

**SMALL SIGNAL STABILITY ANALYSIS OF GRID  
CONNECTED WITH VARIOUS SOLAR PHOTOVOLTAIC  
PENETRATION LEVELS AT DIFFERENT LOAD AND  
REACTIVE LOAD LEVELS**

**SHALOM LIM ZHU AUN**

**COLLEGE OF GRADUATE STUDIES  
UNIVERSITI TENAGA NASIONAL**

**2019**

**SMALL SIGNAL STABILITY ANALYSIS OF GRID  
CONNECTED WITH VARIOUS SOLAR PHOTOVOLTAIC PENETRATION  
LEVELS AT DIFFERENT LOAD AND REACTIVE LOAD LEVELS**

**By**

**SHALOM LIM ZHU AUN**

**A Dissertation Submitted in Partial Fulfillment of the Requirements for  
the Degree of Master of Electrical Engineering**

**College of Graduate Studies  
Universiti Tenaga Nasional**

**September 2019**

## **ABSTRACT**

The utilization of fossil fuels at an alarming rate has brought adverse effects on the environment and have accelerated the need for the development of alternative renewable energy resources. This dissertation primarily focuses on the small signal stability analysis of a power system integrated with solar photovoltaics (PV). The test systems utilized in this study are a small and large scaled power system which is the IEEE 9-bus and 39-bus power system respectively. The small signal stability of the test systems is broken down and examined in terms of eigenvalue analysis, damped frequency, damping ratio and participation factor. Different states are analyzed in this study which consist of the effects of incremental solar PV penetration into the systems, load variation and reactive load variation. For incremental solar PV penetration, the results observed indicate that there are no significant adverse impacts of solar PV penetration on the small signal stability of both the small and large scaled power systems. When the overall load and reactive loads are increased, no significant impact is observed on small signal stability and the power systems still remained in a stable state. The software used in this study is DigSILENT Powerfactory.

## ACKNOWLEDGEMENTS

The success of any project depends essentially on the support and guidance of many others. It would not have been possible to compose this dissertation without the support and help of the individuals around me, to only a few of whom it is conceivable to recognize here.

Above all, I take this opportunity to express my appreciation to the individuals who have guided me in completing this dissertation. I would like to show my greatest appreciation to Dr. Marayati Bte Marsadek, my supervisor for her constant support, guidance and dedication. She consistently steered me in the right direction whenever she thought I needed it. I am grateful for her invaluable advice and guidance.

I would also like to thank Associate Professor Dr. Agileswari K. Ramasamy for her aid, support and her consent on this project. Apart from that, I am grateful for her guidance in the publication of my journal.

At last, I must express my exceptionally significant appreciation to my parents for giving me unfailing bolster and ceaseless support throughout my years of study and throughout the process of composing this dissertation. This achievement would not have been possible without them.

## **DECLARATION**

I hereby declare that the thesis is my original work except for quotations and citations which have been duly acknowledged. I also declare that it has not been previously, and is not concurrently submitted for any other degree at Universiti Tenaga Nasional or at any other institutions. This thesis may be made available within the university library and may be photocopies and loaned to other libraries for the purpose of consultation.

---

(Signature)

**SHALOM LIM ZHU AUN**

Date: 1<sup>st</sup> October 2019

## TABLE OF CONTENTS

	<b>Page</b>
<b>ABSTRACT</b>	iii
<b>ACKNOWLEDGEMENTS</b>	iv
<b>DECLARATION</b>	v
<b>TABLE OF CONTENTS</b>	vi
<b>LIST OF TABLES</b>	ix
<b>LIST OF FIGURES</b>	xii
<b>LIST OF ABBREVIATIONS</b>	xv
<b>LIST OF PUBLICATIONS</b>	xvi
<b>CHAPTER 1 INTRODUCTION</b>	<b>1</b>
1.1 Introduction	1
1.2 Problem Statement	1
1.3 Research Objectives	3
1.4 Research Scope	3
1.5 Summary of Chapter	4
<b>CHAPTER 2 LITERATURE REVIEW</b>	<b>5</b>
2.1 Evolution of renewable energy	5
2.2 Issues Faced by Integration of Renewable Energy Sources into Existing Grids	6
2.3 Power System Stability	8
2.4 Studies done on Small Signal Stability Performance in grid integrated solar PV	10
2.5 Summary of Chapter	14

<b>CHAPTER 3 METHODOLOGY</b>	<b>15</b>
3.1 Introduction	15
3.2 Simulation Methods	15
3.2.1 Load Flow Analysis	15
3.2.2 Newton-Raphson Method	17
3.2.3 Small Signal Stability Analysis	20
3.3 IEEE 9-Bus and 39-Bus Power System	23
3.4 Research Proposed Approach and Design	28
3.5 Summary of Chapter	32
<b>CHAPTER 4 RESULTS AND DISCUSSION</b>	<b>33</b>
4.1 Introduction	33
4.2 Case 1: Base model simulation for 9-bus and 39-bus power system	33
4.2.1 Load flow simulation for 9-bus power system	34
4.2.2 Load flow simulation for 39-bus power system	36
4.3 Case 2: Increments of AC solar PV penetration in the power system	39
4.3.1 9-bus power system for incremental penetration of AC solar PV generation	39
4.3.2 39-bus incremental penetration of AC solar PV generation	43
4.4 Case 3: Load variation simultaneously with penetration of AC solar PV generation on power system	47
4.4.1 9-bus load variation with incremental penetration of AC solar PV generation	48
4.4.2 39-bus load variation with incremental penetration of AC solar PV generation	52
4.5 Case 4: Incremental penetration of AC solar PV generation with various reactive load percentages	58
4.5.1 Reactive load variation for various AC solar PV penetration values for the 9-bus power system	59

4.5.2 Reactive load variation for various AC solar PV penetration values for the 39-bus power system	63
4.6 Summary of Chapter	70
<b>CHAPTER 5 CONCLUSION AND RECOMMENDATIONS FOR FUTURE WORK</b>	<b>70</b>
5.1 Conclusion	71
5.2 Recommendations for Future Work	73
<b>REFERENCES</b>	<b>74</b>
<b>APPENDICES</b>	<b>79</b>
Appendix A: Power generation and load data of 9-bus power system	79
Appendix B: Power generation and load data of 39-bus power system	84

## LIST OF TABLES

Table 3.1	Inter-area and local modes frequency range	21
Table 3.2	IEEE 9-Bus modified test system machine data	24
Table 3.3	IEEE 9-Bus modified test system exciter data	24
Table 3.4	IEEE 9-Bus modified test system governor data	25
Table 3.5	IEEE 39-Bus modified test system machine data	26
Table 3.6	IEEE 39-Bus modified test system governor data	27
Table 3.7	IEEE 39-Bus modified test system exciter data	27
Table 4.1	Voltage magnitude validation for 9-bus system	35
Table 4.2	Load flow result comparison for distribution lines in 9-bus the system	35
Table 4.3	Voltage magnitude and deviation for 39-bus system	36
Table 4.4	Load flow result for distribution lines in 39-bus the system	38
Table 4.5	Lowest damping ratio mode for AC solar PV penetration of 0 MW to 163 MW	40
Table 4.6	Highest damping ratio mode for AC solar PV penetration of 0 MW to 163 MW	41
Table 4.7	Lowest damping ratio eigenvalues for AC solar PV penetration of 0 MW to 250 MW	44
Table 4.8	Highest damping ratio eigenvalues for AC solar PV penetration of 0 MW to 250 MW	45
Table 4.9	Lowest damping ratio eigenvalues for various AC solar PV penetration and overall load variation	48
Table 4.10	Highest damping ratio eigenvalues for various AC solar PV penetration and overall load variation	49
Table 4.11	Critical lowest damping ratio for critical eigenvalues for overall load variation of 5% to 15%	53
Table 4.12	Critical highest damping ratio for critical eigenvalues for overall load variation of 5% to 15%	55

Table 4.13	Lowest damping ratio eigenvalues for various AC solar PV penetration and reactive load variation	59
Table 4.14	Highest damping ratio eigenvalues for various AC solar PV penetration and reactive load variation	60
Table 4.15	Lowest damping ratio eigenvalues for various AC solar PV penetration and reactive load variation	64
Table 4.16	Highest damping ratio eigenvalues for various AC solar PV penetration and reactive load variation	66
Table 4.17	Results summary of Case 1, Case 2, Case 3 and Case 4	70
Table A.1	Power generation data for AC solar PV penetration of 0 MW to 163 MW	79
Table A.2	9-bus system overall load data at 5%, 10% and 15% increments	79
Table A.3	9-bus system generation data for AC solar PV penetration of 0 MW to 163 MW at 5% overall load increment	80
Table A.4	9-bus system generation data for AC solar PV penetration of 0 MW to 163 MW at 10% overall load increment	80
Table A.5	9-bus system generation data for AC solar PV penetration of 0 MW to 163 MW at 15% overall load increment	81
Table A.6	9-bus system reactive load data at 5%, 10% and 15% increments	81
Table A.7	9-bus system generation data for AC solar PV penetration of 0 MW to 163 MW at 5% reactive load increment	82
Table A.8	9-bus system generation data for AC solar PV penetration of 0 MW to 163 MW at 10% reactive load increment	82
Table A.9	9-bus system generation data for AC solar PV penetration of 0 MW to 163 MW at 15% reactive load increment	83
Table B.1	Power generation data for AC solar PV penetration of 0 MW to 250 MW	84
Table B.2	39-bus system overall load data at 5%, 10% and 15% increments	86
Table B.3	39-bus system generation data for AC solar PV penetration of 0 MW to 250 MW at 5% overall load increment	89

Table B.4	39-bus system generation data for AC solar PV penetration of 0 MW to 250 MW at 10% overall load increment	91
Table B.5	39-bus system generation data for AC solar PV penetration of 0 MW to 250 MW at 15% overall load increment	93
Table B.6	39-bus system reactive load data at 5%, 10% and 15% increments	95
Table B.7	39-bus system generation data for AC solar PV penetration of 0 MW to 250 MW at 5% reactive load increment	98
Table B.8	39-bus system generation data for AC solar PV penetration of 0 MW to 250 MW at 10% reactive load increment	100
Table B.9	39-bus system generation data for AC solar PV penetration of 0 MW to 250 MW at 15% reactive load increment	102

## LIST OF FIGURES

Figure 2.1	Classification of Power System Stability	8
Figure 3.1	Modified IEEE 9-bus system in DIgSILENT Powerfactory software	23
Figure 3.2	Modified IEEE 39-bus system in DIgSILENT Powerfactory software	26
Figure 3.3	50 MW AC Solar PV Penetration with 200 MW Synchronous Generator	29
Figure 3.4	100 MW AC Solar PV Penetration with 150 MW Synchronous Generator	29
Figure 3.5	150 MW AC Solar PV Penetration with 100 MW Synchronous Generator	30
Figure 3.6	200 M WAC Solar PV Penetration with 50 MW Synchronous Generator	30
Figure 3.7	250 MW AC Solar PV Penetration without Synchronous Generator	30
Figure 3.8	Methodology flow chart	32
Figure 4.1	Graph of voltage in p.u. for each bus in the 9-bus power system.	34
Figure 4.2	Graph of voltage deviation for each bus in the 39-bus power system	36
Figure 4.3	Graph of damping ratio against AC solar PV penetration for lowest damping ratio mode	40
Figure 4.4	Graph of damping ratio against AC solar PV penetration for highest damping ratio mode	41
Figure 4.5	Eigenvalue plot, AC solar PV penetration of 163 MW	42
Figure 4.6	Participation factor bar plot with AC solar PV penetration of 163 MW (Positive imaginary part)	43
Figure 4.7	Graph of damping ratio against AC solar PV penetration for mode with lowest damping ratio	44
Figure 4.8	Graph of damping ratio against AC solar PV penetration for mode with highest damping ratio	45
Figure 4.9	Eigenvalue plot, AC solar PV penetration of 250 MW	46

Figure 4.10	Participation factor bar plot with AC solar PV penetration of 250 MW (Positive imaginary part)	47
Figure 4.11	Graph of damping ratio against AC solar PV penetration at various loads for lowest damping ratio mode	49
Figure 4.12	Graph of damping ratio against AC solar PV penetration at various loads for highest damping ratio mode	50
Figure 4.13	Eigenvalue plot, AC solar PV penetration of 163 MW at 15% loading	51
Figure 4.14	Participation factor bar plot with PV penetration of 163 MW at 15% loading (Positive imaginary part)	52
Figure 4.15	Graph of damping ratio against AC solar PV penetration at various loads critical mode with lowest damping ratio	54
Figure 4.16	Graph of damping ratio against AC solar PV penetration at various loads critical mode with highest damping ratio	56
Figure 4.17	Eigenvalue plot, AC solar PV penetration of 250 MW at 15% loading	57
Figure 4.18	Participation factor bar plot with PV penetration of 250 MW at 15% loading (Positive imaginary part)	58
Figure 4.19	Graph of damping ratio against AC solar PV penetration at various reactive loads for lowest damping ratio mode	60
Figure 4.20	Graph of damping ratio against AC solar PV penetration at various reactive loads for highest damping ratio mode	61
Figure 4.21	Eigenvalue plot, AC solar PV penetration of 163 MW at 15% reactive loading	62
Figure 4.22	Participation factor bar plot with PV penetration of 163 MW at 15% reactive loading (Positive imaginary part)	63
Figure 4.23	Graph of damping ratio against AC solar PV penetration at various reactive loads for critical mode with lowest damping ratio	65
Figure 4.24	Graph of damping ratio against AC solar PV penetration at various reactive loads for critical mode with highest damping ratio	67

Figure 4.25	Eigenvalue plot, AC solar PV penetration of 250 MW at 15% reactive loading	68
Figure 4.26	Participation factor bar plot with PV penetration of 250 MW at 15% reactive loading (Positive imaginary part)	69

## LIST OF ABBREVIATIONS

AVR	Automatic Voltage Regulator
DFIG	Doubly Fed Induction Generator
FACTS	Flexible AC Transmission System
PSAT	Power System Analysis Toolbox
PSLF	General Electric's Positive Sequence Load Flow
PSS	Power System Stabilizer
PV	Photovoltaics
SSAT	Small Signal Analysis Tool
SVC	Static Var Compensator
TSCS	Thyristor Controlled Series Capacitor
WECC	Western Electric Coordinating Council

## LIST OF PUBLICATION

- [1] S. L. Z. Aun, M. B. Marsadek, and A. K. Ramasamy. (2017, June). Small signal stability analysis of grid connected photovoltaic. *Indones. J. Electr. Eng. Comput. Sci.* [Online]. 6 (3), pp. 553–562.

# CHAPTER 1

## INTRODUCTION

### 1.1 Research Background

This research focuses on small signal stability analysis of grid connected with solar photovoltaic. The research involves the investigation that consist of eigenvalue analysis, damped frequency, damping ratio and participation factor for increased photovoltaic penetration and load variation into the grid. The obtained results would indicate the effects and impact of photovoltaic penetration on the small signal stability of the power system.

### 1.2 Problem Statement

In later times, the utilization and exhaustion of the world's fossil fuels have been growing at a disturbing exponential rate. 3.7 million tons of carbon dioxide and various greenhouse gases is released into the world's atmosphere annually by the average 500 MW coal plant [1]. One of the main disadvantages of fossil fuels power plants are the emission of carbon dioxide gases. A report estimated that global carbon dioxide emissions from fossil fuel use were 32.2 billion tons in 2013, reaching a record high which is 56.1% above the emission level in 1990 and 2.3% above 2012. In other words, at current rates, remaining resources would be used up in the next 30 years [2].

Fossil fuel power plants utilizes coal that is a sedimentary rock consisting mainly of organic, inorganic minerals and elements deposited during its formation. Coal contains low levels of thorium, uranium and other radioactive isotopes which causes radioactive contamination in the environment. A typical active 1000 MW coal power plant could release of up to 12.8 tons of thorium and 5.2 tons of uranium annually [3]. These emissions are harmful and could potentially cause unwanted side effects on humans and also cause contamination on environment. This also raises an awareness and concern on global warming, greenhouse effects and energy shortage in the near future.

The growth of non-renewable energy resources would also lead to the possibility of a resource scarcity which in return would increase the costs involved. Furthermore, conventional power plants are becoming costlier because of societal demand of reducing pollution and increasing safety. When relying on conventional power generation methods, successful economic development would raise prices and make further economic development more difficult to be achieved. However, this cost driving factor is not faced for renewable electricity. The development and utilization of renewable energy would in return pave the way for further economic development. Even though initial investments for renewable energy resources may be higher, with technology advancement in the long run it will outcompete non-renewable resources [4]. Therefore, this accelerates the need to seek for alternative energy resources to guarantee a sustainable future.

In Malaysia, gas and coal remained the most used fossil fuels for power generation at 49.4% and 42.6% respectively, followed by hydroelectric at 4.8% and oil/distillate at 2.5%. With estimated annual consumption of 21 million tons in 2013, coal is poised to be the main fuel for power generation as additional 5000 MW of coal-fired capacity will be commissioned from 2015 to 2019 [5]. Nevertheless, over the years, numerous policies have been drafted and implemented by the government in order to develop the renewable energy sector in the country [6]. This would increase the amount of renewable energy being fed into the power system grid.

The conventional power systems now mainly consist of synchronous generators that are highly nonlinear. When connected to renewable resources, this may result in a change of dynamics and operational characteristics which may affect its small signal stability performance. Thus, the need arises to study the interaction when the conventional power system is integrated with renewable energy resources. Since the development of renewable energy in Malaysia is headed towards solar PV systems, an in-depth study on the interaction of solar PV penetration into a power system in terms of small signal stability is to be done. Furthermore, the load demand and reactive load vary as the demand for electricity changes throughout the day. Power systems must match generation and load

in real time, which may also impact the small signal stability of the system. This study would also evaluate the small signal stability performance at various load demands and reactive loads in the power system which is integrated with solar PV generation.

### **1.3 Research Objective**

This research embarks on the following objectives:

- 1) To investigate the impact of increased solar PV penetration on the grid towards small signal stability
- 2) To investigate the effect of increasing the overall base load by 5%, 10% and 15% at different levels of solar PV penetration in the grid towards small signal stability
- 3) To study the effect of increasing the overall reactive base load by 5%, 10% and 15% at different levels of solar PV penetration in the grid towards small signal stability

### **1.4 Research Scope**

The performance of the power system with penetration of solar PV will be evaluated and assessed using small signal stability analysis. The power system used in this study will be the typical IEEE 9-bus and 39-bus system which consists of synchronous generators. The impact of solar PV penetration in the power system in terms of small signal stability will be studied from the eigenvalue of all states computed using modal analysis. In addition, the damping ratio, damped frequency and participation factor would also be investigated. DIgSILENT Powerfactory simulation software is utilized in this research for modal analysis.

## **1.5 Summary of Chapter**

The alarming rates of fossil fuels being consumed for the generation of electricity in the world today has raised a concern towards an increase in greenhouse gases leading to global warming. This has raised awareness on the importance of the development of alternative energy resources, particularly renewable energy. However, with the advancement of renewable energy, this also raised a concern on its small signal stability when integrated into the existing power system grids. Given Malaysia's high irradiance levels, it is suitable for generation of solar PV systems. This research focuses on three main objectives. Firstly, this research investigates the impact of increased solar PV penetration on the grid towards small signal stability. Next, the effect of increasing the overall base load by 5%, 10% and 15% at different levels of solar PV penetration in the grid towards small signal stability is investigated. Lastly, the effect of increasing the overall reactive base load by 5%, 10% and 15% at different levels of solar PV penetration in the grid towards small signal stability is examined. The research scope involves the small signal stability analysis of two power systems; IEEE 9-bus and IEEE 39-bus power systems.

## CHAPTER 2

### LITERATURE REVIEW

#### 2.1 Evolution of renewable energy

Traditional farming labor and manual manufacturing were replaced by machinery in the first industrial revolution which took place in Great Britain. The very first industry to be dominated by machines was the textile industry. Towards the end of the 18th century, the first industrial revolutions were energized via steam engine, coal and steam. Moving forward, in the mid-19th century, expeditious growth of steamships and steam railways emerged from the heavy steel-making industry in Great Britain, the United States and Germany. Besides that, early electrical technologies such as the telegraph emerged in the 19th century. In 1870, the second industrial revolution was driven by the rise of electric power and technology contributed by none other than Thomas Edison, Antonio Meucci, Alexander Bell, Galileo Ferraris, George Westinghouse, Nikola Tesla and Guglielmo Marconi. At the start of the new century, electro-powered factories started to outperformed coal-powered factories due to the vast availability, versatility and efficiency of electrical machinery mainly hydropower in locations such as the Great Lakes (United States) and Alps (Europe). During the first half of the 20th century, thermal power stations fed by coal or oil multiplied rapidly. Towards the mid-20th century, there was growth in the solid-state electronics, information technology and automation sector. This helped boost the information processing and transmission sectors. Throughout these industrial phases, fossil fuels have been consumed at alarming exponential rates and have increased the greenhouse effects. Today, the world is developing means to use renewable energy sources to support industrialization in a sustainable manner [7].

Countries such as Spain, Denmark, Germany and the United States have created critical markets for renewable energy, that drove the early technological advances and economies of scale, setting the stage and aiding to fueled the past decade of explosive market expansion. There is a steady increase in contribution of renewable energy to the global

heat, power and transport sectors, most notable in developing and emerging economies, whereby its markets and technology developments have excelled quickly. In this modern era, renewable energy technologies are tools for proving energy security, mitigating and adapting to climate change, reducing dependency on imported fuels, improving local air quality and safety, advancing energy access and security, propelling economic development and creating more jobs. Over the past decade, China has taken the lead in renewables manufacturing and installed capacity, having increased investment in this sector almost every year in the past 10 years. Energy demand and growing interests in renewable energy in developing and emerging countries across Latin America, Africa, Middle East and Asia are expanding. Furthermore, foreign direct investments in renewable energy and the mobilization of private capital in emerging economies have contributed to growth across technologies and regions [8]. The excellent growth in renewable energy markets has led to an increase in manufacturers and an overall increase in the number of jobs installing and servicing renewable energy technologies. With the increased growth rate of renewable energy sources, it also brought along issues related to its integration into existing grids.

## **2.2 Issues Faced by Integration of Renewable Energy Sources into Existing Grids**

The integration of renewable energy sources into existing power grids bring about technical challenges. It is commonly known that the renewable energy implementation within the electrical power system is a new challenge, such implementations have constraints and can cause some perturbation. The intermittent nature of renewable energy generation has raised concerns on its power system stability and hence been deduced that renewable energy is a potential source of power quality disturbances of the future power grid [9] - [10]. There are various constrains on integrating renewable energy sources to the power grid such as harmonics, frequency, voltage fluctuations, voltage imbalances, voltage sags/swells, flickers and degradation of minimum current [11] - [12]. Furthermore, power system stability is also another issue faced by the integration of large scale renewable energy sources into the existing grids.

Based on a research done in [13], the small signal stability performance is impacted when DFIG-based wind turbine generators are integrated into the power system grid. In addition, another study done in [14] confirms that small signal stability issues arose when wind renewable energy is integrated to the grid. Results showed dynamically unstable characteristics and transformed local and inter-area mode shapes. Another study was done on the impact of DFIG-based wind and solar PV generation on the power system grid. It was observed that the stability of the system was enhanced [15]. Apart from that, in [16], when a 2 MW wind farm with DGIF wind turbines is integrated into a small grid, results show that the small signal stability is improved under certain conditions. Furthermore, [17] found that integration of wind energy improved stability by reducing the settling and overshoot time under the action of power system stabilizers. Besides that, integration of renewable energy at the distribution level was investigated in [18]. It was observed that solar PV generations enhances small signal stability performance and the dynamics of wind energy induced more system oscillations. In [19], when renewable energy penetration increased, there was an increase in frequency of modes, however the damping ratio remained relatively constant. There were also no negative effects when renewable generation increased. Moreover, another study done in [20] discovered that damping ratio of inter-area modes improved when wind farms were equipped with Power System Stabilizer (PSS). Based on [21], damping performance and small signal stability at a microgrid level is seen to have improved when during the integration of wind and solar PV energy conversion systems.

Therefore, this shows the importance of assessing and analyzing the impact and performance of the integration of renewable energy into the grid. Though Malaysia's geographic location may not be suited for harvesting wind energy, it does have great potential for solar renewable energy. Malaysia lies in the equatorial region making it a hot and relatively humid country with stable climate throughout the whole year. A study done in [22], states that on average, Malaysia's solar irradiations falls between 4.21 kWh/m<sup>2</sup> to 5.56 kWh/m<sup>2</sup> which encourages the development of solar PV systems. Therefore, solar PV systems does indeed have good potential to be developed in Malaysia.

### 2.3 Power System Stability

Power system stability can be classified into rotor angle stability, frequency stability and voltage stability. Figure 2.1 shows the various classifications of power system stability. Rotor angle stability is the system's ability to maintain the equilibrium between electromagnetic torque and mechanical torque of each generator in the system. Rotor angle instability occur due to angular swings of certain generators which leads to their loss of synchronism among other generators. Voltage stability refers to the ability of a power system to maintain its steady voltage at all buses in the system from a given initial operating condition, after subjecting to a disturbance [23] - [24].

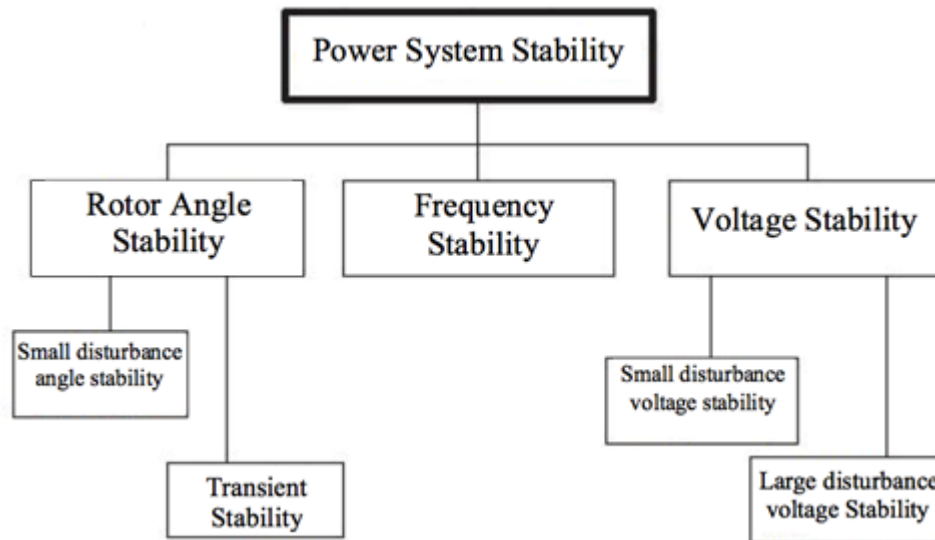


Figure 2.1. Classification of Power System Stability [13].

More solar PV systems are being built into existing power systems, the conventional generation systems could be replaced due to higher operating costs, lower efficiencies, aging and other factors. Thus, with these changes in the power grid, actions have to be taken in order to sustain the requirements of the future power systems.

The increase in solar PV generation would reduce system inertia that may affect the response of the power systems. Most conventional generators in the grid consists of synchronous generators. The increase in solar PV generation would indicate a displacement of synchronous generation which in turn causes a reduced rotating mass in the power system. Therefore, this reduces the overall system inertia [25]. The essentials of a reliable system operation include the system's ability to respond and adapt to the operating conditions in a timely manner when faced with different disturbances. With the increase in PV resources in the grid, the effects of these systems are not adequately studied. Literature states that voltage profiles at the distribution level may be affected depending on the amount of solar PV penetration and loading conditions [26] - [27]. These studies have determined various issues associated with solar PV system in direct relation affecting distribution systems. Researchers suggested that the present equipment used for voltage regulation is not suitable for mitigating the detrimental impacts of solar PV system transients.

Studies performed in [28] - [29], transient behaviour towards transmission system in response to solar PV penetration has been investigated. The results showed that various amounts of PV penetration can have detrimental and beneficial effects on transient voltages. Nevertheless, the studies are not conducted on actual representations of larger interconnected power systems.

Various case studies to analyse transmission system performance was conducted on an IEEE 39-bus system done by [29]. The analysis was done to investigate the transient stability and steady state. In this study, it was observed that with reduced system inertia, this indicated that small signal stability performance of the system could be affected.

## **2.4 Studies done on Small Signal Stability Performance in grid integrated solar PV**

This section discusses in more detail the previous researches on the small signal stability with solar PV penetration in the grid.

In [30], analyzed the impact of increased solar PV generation on the inter-area oscillations in the Western North American power system was investigated. The software analysis tools used in this study were General Electric's Positive Sequence Load Flow (PSLF), MATLAB and Small Signal Analysis Tool (SSAT) from Powertech Labs. In the first approach, the modes of oscillation were excited by simulation and then ringdown analysis using Prony's method was performed. PSLF was used to simulate dynamic brake insertions, whereas MATLAB to extract the modal content from the measured ringdowns. The second approach used SSAT to perform analytical linearization techniques to investigate the effects of small signal stability in increased penetration of solar renewable energy. Two different base cases were investigated on from the Western Electric Coordinating Council (WECC). It was observed that under low load conditions, there was an increase in observability and decrease in damping ratio in the mode of oscillation which may have been a potential concern. Furthermore, the mode of frequency is found to increase as penetration of solar PV increases, while the system's damping remains relatively unaffected [30].

A model of a single-machine infinite-bus power system that is integrated with solar PV generation is established in [31]. The damping torque analysis is conducted to examine the effects of solar PV on the damping of power system local mode oscillations. Solar PV does not add any additional oscillation mode to the power system due to it lacking rotational components. However, it affects the small signal stability due to its interaction with synchronous generators. The small signal stability performance of the power system varies and is dependent on the system operating conditions. This is because to the damping torque contribution from the solar PV could be either positive or negative. A critical condition is formed when the solar PV generation changes from being positive to negative and vice versa [31].

Modal analysis is used to determine the oscillation frequency, damping ratio and mode shape. In [32], results are further analyzed using the non-linear time-domain simulation. An equivalent single-machine model for a solar PV power plant is used in the study. The method used in this study is that the power output of a generator is partially or fully displaced with solar PV generator. DSA Tools by Powertech Labs Inc. is used in this modal analysis. Simulation results show that the penetration of solar PV can be both beneficial or detrimental to the power system [32].

Investigation of the impact of small signal stability at different penetration levels of solar PV generation in a two-area system was conducted by [33]. The synchronous generators were displaced with solar PV generation in order to keep the total generation constant for all cases. The penetration levels used in the study were 25%, 45%, 65% and 85%. The power system being studied on is equipped with Flexible AC Transmission System (FACTS) devices namely Static Var Compensator (SVC) and Thyristor Controlled Series Capacitor (TSCS). Three cases were considered in the study. Firstly, the analysis of PV penetration is done on the power system without incorporating FACTS. The second case incorporates the use of Static Var Compensator (SVC) and finally the third case uses Thyristor Controlled Series Capacitor (TSCS) into the power system. Impact of solar PV penetration is found to benefit the two-area system to a certain point. At 85% penetration however, it is found that the system's damping ratio deteriorates. Nevertheless, the incorporation of SVC and TCSC is shown to have improved the damping greatly [33].

According to [15], the impact of small signal stability on the integration of solar PV and wind power generation was done. The conventional synchronous generators were substituted with solar PV generation and doubly fed induction generator (DFIG). The impact of different levels of solar and wind power penetration to the power system is also examined. Eigenvalue analysis was used to calculate the damping ratio and frequency of oscillatory components for minor disturbances. A spectral analysis known as discrete wavelet transform is used to identify oscillatory modes. Hidden frequency information within the signal are extracted using power spectral density and time frequency curves.

MATLAB PSAT is used as the software analysis tool. It is found that renewable energy integrated into the power system causes the system to be more dynamic. This is due to the intermittent nature of renewable energy resources. This study shows an improvement in the damping when solar PV penetration is increased. Wind energy enhances damping up at a penetration level of 50%. A penetration of 50% level alone would negatively affect the power system damping [15].

The effect of solar PV penetration on the small signal stability of the power system was also studied in [34]. The software used in this study is Power System Analysis Toolbox (PSAT) of MATLAB. The synchronous generator is displaced with various penetration levels of solar PV. Small signal stability of the power system is investigated in terms of eigenvalue analysis and critical modes. Transient analysis is also done to verify the results obtained in small signal stability analysis. This research consists of four cases. Firstly, the base case is analyzed first to uncover the existing system's critical modes. Next, various levels of solar PV penetration are investigated using eigenvalue analysis. The results are then compared to the base case and then analyzed. Lastly, transient analysis is used to validate the small signal stability analysis. In this study, it is observed that when the conventional generator is displaced by solar PV system, the eigenvalues are observed to move more to the left-hand side of the complex plane. Thus, this indicates the system is becoming more stable due to the reduction of inertia [34].

According to [18], an investigation of renewable energy based of distribution system. Renewable energy used in the study are wind and solar PV. In the future, there will be a widespread of renewable energy resource being integrated into the distribution systems. The method used in this research was firstly to examine the base case. Then, solar PV generation is set to a constant of 1 MW and wind generation was increased to 6 MW which is equivalent to a 20% increment. Lastly, wind generation was set to a constant 2 MW and solar PV generation increased to 6 MW which is equivalent to a 20% increment. The three cases were evaluated using eigenvalue analysis and participation factor. Results show an increase in solar PV penetration, it causes a decreases in the eigensensitivity, thus causing an improvement of the small signal system performance. It is observed that wind energy

and solar PV penetration positively impact the oscillation damping of the synchronous generator [18].

In another research, penetration of solar PV and wind energy conversion system from microgrid into actual grid was studied. In this research, 50% solar PV and 50% WECS from microgrid and the microgrid is gradually increased from 10 MW to 80 MW penetration. It was observed that with a higher penetration from the microgrid, the damping performance was enhanced and the power system becomes more stable. The eigenvalue real parts are more negative and there is a higher damping ratio which corresponds to the penetration increase [21].

Apart from solar PV penetration, there are also studies done on the influence of load modeling on small signal stability investigations. In [35], various load classes such as residential, commercial and industrial were simulated and the small signal stability was analyzed. The results had shown that a residential load class would lead to the lowest damping and eigenfrequency, whereas the industrial load class revealed the highest damping and eigenfrequency. Furthermore, a study done by [36] revealed that load changes and capacity changes in a large-scale power system can affect the oscillation mode. It is observed that as load increases, the oscillation stability is improved.

Various studies have been conducted in the efforts of investigating the impact of small signal stability analysis for grid connected solar PV penetration. Research shows that the power system can behave differently on a case-by-case basis. Currently, there is no research on the impact of small signal stability at various load and reactive load levels on a grid connected with solar PV. Thus, this brings the need to investigate further on small signal stability performance in this aspect. Proposed approaches would be discussed in the following methodology section.

## **2.5 Summary of Chapter**

The world is looking towards renewable energy resources to support the on-going industrialization. There are several issues faced by the integration of renewable energy resources into the existing grids. Some studies have shown that there is a negative impact when renewable energy is integrated into the grid. Whereas, other studies observed that the integration of renewable energy enhanced the stability of the power system. Thus, the need to investigate the small signal stability impact of solar PV on the grid arises.

## CHAPTER 3

### METHODOLOGY

#### 3.1 Introduction

In this section, the methodology used to achieve research objectives would be presented. Simulation methods that are used such as Newton-Raphson load flow analysis and small signal stability analysis will be elaborated in the sections below. The test systems that are utilized in this research is the IEEE 9-bus and 39-bus systems. Their characteristics and properties will also be reviewed. Furthermore, the research proposed approach and design that consist of four cases would also be discussed here.

#### 3.2 Simulation Methods

There are various simulation methods used in this research. For the load flow analysis, Newton Raphson method is utilized. Besides that, small signal stability analysis is used to determine the stability of the power system . These analysis methods are detailed in the following sections below.

##### 3.2.1 Load Flow Analysis

The complex power injected to the  $i^{\text{th}}$  bus of a system is shown below [37]:

$$S_i = P_i + jQ_i = V_i J_i^* ; \quad i = 1, 2, \dots, n \quad (\text{Equation 3.1})$$

where  $V_i$  is the bus voltage with respect to the ground and  $J_i$  is the bus current. From the complex conjugate in Equation 3.1, equation below is obtained:

$$P_i - jQ_i = V_i^* J_i ; \quad i = 1, 2, \dots, n \quad (\text{Equation 3.2})$$

$J_i$  is then substituted in to Equation 3.2 using:

$$J_i = \sum_{k=1}^n Y_{ik} V_k ; \quad i = 1, 2, \dots, n \quad (\text{Equation 3.3})$$

Equation 3.4 is then derived as below:

$$P_i - jQ_i = V_i^* \sum_{k=1}^n Y_{ik} V_k; \quad i = 1, 2, \dots, n \quad (\text{Equation 3.4})$$

The real and imaginary parts are then separated as below:

$$P_i = \{V_i^* \sum_{k=1}^n Y_{ik} V_k\} \quad (\text{Equation 3.5})$$

$$Q_i = -\text{Im} \{V_i^* \sum_{k=1}^n Y_{ik} V_k\} \quad (\text{Equation 3.6})$$

By breaking down the complex equations into their respective real and imaginary parts, the static load flow equations can be obtained as below:

$$P_i = |V_i| \sum_{k=1}^n |V_k| |Y_{ik}| \cos(\theta_{ik} + \delta_k - \delta_i); \quad i = 1, 2, \dots, n \quad (\text{Equation 3.7})$$

$$Q_i = -|V_i| \sum_{k=1}^n |V_k| |Y_{ik}| \sin(\theta_{ik} + \delta_k - \delta_i); \quad i = 1, 2, \dots, n \quad (\text{Equation 3.8})$$

The state and control variables must be within the specified limits as below [37]:

i) Voltage magnitude limits:

$$|V_i|_{min} \leq |V_i| \leq |V_i|_{max} \quad (\text{Equation 3.9})$$

The voltage magnitude should be within 0.95 to 1.05 per unit.

ii) Power angle limits:

$$|\delta_i - \delta_k|_{min} \leq |\delta_i - \delta_k| \leq |\delta_i - \delta_k|_{max} \quad (\text{Equation 3.10})$$

The power angle determines stability of power and should be within the limits specified in Equation 3.10.

iii) Real and reactive power limits

$$P_{Gi,min} \leq P_{Gi} \leq P_{Gi,max} \quad (\text{Equation 3.11})$$

$$Q_{Gi,min} \leq Q_{Gi} \leq Q_{Gi,max} \quad (\text{Equation 3.12})$$

The generation of power is equal to the load demand including losses:

$$\sum_i^n P_{Gi} = \sum_i^n P_{Di} + P_L \quad (\text{Equation 3.13})$$

### 3.2.2 Newton-Raphson Method

In order to solve the power load problem, the Newton-Raphson Method is implemented. This method is based upon the Taylor series expansion which uses an iterative method that approximates non-linear simultaneous equations into a set of linear equations up to the first order approximation. Equations below discuss the application of Newton-Raphson method [37].

A set of n non-linear algebraic equations is given as below:

$$f_i(x_1, x_2, \dots, x_n) \quad (\text{Equation 3.14})$$

Initial estimate is assumed by:

$$x_1^{(0)}, x_2^{(0)}, \dots, x_n^{(0)} \quad (\text{Equation 3.15})$$

Corrections to the terms are as:

$$\Delta x_1, \Delta x_2, \dots, \Delta x_n \quad (\text{Equation 3.16})$$

The corrections are added to the initial estimate to obtain Equation 3.17 as below:

$$f_i(x_1^{(0)} + \Delta x_1, x_2^{(0)} + \Delta x_2, \dots, x_n^{(0)} + \Delta x_n) = 0 \quad (\text{Equation 3.17})$$

Taylor series expansion is used to expand Equation 3.18 as below:

$$f_i(x_1^{(0)}, x_2^{(0)}, \dots, x_n^{(0)}) + \left[ \Delta x_1 \frac{df_i}{dx_1} \Big|_0 + \Delta x_2 \frac{df_i}{dx_2} \Big|_0 + \dots + \Delta x_n \frac{df_i}{dx_n} \Big|_0 \right] + \text{higher order terms} = 0 \quad (\text{Equation 3.18})$$

The higher order terms are ignored as there are generally no major loss. The equations are rewritten as Equation 3.19 below:

$$\begin{bmatrix} y_1 - f_1(x_1^{(0)}, x_2^{(0)}, \dots, x_n^{(0)}) \\ y_2 - f_2(x_1^{(0)}, x_2^{(0)}, \dots, x_n^{(0)}) \\ y_3 - f_3(x_1^{(0)}, x_2^{(0)}, \dots, x_n^{(0)}) \end{bmatrix} = \begin{bmatrix} \frac{df_1}{dx_1} \Big|_0 & \frac{df_1}{dx_2} \Big|_0 & \frac{df_1}{dx_n} \Big|_0 \\ \frac{df_2}{dx_1} \Big|_0 & \frac{df_2}{dx_2} \Big|_0 & \frac{df_2}{dx_n} \Big|_0 \\ \frac{df_n}{dx_1} \Big|_0 & \frac{df_n}{dx_2} \Big|_0 & \frac{df_n}{dx_n} \Big|_0 \end{bmatrix} \begin{bmatrix} \Delta x_1 \\ \Delta x_2 \\ \Delta x_n \end{bmatrix} \quad (\text{Equation 3.19})$$

The equation can be simplified as Equation 3.20:

$$[M] = [J][R] \quad (\text{Equation 3.20})$$

Where J is the Jacobian Matrix, M is the Mismatch Matrix and R is the matrix of the corrections  $\Delta x_i$ . The equation can be written as an iterative in Equation 3.21 and Equation 3.22 below:

$$M^{(r)} = J^{(r)} R^{(r)} \quad (\text{Equation 3.21})$$

$$R^{(r)} = [J^{(r)}]^{-1} M^{(r)} \quad (\text{Equation 3.22})$$

Thus,  $x_i$  can be given by Equation 3.23:

$$x_i^{(r+1)} = x_i^{(r)} + \Delta x_i^{(r)} \quad (\text{Equation 3.23})$$

This process is repeated until there is a small tolerance difference between two successive values of  $x_i$ . Nevertheless, the Newton-Raphson method is more accurate using polar coordinates. The real and reactive powers are represented as Equation 3.24 and Equation 3.25:

$$P_i = \sum_{k=1}^n |V_i| |V_k| |Y_{ik}| \cos(\theta_{ik} + \delta_k - \delta_i); \quad (\text{Equation 3.24})$$

$$Q_i = -\sum_{k=1}^n |V_i| |V_k| |Y_{ik}| \sin(\theta_{ik} + \delta_k - \delta_i); \quad (\text{Equation 3.25})$$

All buses are assumed PQ and using estimated values, the difference between the buses are calculated as Equation 3.26 and Equation 3.27:

$$\Delta P_i = P_{i,spec} - P_{i,cal} \quad (\text{Equation 3.26})$$

$$\Delta Q_i = Q_{i,spec} - Q_{i,cal} \quad (\text{Equation 3.27})$$

The Jacobian in this set of equations consists of partial derivations of P and Q with respect to each of the variables in the static load flow equations. The matrix consists of corrections to be added to the original estimates of voltage magnitude and angle to obtain new calculations for computing the mismatches  $\Delta P_i^p$  and  $\Delta Q_i^p$ .

The matrix representation is finally derived as Equation 3.28:

$$\begin{bmatrix} \Delta P_2 \\ \vdots \\ \Delta P_n \\ \Delta Q_2 \\ \vdots \\ \Delta Q_n \end{bmatrix} = \begin{bmatrix} \left( \frac{\partial P_2}{\partial \delta_2} \right) & \dots & \left( \frac{\partial P_2}{\partial \delta_n} \right) & \left( \frac{\partial P_2}{\partial |V|_2} \right) & \dots & \left( \frac{\partial P_2}{\partial |V|_n} \right) \\ \vdots & \ddots & \vdots & \vdots & \ddots & \vdots \\ \left( \frac{\partial P_n}{\partial \delta_2} \right) & \dots & \left( \frac{\partial P_n}{\partial \delta_n} \right) & \left( \frac{\partial P_n}{\partial |V|_2} \right) & \dots & \left( \frac{\partial P_n}{\partial |V|_n} \right) \\ \left( \frac{\partial Q_2}{\partial \delta_2} \right) & \dots & \left( \frac{\partial Q_2}{\partial \delta_n} \right) & \left( \frac{\partial Q_2}{\partial |V|_2} \right) & \dots & \left( \frac{\partial Q_2}{\partial |V|_n} \right) \\ \vdots & \ddots & \vdots & \vdots & \ddots & \vdots \\ \left( \frac{\partial Q_n}{\partial \delta_2} \right) & \dots & \left( \frac{\partial Q_n}{\partial \delta_n} \right) & \left( \frac{\partial Q_n}{\partial |V|_2} \right) & \dots & \left( \frac{\partial Q_n}{\partial |V|_n} \right) \end{bmatrix} \begin{bmatrix} \Delta \delta_2 \\ \vdots \\ \Delta \delta_n \\ \Delta |V_2| \\ \vdots \\ \Delta |V_n| \end{bmatrix} \quad (\text{Equation 3.28})$$

Equation 3.29 can be simplified into the following:

$$\begin{bmatrix} \Delta P \\ \Delta Q \end{bmatrix} = \begin{bmatrix} J_1 & J_2 \\ J_3 & J_4 \end{bmatrix} \begin{bmatrix} \Delta \delta \\ \Delta |V| \end{bmatrix} \quad (\text{Equation 3.29})$$

The Jacobian is then inverted as Equation 3.30 below:

$$\begin{bmatrix} \Delta \delta^{(p)} \\ \Delta |V|^{(p)} \end{bmatrix} = \begin{bmatrix} \Delta P \\ \Delta Q \end{bmatrix} \begin{bmatrix} J_1 & J_2 \\ J_3 & J_4 \end{bmatrix}^{-1} \quad (\text{Equation 3.30})$$

The values  $\Delta \delta^{(p)}$  and  $\Delta |V|^{(p)}$  are added to the previous voltage magnitude and angles. These new values are then inserted back into Equation 3.29 and Equation 3.30 to obtain new values of real and reactive power. The iterations and processes are repeated until convergence is achieved.

### 3.2.3 Small Signal Stability Analysis

Small signal stability is the power system's ability to preserve synchronism after being subjected to small variations in generation or load [38]. The stability of a power system can be affected by its load characteristics, discrete and continuous controls. Small signal stability analysis examines the system's response to disturbances. System instability normally occurs under the following conditions [38]:

- i) Constant increase in rotor angle due to insufficient synchronizing torque
- ii) Increasing amplitude of rotor oscillations due to insufficient damping torque

Generally, the small signal stability oscillations can be classified into either local mode or inter-area mode. Local modes are divided into three categories which are [38]:

- i) Rotor angle oscillations of a single generator against the rest of the power system with frequencies ranging from 1 Hz to 3 Hz
- ii) Oscillations between rotors of several generators close to one another with frequencies ranging from 0.7 Hz to 2 Hz
- iii) Inadequate tuning of control systems

Inter-area mode oscillations are caused by the interactions among two or more large groups of generators that are swinging against each other in different locations. Inter-area oscillations can be divided into two categories which are [38]:

- i) Low frequency mode that occurs when generators in two different areas are swinging against each other. The frequency of oscillation range is from 0.1 Hz to 0.3 Hz
- ii) High frequency mode involving subgroups of generators swinging The frequency of oscillation range is from 0.4 Hz to 0.7 Hz

Table 3.1 shows the inter-area and local modes frequency range

Table 3.1. Inter-area and local modes frequency range [38].

<b>Mode Type</b>	<b>Frequency Range (Hz)</b>
Inter-area	0.1 to 0.3 (Low frequency)
	0.4 to 0.7 (High frequency)
Local	0.7 to 3

A complex pole can be represented as Equation 3.28 below:

$$s = \sigma \pm j\omega \quad (\text{Equation 3.28})$$

where  $\sigma$  is the real part of the pole known as the exponential damping frequency and  $\omega$  represents the imaginary part which is the damped frequency of oscillation.

The damped frequency of oscillation of any pole is represented by Equation 3.29:

$$f = \frac{\omega}{2\pi} \quad (\text{Equation 3.29})$$

The damping ratio,  $\xi$  is the amplitude of oscillation decay rate. The damping ratio is represented as Equation 3.30 or Equation 3.31 [38]:

$$\xi = \frac{\text{Exponential decay frequency}}{\text{Natural frequency } \left(\frac{\text{rad}}{\text{sec}}\right)} = \frac{|\sigma|}{\omega_n} \quad (\text{Equation 3.30})$$

or

$$\xi = \frac{-\sigma}{\sqrt{\sigma^2 + \omega^2}} \quad (\text{Equation 3.31})$$

The damping ratio plays a significant role in small signal stability because it indicates how well a power system is able to return to its stable state following small disturbances in oscillations.

### 3.3 Test System

The test systems used in this study are the IEEE 9-bus and IEEE 39-bus power systems. Both bus systems are modified to take in to account the dynamic data for time-domain simulations. Each generator in the IEEE bus system has a pre-defined set of dynamic parameters for a sixth order full machine model [39].

The IEEE 9-bus modified system contains three synchronous machines with IEEE type-1 exciters. The system consists of 11 buses, six distribution lines, six transformers and three constant impedance loads. The total load demand is 315 MW and 115 MVar. Figure 3.1 shows the IEEE 9-bus system used. Table 3.2 –Table 3.4 shows the synchronous dynamic data used for the IEEE 9-bus system. The 9-bus system is simulated using DIgSILENT Powerfactory software.

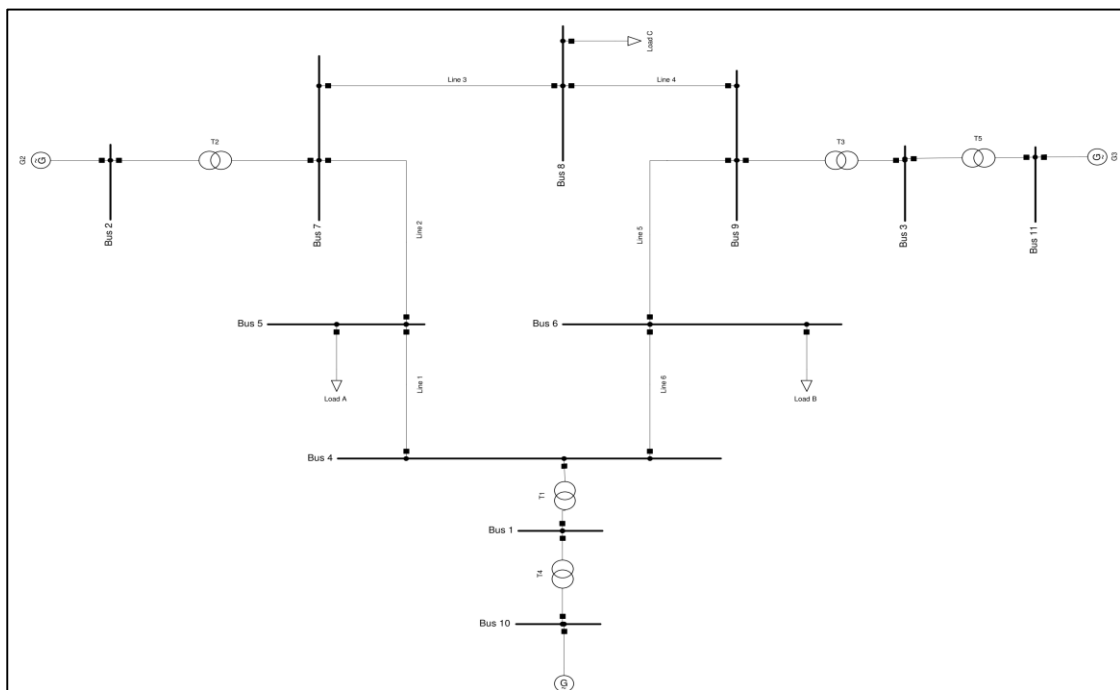


Figure 3.1. Modified IEEE 9-bus system in DIgSILENT Powerfactory software

Table 3.2. IEEE 9-Bus modified test system machine data.

Type	GENROU	GENROU	GENROU
Operation	Sync. Gen.	Sync. Gen.	Sync. Gen.
Default Unit no. (New Unit no.)	1(12)	2(10)	3(11)
Rated power (MVA)	512	270	125
Rated voltage (kV)	24	18	15.5
Rated pf	0.9	0.85	0.85
$H$ (s)	2.6312	4.1296	4.768
$D$	2.000	2.000	2
$r_a$ (p.u)	0.004	0.0016	0.004
$x_d$ (p.u)	1.700	1.700	1.220
$x_q$ (p.u)	1.650	1.620	1.160
$x'_d$ (p.u)	0.270	0.256	0.174
$x'_q$ (p.u)	0.470	0.245	0.250
$x''_d$ (p.u)	0.200	0.185	0.134
$x''_q$ (p.u)	0.200	0.185	0.134
$x_l$ or $x_p$ (p.u)	0.160	0.155	0.0078
$T'_{d0}$ (s)	3.800	4.800	8.970
$T'_{q0}$ (s)	0.480	0.500	0.500
$T''_{d0}$ (s)	0.010	0.010	0.033
$T''_{q0}$ (s)	0.0007	0.0007	0.070
$S(1.0)$	0.090	0.125	0.1026
$S(1.2)$	0.400	0.450	0.432

Table 3.3. IEEE 9-Bus modified test system exciter data.

Type	IEEET1	IEEET1	IEEET1
Default Unit no. (New Unit no.)	1(12)	2(10)	3(11)
Rated power (MVA)	512	270	125
Rated voltage (kV)	24	18	15.5
$T_r$ (s)	0.000	0.000	0.060
$K_a$ (p.u)	200	30	25
$T_a$ (s)	0.395	0.400	0.200
$V_{Rmax}$ (p.u)	3.840	4.590	1.000
$V_{Rmin}$ (p.u)	-3.840	-4.590	-1.000
$K_e$ (p.u)	1.000	-0.020	-0.0601
$T_e$ (s)	0.000	0.560	0.6758
$K_f$ (p.u)	0.0635	0.050	0.108
$T_f$ (s)	1.000	1.300	0.350
$E_1$ (p.u)	2.880	2.5875	2.4975
$SE(E_1)$	0.000	0.7298	0.0949
$E_2$ (p.u)	3.840	3.450	3.330
$SE(E_2)$	0.000	1.3496	0.37026

Table 3.4. IEEE 9-Bus modified test system governor data.

Type	BPA_GG	BPA_GG	BPA_GG
Default Unit no. (New Unit no.)	1(12)	2(10)	3(11)
Rated power (MVA)	512	270	125
Rated voltage (kV)	24	18	15.5
$P_{max}$ (p.u)	0.8984	0.8518	1.056
$R$ (p.u)	0.00976	0.01852	0.040
$T_1$ (s)	0.150	0.100	0.083
$T_2$ (s)	0.050	0.000	0.000
$T_3$ (s)	0.300	0.259	0.200
$T_4$ (s)	0.260	0.100	0.050
$T_5$ (s)	8.000	10.000	5.000
$F$	0.270	0.272	0.280

The modified IEEE 39-bus system has 49 buses, 24 transformers, 10 generators, and 32 distribution lines. It consists of 19 impedance loads which has a total of 6097.1 MW and 1408.9 MVAR. All generators except generator 39 (aggregation of high numbers of generators) are equipped with a turbine governor and type-1 exciters, which include the continuous acting AVR and exciter. The 39-bus system is shown in Figure 3.2. The synchronous dynamic data is shown in Table 3.5 to Table 3.7. DIGSILENT Powerfactory is utilized to simulate the power system.

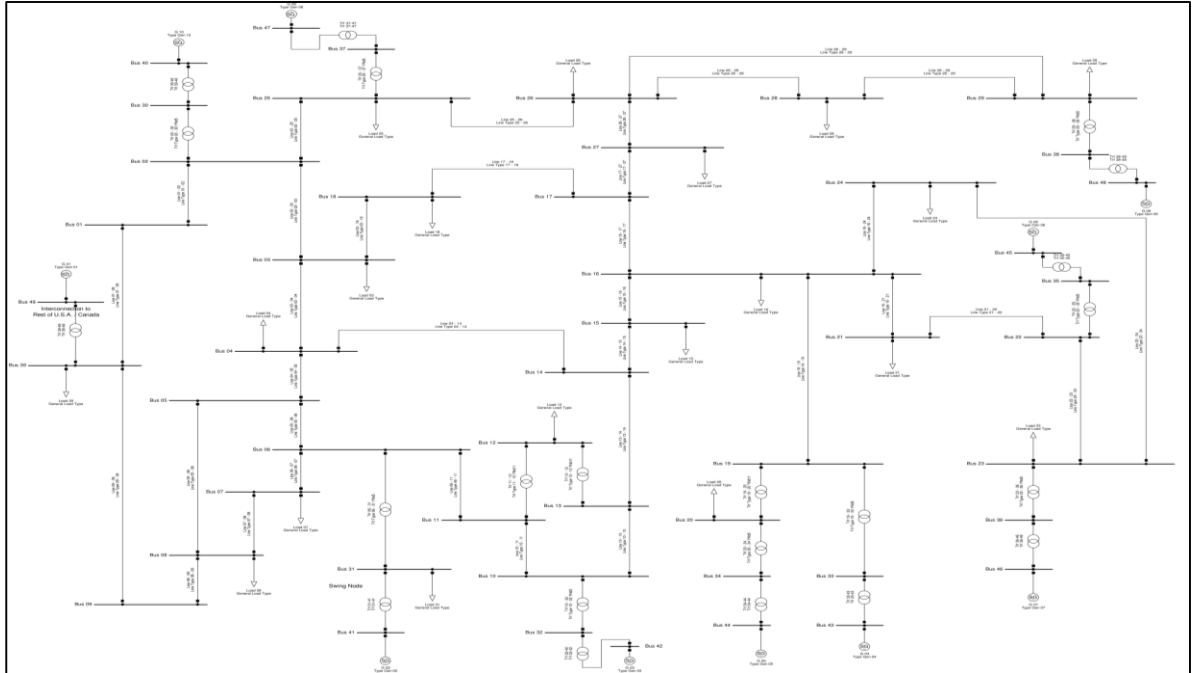


Figure 3.2. Modified IEEE 39-bus system in DigSILENT Powerfactory software.

Table 3.5. IEEE 39-Bus modified test system machine data.

Type Operation	GENROU Sync. Gen.	GENROU Sync. Gen.	GENROU Sync. Gen.
Default Unit no. (New Unit no.)	30(40)	31(41), 32(42), 33(43) 34(44), 35(45), 36(46) 37(47)	38(48) 39(49)
Rated power (MVA)	590	835	911
Rated voltage (kV)	22	20	26
Rated pf	0.95	0.9	0.9
$H$ (s)	2.3186	2.6419	2.4862
$D$	2.00	2.00	2.00
$r_a$ (p.u)	0.0046	0.0019	0.0010
$x_d$ (p.u)	2.110	2.183	2.040
$x_q$ (p.u)	2.020	2.157	1.960
$x'_d$ (p.u)	0.280	0.413	0.266
$x'_q$ (p.u)	0.490	1.285	0.262
$x''_d$ (p.u)	0.215	0.339	0.193
$x''_q$ (p.u)	0.215	0.339	0.193
$x_l$ or $x_p$ (p.u)	0.155	0.246	0.154
$T'_{d0}$ (s)	4.200	5.690	6.000
$T'_{q0}$ (s)	0.565	1.500	0.900
$T''_{d0}$ (s)	0.032	0.041	0.004
$T''_{q0}$ (s)	0.062	0.144	0.004
$S(1.0)$	0.079	0.134	0.340
$S(1.2)$	0.349	0.617	1.120

Table 3.6. IEEE 39-Bus modified test system governor data.

Type	BPA_GG	BPA_GG	BPA_GG
Default Unit no. (New Unit no.)	30(40)	31(41), 32(42), 33(43) 34(44), 35(45), 36(46) 37(47)	38(48)
Rated power (MVA)	590	835	911
Rated voltage (kV)	22	20	26
$P_{max}$ (p.u)	0.9373	0.9177	0.9001
$R$ (p.u)	0.0085	0.006	0.00548
$T_1$ (s)	0.080	0.180	0.100
$T_2$ (s)	0.000	0.030	0.000
$T_3$ (s)	0.150	0.200	0.200
$T_4$ (s)	0.050	0.000	0.100
$T_5$ (s)	10.000	8.000	8.720
$F$	0.280	0.300	0.300

Table 3.7. IEEE 39-Bus modified test system exciter data.

Type	IEEET1	IEEET1	IEEET1
Default Unit no. (New Unit no.)	30(40)	31(41), 32(42), 33(43) 34(44), 35(45), 36(46) 37(47)	38(48)
Rated power (MVA)	590	835	911
Rated voltage (kV)	22	20	26
$T_r$ (s)	0.000	0.000	0.000
$K_a$ (p.u)	200	400	50
$T_a$ (s)	0.3575	0.020	0.060
$V_{Rmax}$ (p.u)	5.730	18.300	1.000
$V_{Rmin}$ (p.u)	-5.730	-18.300	-1.00
$K_e$ (p.u)	1.000	1.000	-0.0393
$T_e$ (s)	0.004	0.942	0.440
$K_f$ (p.u)	0.0529	0.030	0.070
$T_f$	1.000	1.000	1.000
$E_1$	4.2975	3.765	3.375
$SE(E_1)$	0.000	0.8147	0.0644
$E_2$	5.730	5.020	4.5
$SE(E_2)$	0.000	2.6756	0.2363

### **3.4 Research Proposed Approach and Design**

The performance of small signal stability of both the modified IEEE 9-bus and modified IEEE 39-bus system are investigated. Various research and design methods are used in this investigation. The following four cases are implemented to test the performance of the power systems in order to investigate the small signal stability performance of these two power systems.

Case 1: Load flow analysis on base model power system

Case 2: Increments of AC solar PV penetration in the power system

Case 3: Overall load variation at 5%, 10% and 15% at various AC solar PV penetration levels in the power system

Case 4: Overall reactive load variation at 5%, 10% and 15% at various AC solar PV penetration levels in the power system

In Case 1, the power systems would initially undergo a load flow analysis. Load flow analysis is done to determine if the steady-state voltage variation of the system is within the specified limits under normal operating conditions. The load flow calculations are used to analyze the power systems under steady-state conditions without any faults (short-circuit-free) conditions. All parameters and variables are assumed to be constant during the period of load flow calculation. The method used in this load flow analysis is the Newton Raphson method.

In Case 2, Figure 3.3 shows a solar PV plant that generates 50 MW would be installed at a selected bus in the power system. For this case study, unity power factor would be used. The solar PV plant will displace the active power of the synchronous generator, in increments of 50 MW until it is completely displaced. When the synchronous generator is completely displaced, its reactive component will also be displaced. The power factor and small signal stability performance of the system is expected to improve. In this case, Bus 40 is selected. Figure 3.4 shows solar PV generation of 100 MW and synchronous generator of 150 MW followed by Figure 3.5 which is 150 MW on solar PV generation

and 100 MW synchronous generation. Figure 3.6 shows solar PV generation of 200 MW and a displaced synchronous generation to 50 MW. Finally, in Figure 3.7, the synchronous generator will be completely removed and the generation on the respective bus would solely rely on solar PV generation. Similar simulations would be done on the 9-bus power system as well.

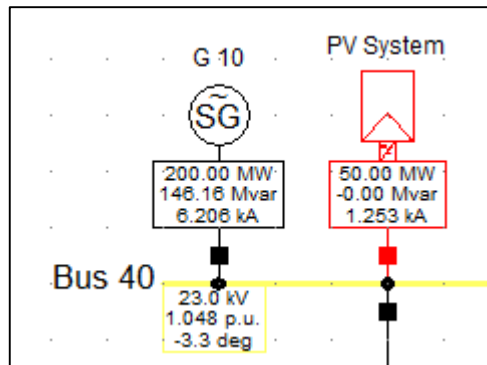


Figure 3.3. 50 MW AC Solar PV Penetration with 200 MW Synchronous Generator.

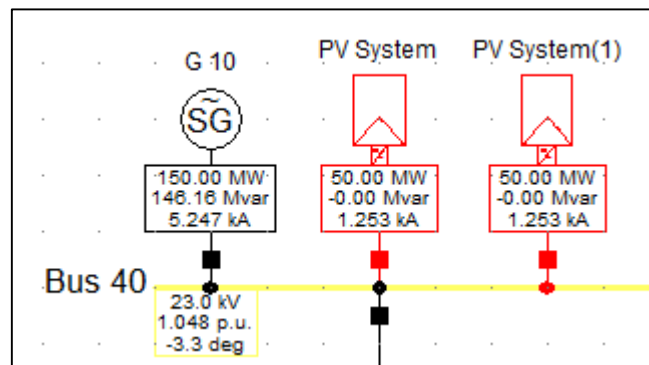


Figure 3.4. 100 MW AC Solar PV Penetration with 150 MW Synchronous Generator.

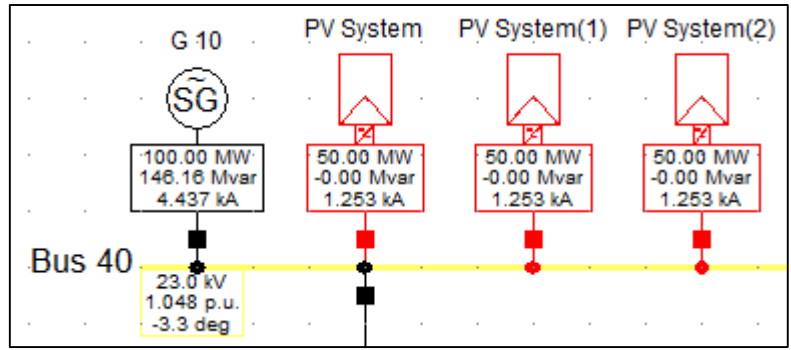


Figure 3.5. 150 MW AC Solar PV Penetration with 100 MW Synchronous Generator.

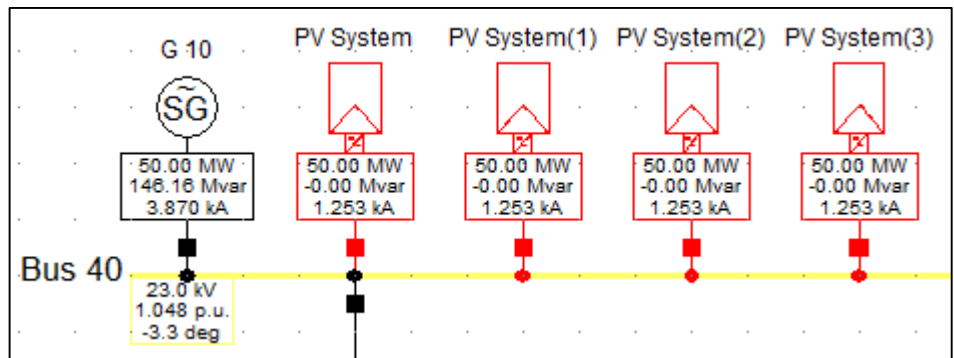


Figure 3.6. 200 M WAC Solar PV Penetration with 50 MW Synchronous Generator.

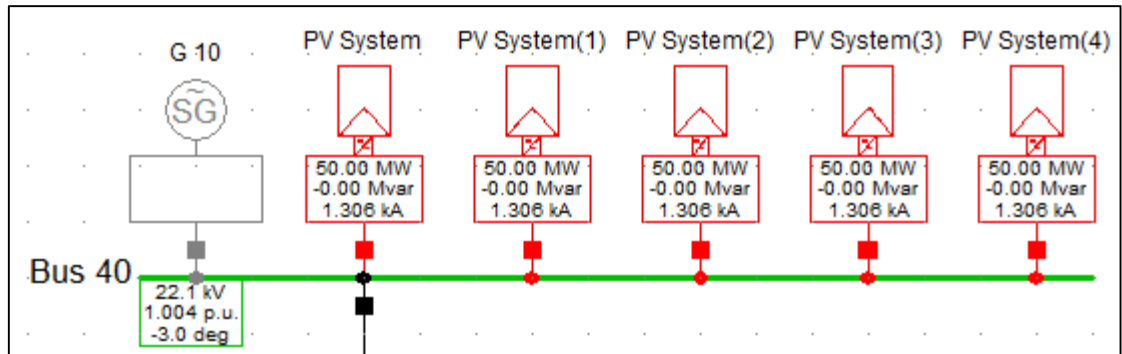


Figure 3.7. 250 MW AC Solar PV Penetration without Synchronous Generator.

Case 3 is conducted by increasing the power system's overall base load by 5%, 10% and 15% [40] simultaneously increasing the AC solar PV generation at unity power factor. The base load is varied to simulate the load changes in a typical power system due to weather conditions, demographic and economic factors using the load scaling factor function in DigSILENT PowerFactory.

Case 4 is conducted by maintaining a fixed AC solar PV penetration (displacing a synchronous generator) by increasing the base reactive load of the entire system by 5%, 10% and 15%. By increasing the reactive load, it simulates a practical situation as the amount of reactive power being drawn changes throughout the day. Unity power factor is also used in the AC solar PV generations. This investigates how an increase in reactive load affects the system's small signal stability performance.

Each case is simulated and its small signal stability performance is assessed. The modes with the lowest and highest damping ratios are taken into consideration. The two extreme scenarios are taken in order to investigate how the system reacts under different conditions. The parameters such as eigenvalue, damped frequency, damping ratio and participation factor of these modes are then analyzed.

### 3.5 Summary of Chapter

Figure 3.8 shows the flowchart of the methodology used in this research. A load flow analysis is done in Case 1. The small signal stability of Case 2, Case 3 and Case 4 would be evaluated based on the respective eigenvalues, damped frequency, damping ratio and participation factor. Results and discussions are presented in Chapter 4.

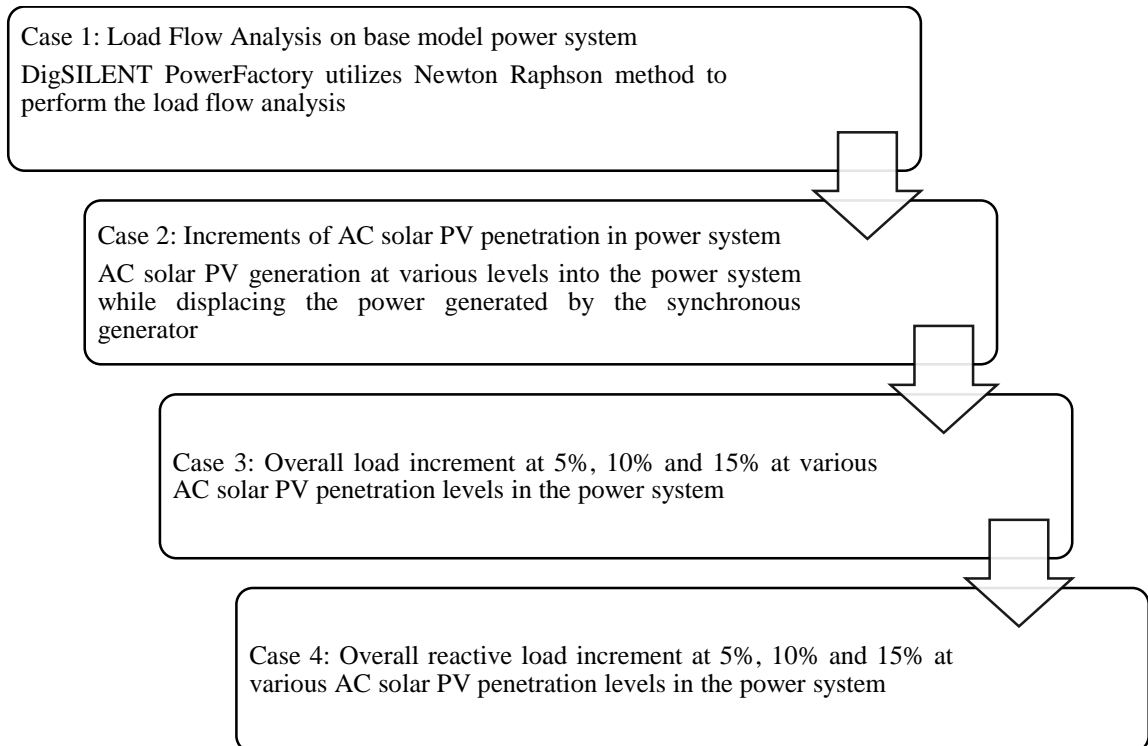


Figure 3.8. Methodology flow chart

## CHAPTER 4

### RESULTS AND DISCUSSION

#### 4.1 Introduction

The results of the study are presented and discussed with reference to the objectives of the study. The first objective is to investigate the small signal stability impacts on the grid when AC solar PV penetration is increased. Next, the impact of load variation together with AC solar PV penetration in the grid would also be discussed. Last of all, the effect of reactive load variation on the penetration of AC solar PV in the grid will be reviewed.

#### 4.2 Case 1: Base model simulation for 9-bus and 39-bus power system

In this case, a load flow is performed on both the systems and their voltage magnitudes are evaluated. The voltage magnitudes at each individual bus are analyzed based on the Malaysian Distribution Code, which states [41]:

##### *“5.4.4.1 Steady-state Voltage Variation under Normal conditions*

*Under normal conditions, when all circuit elements are in service, the voltage at all points in the Distributor’s Distribution System including the points before the Users Connection Point shall be planned to be maintained as follows:*

*a) Medium voltage of 6.6 kV, 11 kV, 22 kV, and 33 kV within  $\pm 5\%$  of nominal voltage”*

The load flow analysis for base case model should represent a system condition in which none of the branch or generator limits is exceeded.

#### 4.2.1 Load flow simulation for 9-bus power system

A load flow analysis is performed on the 9-bus system and results obtained are as shown in Figure 4.1 as a bar chart.

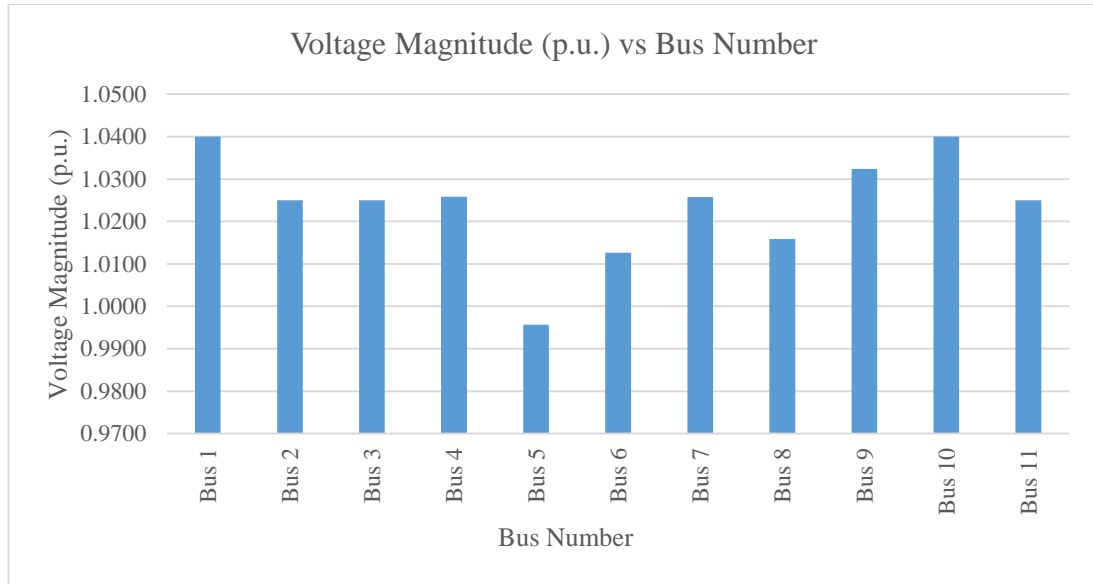


Figure 4.1. Graph of voltage in p.u. for each bus in the 9-bus power system.

Table 4.1. Voltage magnitude validation for 9-bus system. shows the voltage magnitude validation for the 9-bus system. The data shows that voltage magnitudes from Bus 1 to Bus 9 have repeatability and consistency when compared to the results from PSSE and HYPERSIM simulation softwares [42]. Apart from that, it is observed that the voltage magnitudes are within 0.95 p.u. to 1.05 p.u. limit which corresponds to the 5% limit of the Malaysia Distribution Code [41]. Bus 10 and Bus 11 are the newly added buses in this model and hence it is there is no data from PSSE and HYPERSIM models. Nevertheless, its voltage magnitude is within the respective limits.

Table 4.1. Voltage magnitude validation for 9-bus system.

Bus Name	DIGSILENT	PSSE [42]	HYPERSIM [42]
	Voltage Magnitude (p.u.)	Voltage Magnitude (p.u.)	Voltage Magnitude (p.u.)
Bus 1	1.04	1.04	1.04
Bus 2	1.03	1.03	1.03
Bus 3	1.03	1.03	1.03
Bus 4	1.03	1.03	1.03
Bus 5	1.00	1.00	1.00
Bus 6	1.01	1.01	1.01
Bus 7	1.03	1.03	1.03
Bus 8	1.02	1.02	1.02
Bus 9	1.03	1.03	1.03
Bus 10	1.04	-	-
Bus 11	1.03	-	-

Table 4.2 shows the load flow results for distribution line 1 to line 6 in comparison to the PSSE and HYPERSIM simulation softwares. As observed, the results are also repeatable and consistent when compared to the other simulation softwares. Therefore, with the results of voltage magnitudes and power flow being validated, these signify that the system's data and model are suitable to undergo small signal stability analysis.

Table 4.2. Load flow result comparison for distribution lines in 9-bus the system.

Line Number	Busbar Number	DIGSILENT		PSSE[42]		HYPERSIM [42]	
		Active Power (p.u.)	Reactive Power (p.u.)	Active Power (p.u.)	Reactive Power (p.u.)	Active Power (p.u.)	Reactive Power (p.u.)
Line 1	Bus 4 - Bus 5	0.41	0.23	0.41	0.23	0.41	0.23
Line 2	Bus 5 - Bus 7	0.84	0.11	0.84	0.11	0.84	0.11
Line 3	Bus 7 - Bus 8	0.76	0.01	0.76	0.01	0.76	0.01
Line 4	Bus 8 - Bus 9	0.24	0.24	0.24	0.24	0.24	0.24
Line 5	Bus 6 - Bus 9	0.59	0.13	0.59	0.13	0.59	0.14
Line 6	Bus 4 - Bus 6	0.31	0.01	0.31	0.01	0.31	0.01

#### 4.2.2 Load flow simulation for 39-bus power system

Figure 4.2 shows the graph of voltage deviation for each bus in the 39-bus power system.

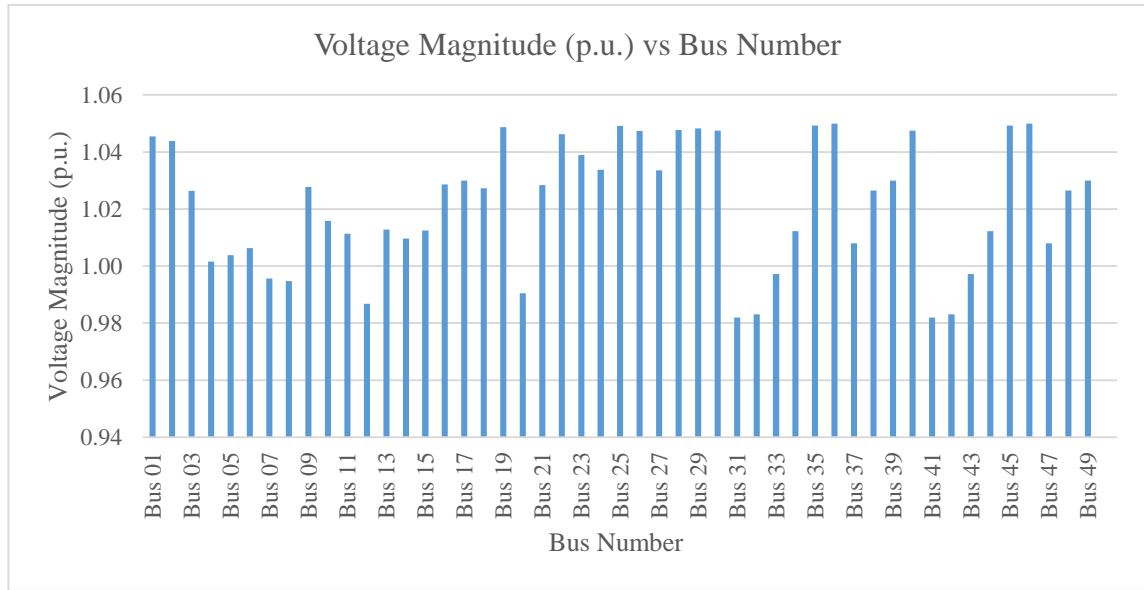


Figure 4.2. Graph of voltage deviation for each bus in the 39-bus power system.

Table 4.3 shows the voltage magnitudes and voltage deviations obtained from the load flow analysis performed on the 39-bus power system. The results show that the voltage magnitudes are all within the 0.95 p.u. to 1.05 p.u. limit during steady-state.

Table 4.3. Voltage magnitude and deviation for 39-bus system.

Bus Name	Voltage Magnitude (p.u.)	Voltage Deviation (%)	Comments
Bus 01	1.05	4.55%	Within limit
Bus 02	1.04	4.39%	Within limit
Bus 03	1.03	2.64%	Within limit
Bus 04	1.00	0.16%	Within limit
Bus 05	1.00	0.38%	Within limit
Bus 06	1.01	0.63%	Within limit
Bus 07	1.00	0.43%	Within limit
Bus 08	0.99	0.53%	Within limit
Bus 09	1.03	2.77%	Within limit

<b>Bus Name</b>	<b>Voltage Magnitude (p.u.)</b>	<b>Voltage Deviation (%)</b>	<b>Comments</b>
Bus 10	1.02	1.58%	Within limit
Bus 11	1.01	1.14%	Within limit
Bus 12	0.99	1.32%	Within limit
Bus 13	1.01	1.28%	Within limit
Bus 14	1.01	0.97%	Within limit
Bus 15	1.01	1.25%	Within limit
Bus 16	1.03	2.86%	Within limit
Bus 17	1.03	3.00%	Within limit
Bus 18	1.03	2.73%	Within limit
Bus 19	1.05	4.87%	Within limit
Bus 20	0.99	0.95%	Within limit
Bus 21	1.03	2.84%	Within limit
Bus 22	1.05	4.63%	Within limit
Bus 23	1.04	3.90%	Within limit
Bus 24	1.03	3.38%	Within limit
Bus 25	1.05	4.92%	Within limit
Bus 26	1.05	4.74%	Within limit
Bus 27	1.03	3.35%	Within limit
Bus 28	1.05	4.77%	Within limit
Bus 29	1.05	4.83%	Within limit
Bus 30	1.05	4.75%	Within limit
Bus 31	0.98	1.80%	Within limit
Bus 32	0.98	1.69%	Within limit
Bus 33	1.00	0.28%	Within limit
Bus 34	1.01	1.23%	Within limit
Bus 35	1.05	4.93%	Within limit
Bus 36	1.05	5.00%	Within limit
Bus 37	1.01	0.80%	Within limit
Bus 38	1.03	2.65%	Within limit
Bus 39	1.03	3.00%	Within limit
Bus 40	1.05	4.75%	Within limit
Bus 41	0.98	1.80%	Within limit
Bus 42	0.98	1.69%	Within limit
Bus 43	1.00	0.28%	Within limit
Bus 44	1.01	1.23%	Within limit
Bus 45	1.05	4.93%	Within limit

<b>Bus Name</b>	<b>Voltage Magnitude (p.u.)</b>	<b>Voltage Deviation (%)</b>	<b>Comments</b>
Bus 46	1.05	5.00%	Within limit
Bus 47	1.01	0.80%	Within limit
Bus 48	1.03	2.65%	Within limit
Bus 49	1.03	3.00%	Within limit

Table 4.4. Load flow result for distribution lines in 39-bus the system.shows the load flow results for each distribution line in the 39-bus system. This validates the load flow analysis for the 39-bus power system.

Table 4.4. Load flow result for distribution lines in 39-bus the system.

<b>Line Number</b>	<b>Busbar Number</b>	<b>Active Power (p.u.)</b>	<b>Reactive Power (p.u.)</b>
Line 01 - 02	Bus 01 - Bus 02	1.24	0.21
Line 01 - 39	Bus 01 - Bus 39	1.24	0.21
Line 02 - 03	Bus 02 - Bus 03	3.62	0.84
Line 02 - 25	Bus 02 - Bus 25	2.36	1.24
Line 03 - 04	Bus 03 - Bus 04	0.92	1.03
Line 03 - 18	Bus 03 - Bus 18	0.54	0.13
Line 04 - 05	Bus 04 - Bus 05	1.37	0.14
Line 04 - 14	Bus 04 - Bus 14	2.71	0.48
Line 05 - 06	Bus 05 - Bus 06	4.55	0.61
Line 05 - 08	Bus 05 - Bus 08	3.17	0.57
Line 06 - 07	Bus 06 - Bus 07	4.21	0.91
Line 06 - 11	Bus 06 - Bus 11	3.64	0.32
Line 07 - 08	Bus 07 - Bus 08	1.86	0.02
Line 08 - 09	Bus 08 - Bus 09	0.20	1.08
Line 09 - 39	Bus 09 - Bus 39	0.20	0.72
Line 10 - 11	Bus 10 - Bus 11	3.65	0.71
Line 10 - 13	Bus 10 - Bus 13	2.85	0.44
Line 13 - 14	Bus 13 - Bus 14	2.77	0.01
Line 14 - 15	Bus 14 - Bus 15	0.05	0.32
Line 15 - 16	Bus 15 - Bus 16	3.15	1.48
Line 16 - 17	Bus 16 - Bus 17	2.29	0.39
Line 16 - 19	Bus 16 - Bus 19	5.03	0.58
Line 16 - 21	Bus 16 - Bus 21	3.30	0.15

Line Number	Busbar Number	Active Power (p.u.)	Reactive Power (p.u.)
Line 16 - 24	Bus 16 - Bus 24	0.42	0.91
Line 17 - 18	Bus 17 - Bus 18	2.12	0.11
Line 17 - 27	Bus 17 - Bus 27	0.17	0.39
Line 21 - 22	Bus 21 - Bus 22	6.05	0.87
Line 22 - 23	Bus 22 - Bus 23	0.42	0.67
Line 23 - 24	Bus 23 - Bus 24	3.53	0.06
Line 25 - 26	Bus 25 - Bus 26	0.73	0.29
Line 26 - 27	Bus 26 - Bus 27	2.65	0.65
Line 26 - 28	Bus 26 - Bus 28	1.41	0.26
Line 26 - 29	Bus 26 - Bus 29	1.90	0.30
Line 28 - 29	Bus 28 - Bus 29	3.48	0.23

### 4.3 Case 2: Increments of AC solar PV penetration in the power system

In this case, small signal stability is analyzed when the penetration of AC solar PV is increased at the same time the synchronous generation is being decreased simultaneously to the point where it is completely displaced. The 9-bus and 39-bus power systems are evaluated here. In this investigation, critical oscillatory modes with the lowest and highest damping ratios are recorded and analyzed. This is to investigate how the lowest and highest damping ratios respond towards various small signal stability disturbances.

#### 4.3.1 9-bus power system for incremental penetration of AC solar PV generation

For the 9-bus power system, the results showed that the system still remains in a stable state even as the solar PV penetration is up to 163 MW. Based on the results in Table 4.5, it is observed that all eigenvalues have negative real parts. Having a negative real part indicates that the system oscillation is decaying. The damped frequencies of all the critical eigenvalues are of local mode as they are ranging between of 0.7 Hz to 3 Hz.

Table 4.5. Lowest damping ratio mode for AC solar PV penetration of 0 MW to 163 MW.

Sync. Gen. Power (MW)	PV Penetration (MW)	Eigenvalues ( $\lambda$ )	Damped Frequency (Hz)	Damping Ratio (%)
163	0	$-0.9085 \pm j7.6855$	1.2232	11.74%
113	50	$-1.0475 \pm j7.6561$	1.2185	13.56%
63	100	$-1.2205 \pm j7.6468$	1.2170	15.76%
0	163	$-1.2144 \pm j8.7654$	1.3951	13.72%

Furthermore, results show an increase in the damping ratio from 11.74% to 15.76% at solar PV penetration of 100 MW in Figure 4.3. However, the damping ratio of the system then reduces back to 13.72% when the entire synchronous generator is displaced. This shows that there is an optimum solar PV penetration value that would provide the highest damping ratio, in this case, that would be at the penetration of 100 MW.

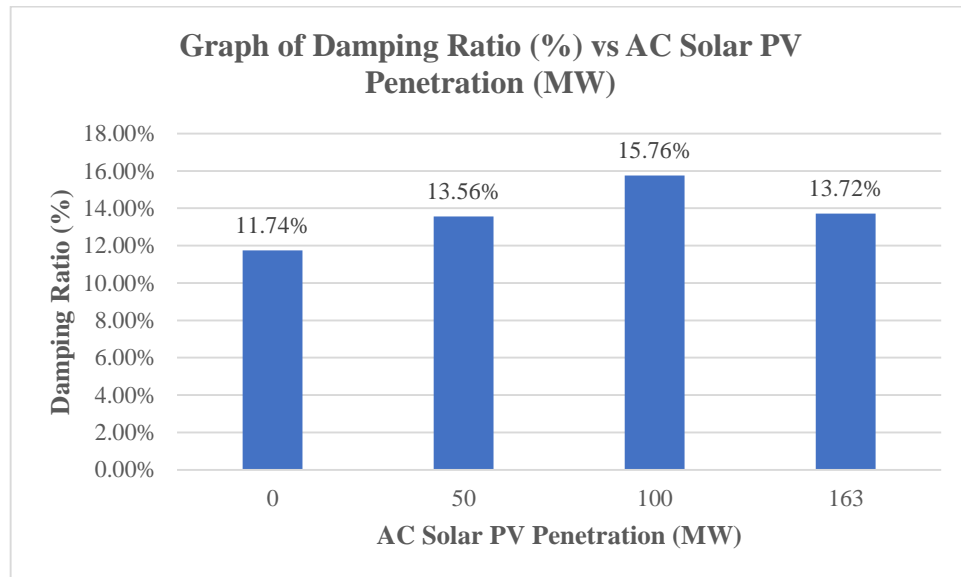


Figure 4.3. Graph of damping ratio against AC solar PV penetration for lowest damping ratio mode.

The oscillatory eigenvalues of highest damping ratio are tabulated in Table 4.6.

Table 4.6. Highest damping ratio mode for solar PV penetration of 0 MW to 163 MW.

Sync. Gen. Power (MW)	PV Penetration (MW)	Eigenvalues ( $\lambda$ )	Damped Frequency (Hz)	Damping Ratio (%)
163	0	$-4.9407 \pm j0.4202$	0.0669	99.64%
113	50	$-4.8615 \pm j0.4834$	0.0769	99.51%
63	100	$-4.7246 \pm j0.4713$	0.0750	99.51%
0	163	$-5.0592 \pm j0.3628$	0.0577	99.74%

The graph of damping ratio against AC solar PV penetration for highest damping ratio mode is shown in Figure 4.4.

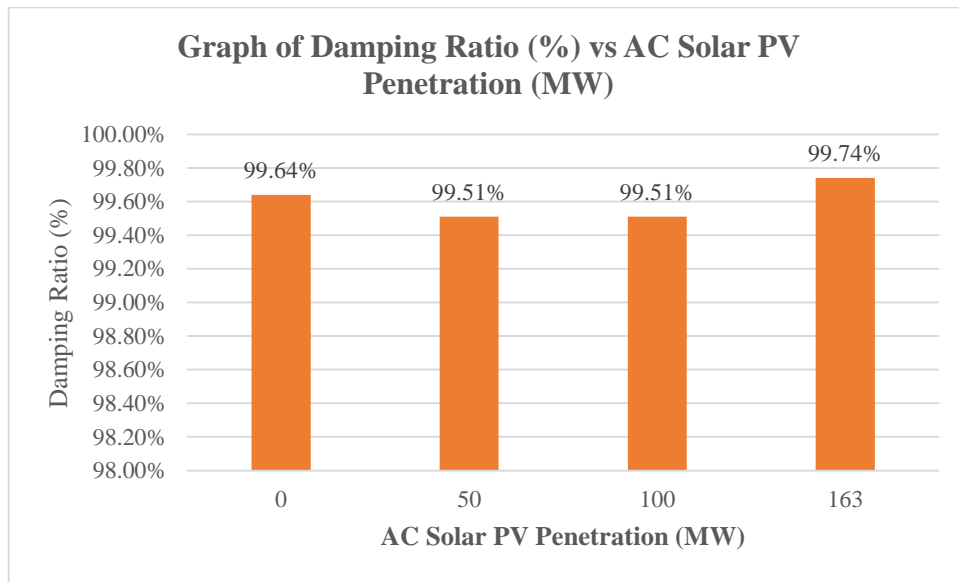


Figure 4.4. Graph of damping ratio against AC solar PV penetration for highest damping ratio mode.

Based on the results, as AC solar PV penetration increase, there is no significant changes in terms of damped frequency and damping ratio for these modes. The damping ratio remains above 99% for all levels of AC solar PV penetration, thus indicating that the system still remains in a stable state.

Figure 4.5 shows the eigenvalue plot for AC solar PV penetration of 163MW. As observed in the eigenvalue plot, all the real parts of the eigenvalue are located on the negative left side of the plane, thus this implies that the power system is in a stable condition. The participation factor bar plot for the AC solar PV penetration of 163 MW is also evaluated.

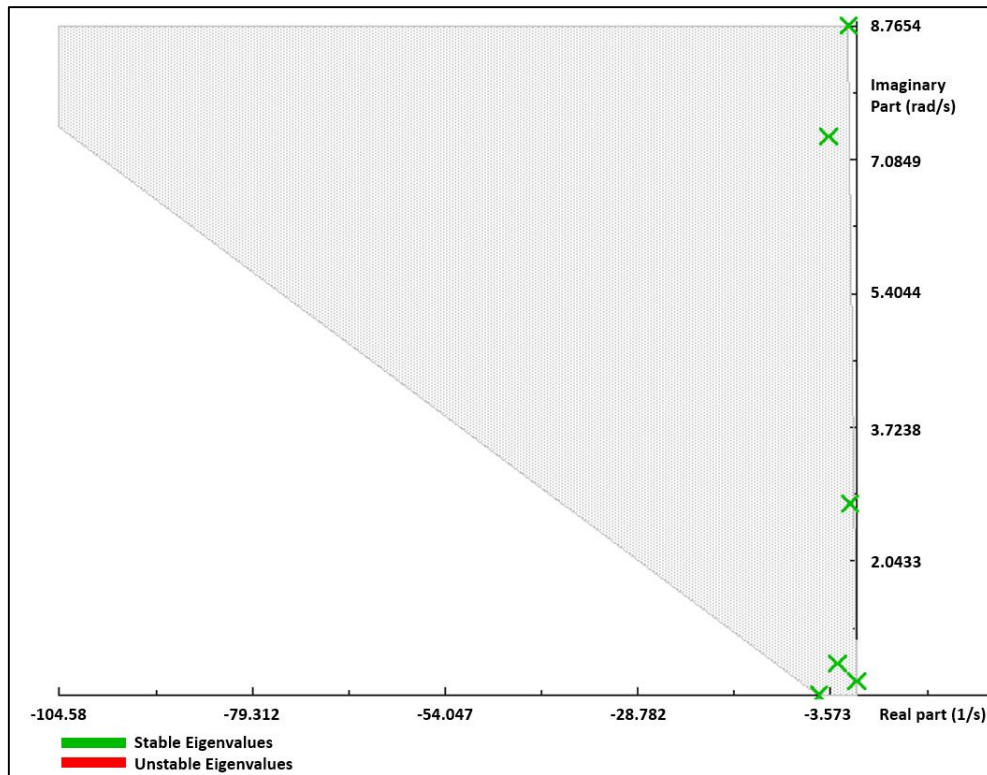


Figure 4.5. Eigenvalue plot, AC solar PV penetration of 163 MW.

The participation factor bar plot is shown in

Figure 4.6. It is observed that the state variable associated with synchronous generator 3 has the highest participation factor contribution. The participation factor is used to measure how each dynamic variable affects a given mode or eigenvalue. The state variable that corresponds the most is the speed of synchronous generator 3. Therefore, the lowest damping ratio modes in this case is contributed by a single generator of local mode oscillation. The power generation data can be referred to in Table A.1 in Appendix A.

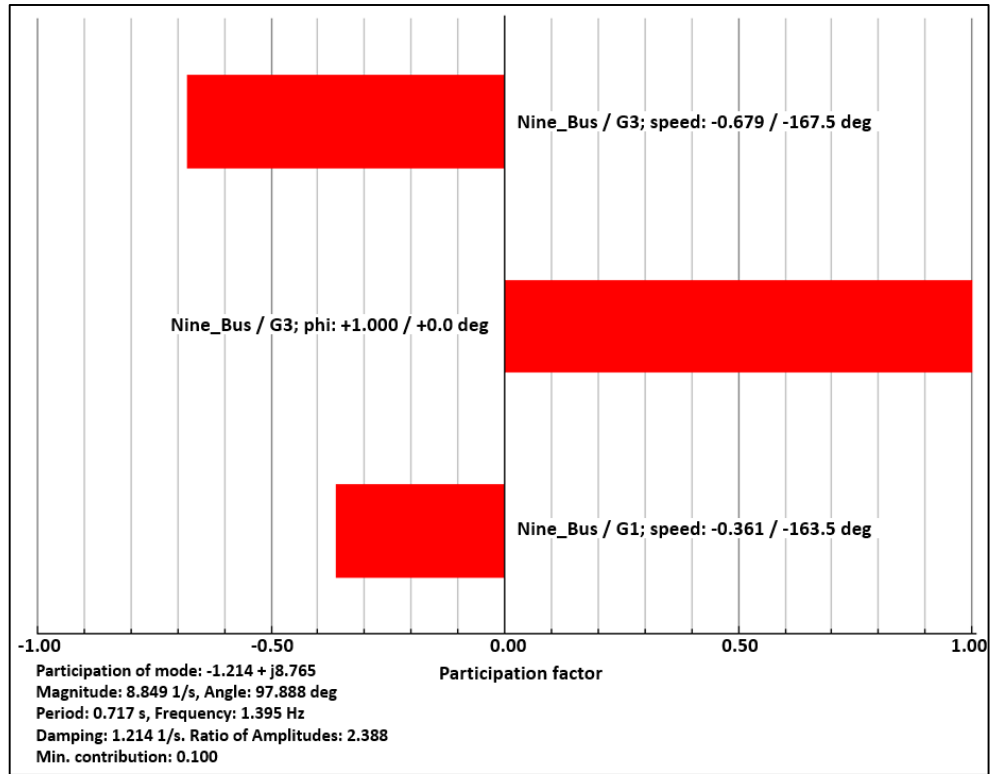


Figure 4.6. Participation factor bar plot with AC solar PV penetration of 163 MW (Positive imaginary part).

### 4.3.2 39-bus incremental penetration of AC solar PV generation

AC solar PV penetration increases from 0 MW to 250 MW at an interval of 50 MW. The data in Table 4.7 shows the lowest damping ratio eigenvalues for AC solar PV penetration.

Table 4.7. Lowest damping ratio eigenvalues for AC solar PV penetration of 0 MW to 250 MW.

Sync. Gen. Power (MW)	PV Penetration (MW)	Eigenvalues ( $\lambda$ )	Damped Frequency (Hz)	Damping Ratio (%)
250	0	$-0.3607 \pm j10.0553$	1.6003	3.59%
200	50	$-0.3744 \pm j10.0400$	1.5979	3.73%
150	100	$-0.3732 \pm j10.0400$	1.5979	3.71%
100	150	$-0.3721 \pm j10.0402$	1.5979	3.70%
50	200	$-0.3711 \pm j10.0405$	1.5980	3.69%
0	250	$-0.3884 \pm j10.0028$	1.5920	3.88%

It is observed that all real parts remain negative. This implies that the system still remains in a stable state even when AC solar PV generation is at its maximum. The damped frequency obtained for this scenario is also of local mode similarly to the 9-bus system. Figure 4.7 shows the graph of damping ratio versus AC solar PV penetration.

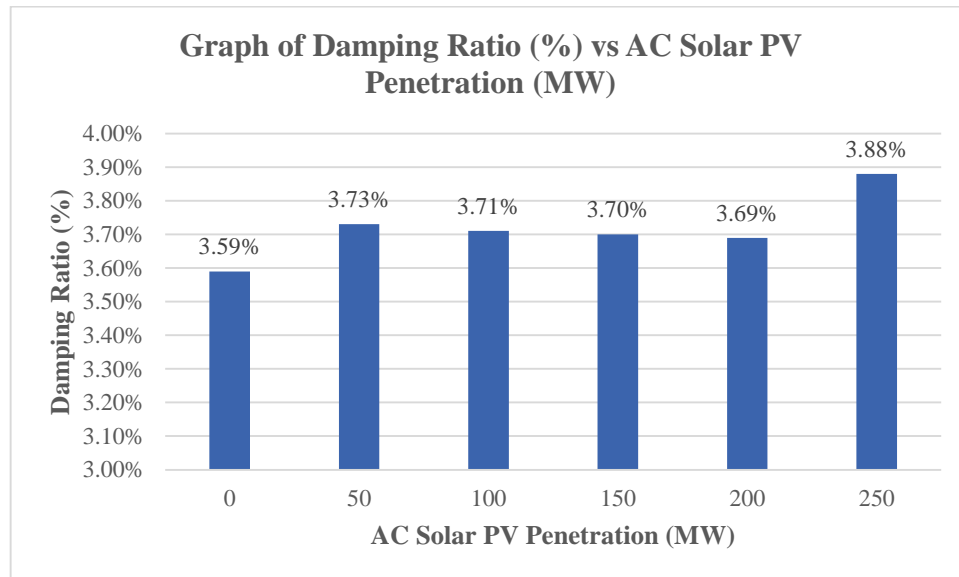


Figure 4.7. Graph of damping ratio against AC solar PV penetration for mode with lowest damping ratio

The damping ratio is observed to be increasing from 3.59% to 3.88% when the synchronous generator is completely displaced. This indicates that the system is growing more stable as there is an increase in the solar PV generation.

Table 4.8 shows the modes with highest damping ratio, which reflects that there is negligible difference in the damping ratio as AC solar PV penetration increases. The majority of damping ratio is at the 99.94% value. Apart from that, the damped frequency is seen to have an increase from 0.0763 Hz to 0.0837 Hz.

Table 4.8. Highest damping ratio eigenvalues for AC solar PV penetration of 0 MW to 250 MW.

Sync. Gen. Power (MW)	PV Penetration (MW)	Eigenvalues ( $\lambda$ )	Damped Frequency (Hz)	Damping Ratio (%)
250	0	-13.6186 ± j0.4794	0.0763	99.94%
200	50	-13.6159 ± j0.4636	0.0738	99.94%
150	100	-13.6167 ± j0.4645	0.0739	99.94%
100	150	-13.6185 ± j0.4648	0.0740	99.94%
50	200	-13.6212 ± j0.4645	0.0739	99.94%
0	250	-13.6801 ± j0.5258	0.0837	99.93%

Figure 4.8 shows the trend for modes with the highest damping ratio.

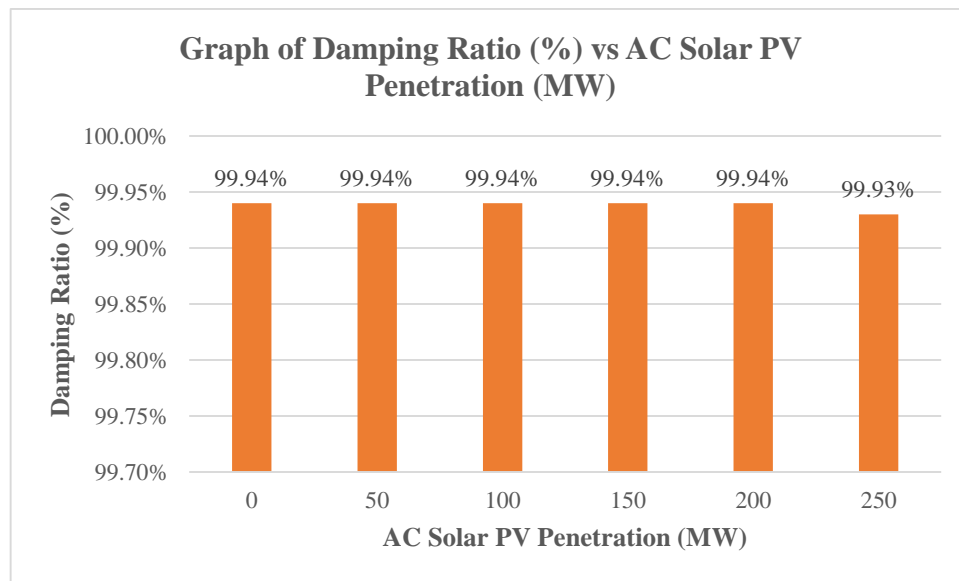


Figure 4.8. Graph of damping ratio against AC solar PV penetration for mode with highest damping ratio.

In Figure 4.9, all the eigenvalues are located on the left portion of the eigenvalue plot. Thus, indicating the system does not lose its stability when AC solar PV penetration is increased from 0 MW up to 250 MW.

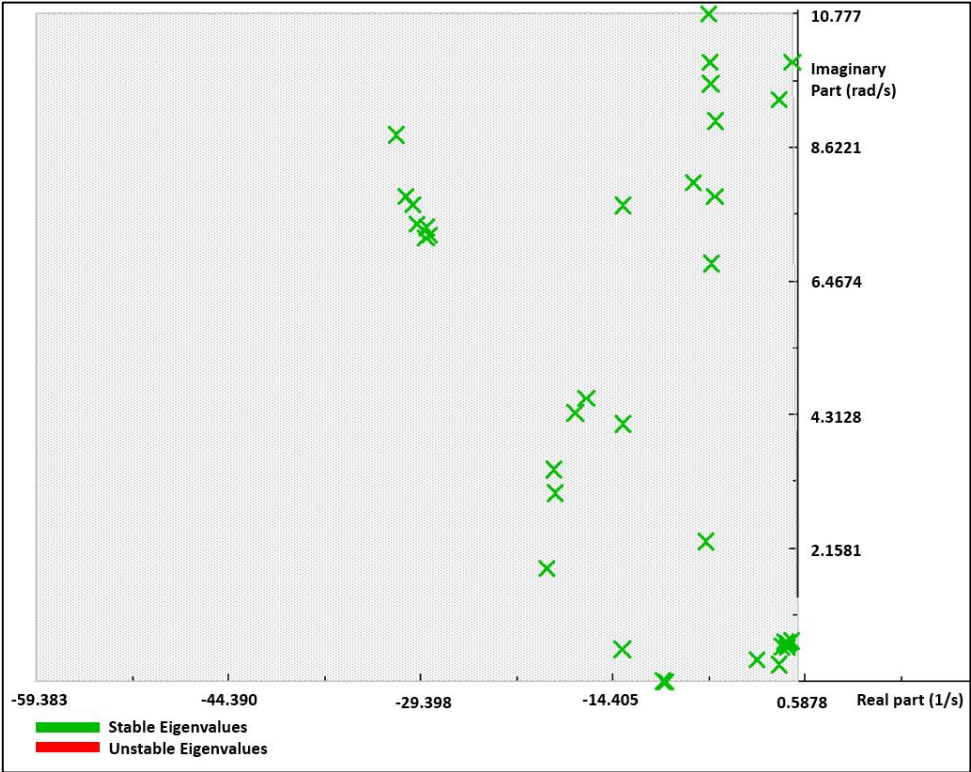


Figure 4.9. Eigenvalue plot, AC solar PV penetration of 250 MW

Figure 4.10 shows that the highest participation factor is contributed by synchronous generator 9. The speed state variable of generator 9 contributes to the lowest critical mode in this simulation.

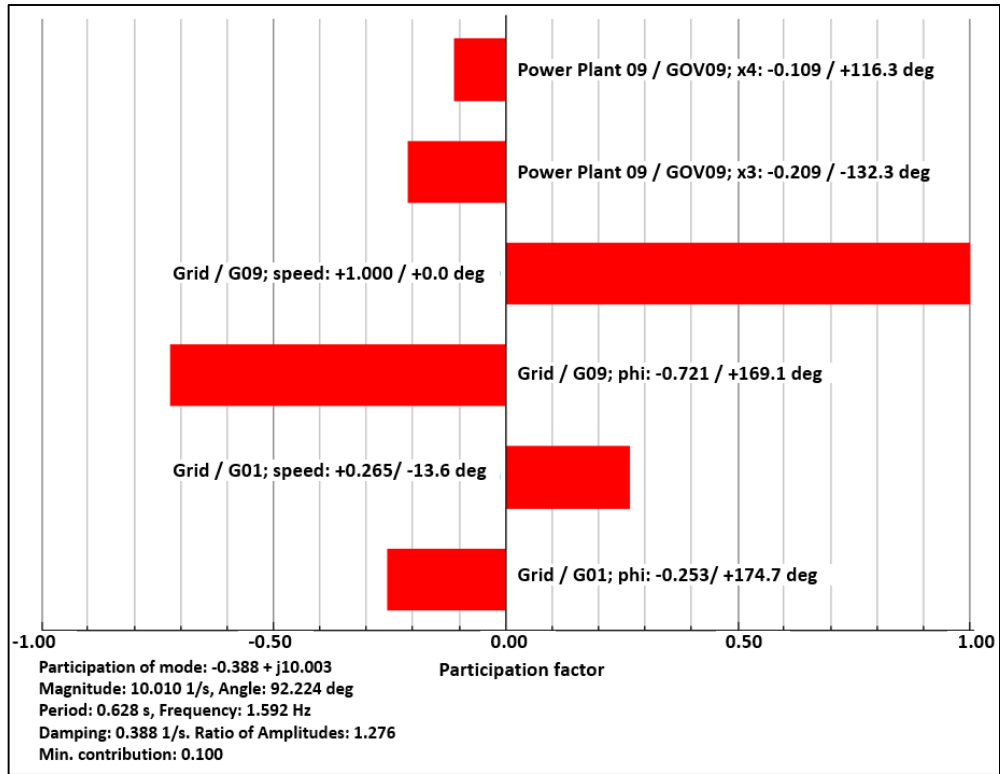


Figure 4.10. Participation factor bar plot with solar PV penetration of 250 MW (Positive imaginary part).

The power generation data for AC solar PV penetration of 0 MW to 250 MW can be found in Table B.1 in Appendix B.

#### 4.4 Case 3: Load variation simultaneously with penetration of AC solar PV generation on power system

The next investigation step is to simulate a base load increment of 5%, 10% and 15% increment in the overall power system load. The eigenvalues, damped frequency, damping ratio and participation factor are analyzed. Similar to Case 2, the lowest and highest damping ratios are taken into consideration.

#### 4.4.1 9-bus load variation with incremental penetration of AC solar PV generation

Based on Table 4.9, all eigenvalue real parts are negative, thus indicating that the power system remains in a stable state throughout the simulation of various load increments from 5% up to 15%. Furthermore, the data shows a similar trend to the simulation Case 2 for the 9-bus power system, whereby as solar PV penetration increases up to a critical penetration value of 100 MW, the damping ratio also increases and then when synchronous generator is taken out of service, the damping ratio drops slightly from 15.71% to 15.59%.

Table 4.9. Lowest damping ratio eigenvalues for various AC solar PV penetration and overall load variation.

Overall Load Variation (%)	Sync. Gen. Power (MW)	PV Penetration (MW)	Eigenvalues ( $\lambda$ )	Damped Frequency (Hz)	Damping Ratio (%)
5	163	0	$-0.9042 \pm j7.6970$	1.2250	11.67%
5	113	50	$-1.0433 \pm j7.6680$	1.2204	13.48%
5	63	100	$-1.2134 \pm j7.6594$	1.2190	15.65%
5	0	163	$-1.2205 \pm j8.7723$	1.3962	13.78%
10	163	0	$-0.8979 \pm j7.7088$	1.2269	11.57%
10	113	50	$-1.0371 \pm j7.6803$	1.2224	13.38%
10	63	100	$-1.2043 \pm j7.6725$	1.2211	15.51%
10	0	163	$-1.2239 \pm j8.7800$	1.3974	13.81%
15	163	0	$-0.8900 \pm j7.7201$	1.2287	11.45%
15	113	50	$-1.0291 \pm j7.6923$	1.2243	13.26%
15	63	100	$-1.1934 \pm j7.6854$	1.2232	15.34%
15	0	163	$-1.2249 \pm j8.7877$	1.3986	13.81%

It is observed that as the load increases from 5% to 15%, the damping ratio for AC solar PV penetration of 0 MW, 50 MW and 100 MW decreases. However, at a penetration level of 163 MW, the trend shows that the damping increases slightly from 13.79% to 13.88%. This may be due to the AC solar PV completely displacing the synchronous generator. This is illustrated in Figure 4.11.

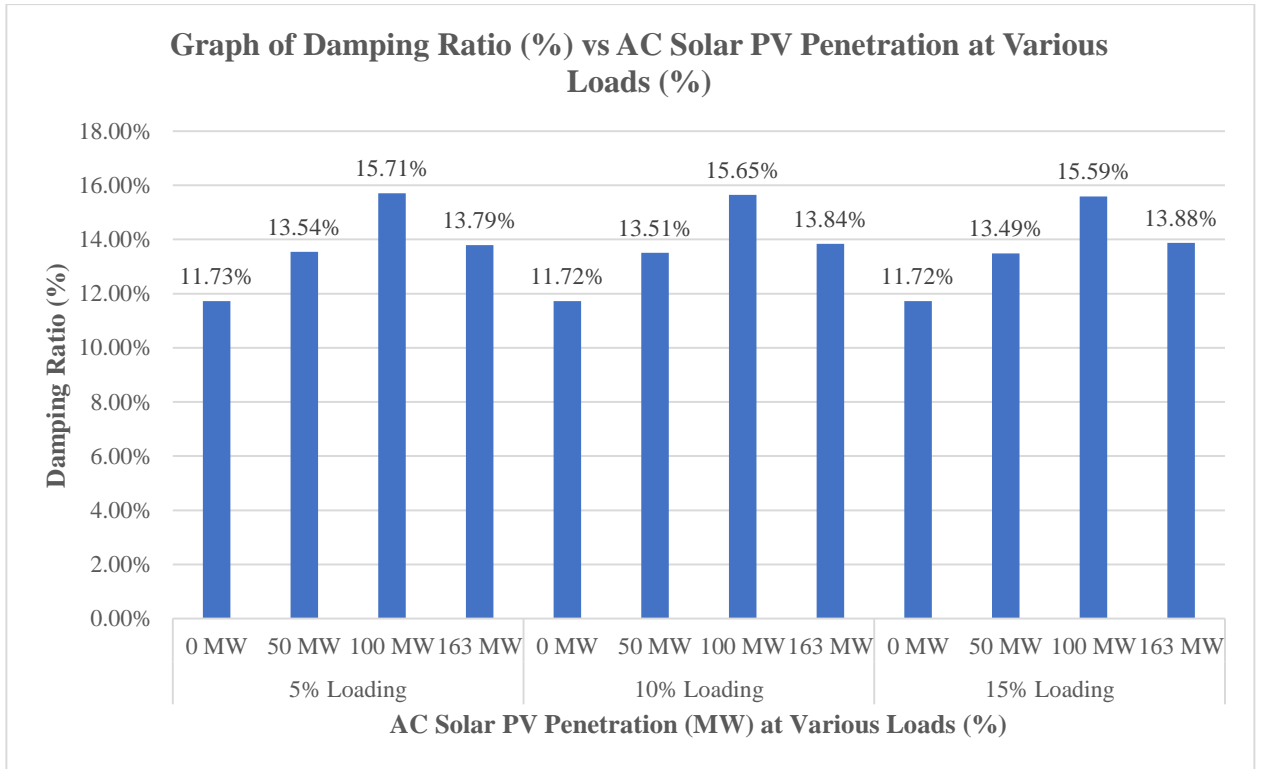


Figure 4.11. Graph of damping ratio against AC solar PV penetration at various loads for lowest damping ratio mode.

Based on the results obtained in Table 4.10, it is observed that the change in load does not affect higher oscillatory modes in the system as their values do not differ significantly from one another.

Table 4.10. Highest damping ratio eigenvalues for various AC solar PV penetration and overall load variation

Overall Load Variation (%)	Sync. Gen. Power (MW)	PV Penetration (MW)	Eigenvalues ( $\lambda$ )	Damped Frequency (Hz)	Damping Ratio (%)
5	163	0	$-4.9582 \pm j0.4243$	0.0675	99.64%
5	113	50	$-4.8776 \pm j0.4887$	0.0778	99.50%
5	63	100	$-4.7398 \pm j0.4730$	0.0753	99.51%
5	0	163	$-5.0674 \pm j0.3618$	0.0576	99.75%
10	163	0	$-4.9759 \pm j0.4256$	0.0677	99.64%

Overall Load Variation (%)	Sync. Gen. Power (MW)	PV Penetration (MW)	Eigenvalues ( $\lambda$ )	Damped Frequency (Hz)	Damping Ratio (%)
10	113	50	$-4.8940 \pm j0.4908$	0.0781	99.50%
10	63	100	$-4.7555 \pm j0.4713$	0.0750	99.51%
10	0	163	$-5.0755 \pm j0.3587$	0.0571	99.75%
15	163	0	$-4.9934 \pm j0.4240$	0.0675	99.64%
15	113	50	$-4.9102 \pm j0.4897$	0.0779	99.51%
15	63	100	$-4.7712 \pm j0.4663$	0.0742	99.53%
15	0	163	$-5.0833 \pm j0.3535$	0.0563	99.76%

The damping ratios remain above 99% for all levels of AC solar PV penetration as observed in Figure 4.12.

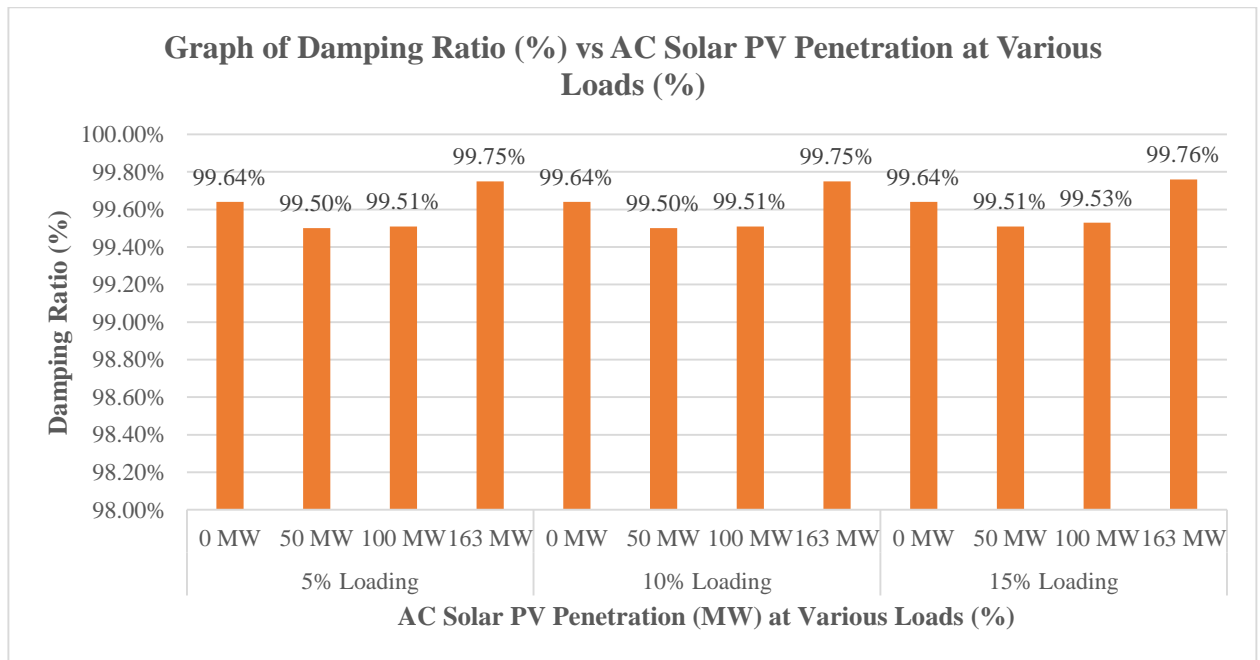


Figure 4.12. Graph of damping ratio against AC solar PV penetration at various loads for highest damping ratio mode.

Figure 4.13 depicts the eigenvalue plot for AC solar PV penetration. The eigenvalue plot shows that all eigenvalues are located on the negative side of the plane, which indicates the system's stability.

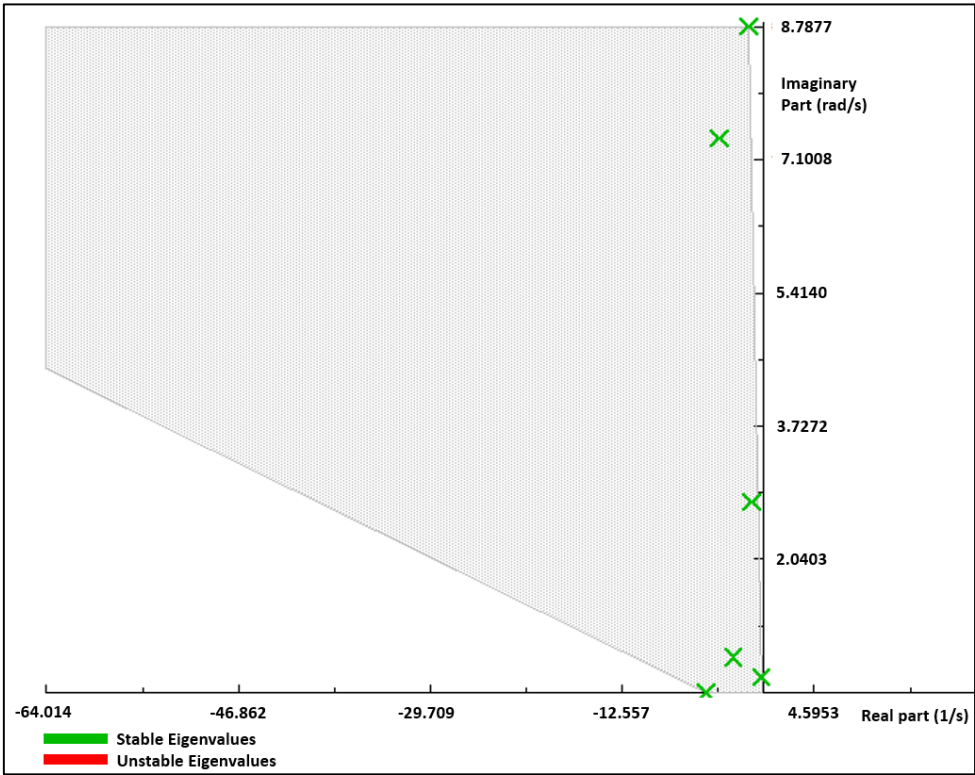


Figure 4.13. Eigenvalue plot, AC solar PV penetration of 163 MW at 15% loading.

Figure 4.14 shows the participation factor bar plot with PV penetration of 163MW at 15%. It is observed that generator 3 speed state variable has the highest contribution of participation factor.

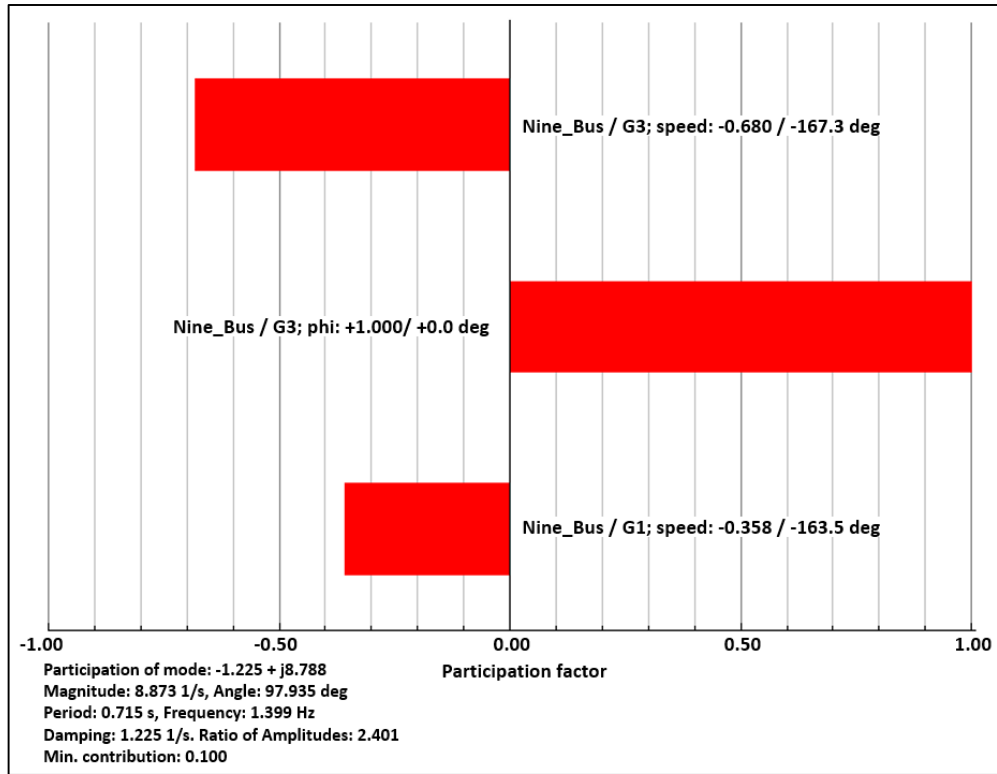


Figure 4.14. Participation factor bar plot with PV penetration of 163 MW at 15% loading (Positive imaginary part).

The 9-bus system overall load data can be referred to in Table A.2 in Appendix A. The power generation data for 5%, 10% and 15% overall load increment can be found in Table A.3, Table A.4 and Table A.5 respectively.

#### 4.4.2 39-bus load variation with incremental penetration of AC solar PV generation

The simulation is applied to the 39-bus power system for load variation. Similar loading percentages are used. The critical lowest damping ratio for critical eigenvalues is shown in Table 4.11, In all loading percentages, the real part of the eigenvalues still remains negative, thus indicating that the system has not lost its stability. There is no changes to the damped frequency in the local mode because it is between 0.7 Hz and 3 Hz.

Table 4.11. Critical lowest damping ratio for critical eigenvalues for overall load variation of 5% to 15%.

Overall Load (%)	PV Penetration (MW)	Eigenvalues ( $\lambda$ )	Damped Frequency (Hz)	Damping Ratio
5	0	$-0.3680 \pm j10.0670$	1.6022	3.65%
5	50	$-0.3659 \pm j10.0655$	1.6020	3.63%
5	100	$-0.3640 \pm j10.0642$	1.6018	3.61%
5	150	$-0.3623 \pm j10.0633$	1.6016	3.60%
5	200	$-0.3608 \pm j10.0631$	1.6016	3.58%
5	250	$-0.4007 \pm j10.0131$	1.5936	4.00%
10	0	$-0.3733 \pm j10.0792$	1.6042	3.70%
10	50	$-0.3714 \pm j10.0776$	1.6039	3.68%
10	100	$-0.3698 \pm j10.0762$	1.6037	3.67%
10	150	$-0.3684 \pm j10.0753$	1.6035	3.65%
10	200	$-0.3670 \pm j10.0751$	1.6035	3.64%
10	250	$-0.4131 \pm j10.0270$	1.5958	4.12%
15	0	$-0.3710 \pm j10.0827$	1.6047	3.68%
15	50	$-0.3694 \pm j10.0813$	1.6045	3.66%
15	100	$-0.3681 \pm j10.0802$	1.6043	3.65%
15	150	$-0.3668 \pm j10.0795$	1.6042	3.64%
15	200	$-0.3657 \pm j10.0794$	1.6042	3.63%
15	250	$-0.4081 \pm j10.0340$	1.5970	4.06%

A down trend of damping ratio is seen at PV penetrations of 0 MW to 200 MW in Figure 4.15. However, upon reaching the 250 MW penetration, the damping ratio shoots up to 4%, 4.12% and 4.06% for 5%, 10% and 15% loading respectively. An observed trend is that the overall damping ratio is peaked at the 10% loading mark.

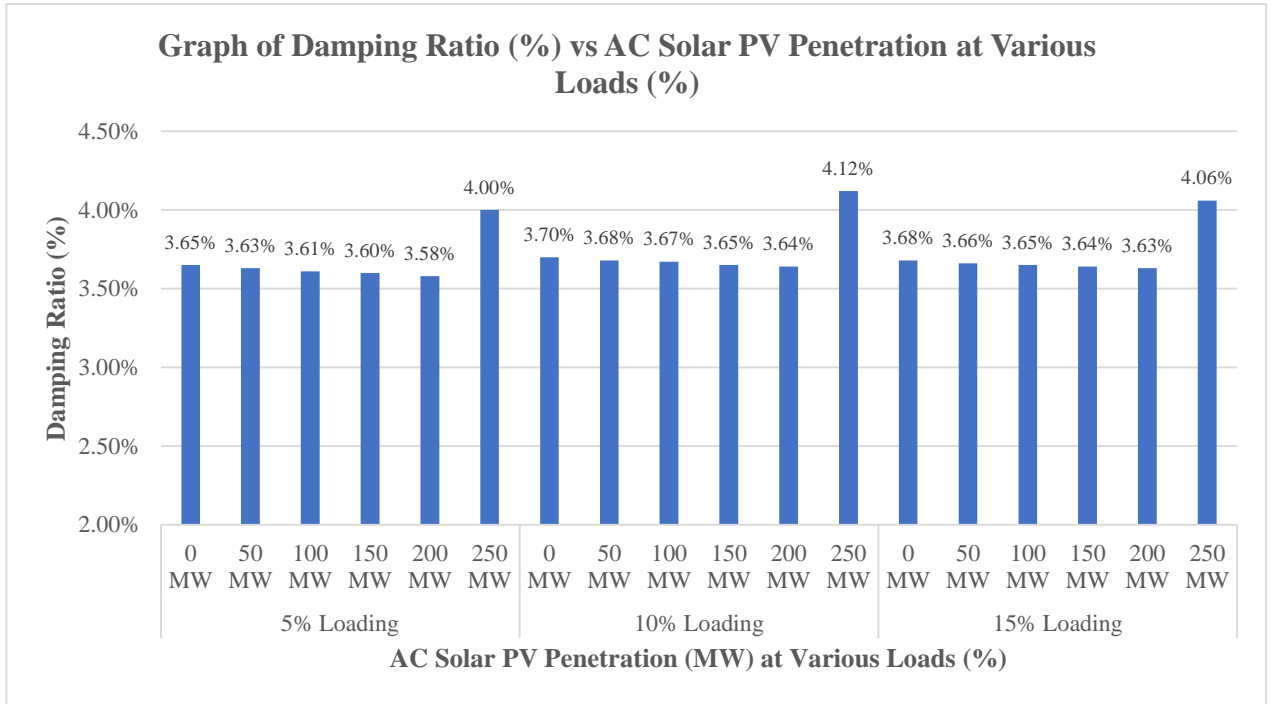


Figure 4.15. Graph of damping ratio against AC solar PV penetration at various loads critical mode with lowest damping ratio.

Table 4.12 shows the critical highest damping ratio for critical eigenvalues for overall load variation of 5% to 15%. Based on the results, all real parts of the eigenvalues are negative, thus the system's stability is maintained.

Table 4.12. Critical highest damping ratio for critical eigenvalues for overall load variation of 5% to 15%.

Overall Load (%)	Solar PV Penetration (MW)	Eigenvalues ( $\lambda$ )	Damped Frequency (Hz)	Damping Ratio
5	0	-19.5434 ± j1.8285	0.2910	99.57%
5	50	-19.5433 ± j1.8286	0.2910	99.57%
5	100	-19.5432 ± j1.8287	0.2910	99.57%
5	150	-3.1072 ± j0.2437	0.0388	99.69%
5	200	-19.5429 ± j1.8291	0.2911	99.56%
5	250	-19.5636 ± j1.6036	0.2552	99.67%
10	0	-21.5696 ± j0.8602	0.1369	99.92%
10	50	-4.0826 ± j0.0678	0.0108	99.99%
10	100	-21.5676 ± j0.8637	0.1375	99.92%
10	150	-0.8558 ± j0.0201	0.0032	99.97%
10	200	-0.8124 ± j0.0145	0.0023	99.98%
10	250	-19.5978 ± j1.2182	0.1939	99.81%
15	0	-19.6245 ± j0.7533	0.1199	99.93%
15	50	-19.6244 ± j0.7535	0.1199	99.93%
15	100	-19.6243 ± j0.7538	0.1200	99.93%
15	150	-0.3998 ± j0.0185	0.0030	99.89%
15	200	-19.6239 ± j0.7546	0.1201	99.93%
15	250	-0.3959 ± j0.0231	0.0037	99.83%

Graph of damping ratio against AC solar PV penetration at various loads critical mode with highest damping ratio is shown in Figure 4.16. The data shows that at incremental 10% and 15% loading, the damping ratio is much higher as compared to 5% loading.

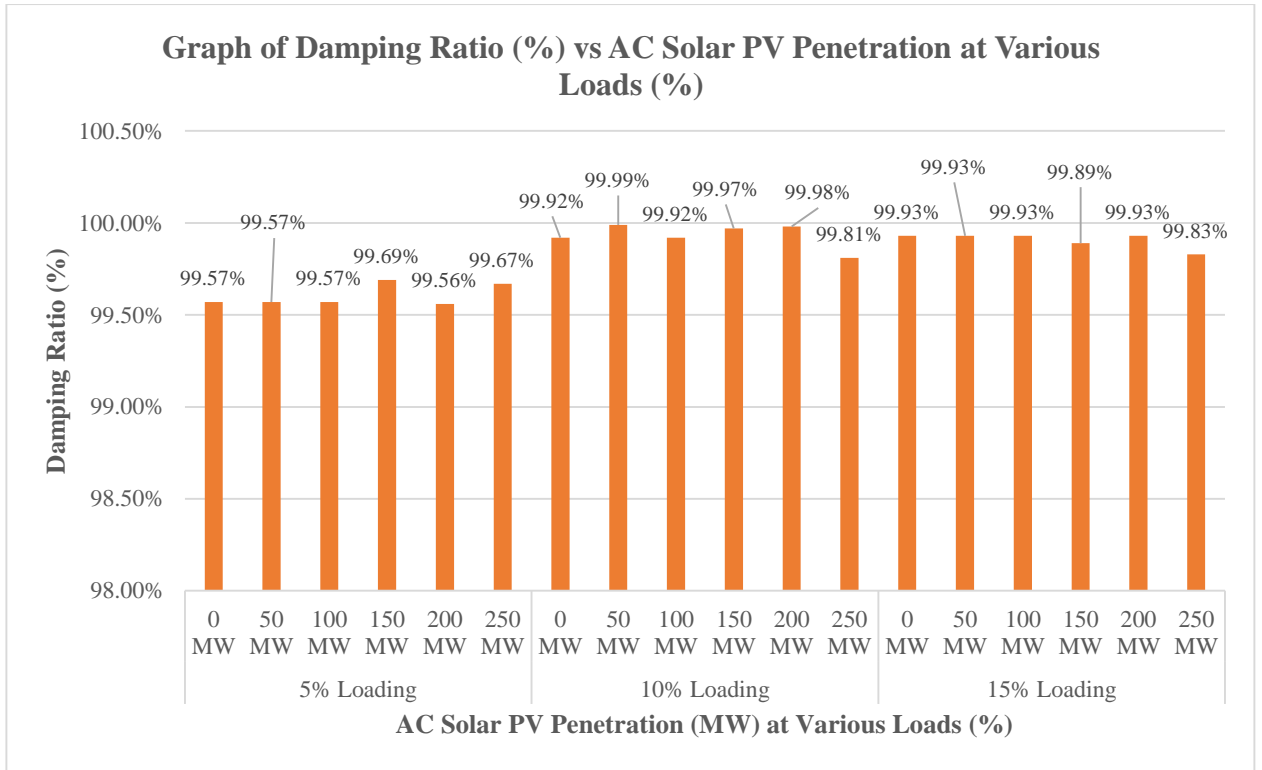


Figure 4.16. Graph of damping ratio against AC solar PV penetration at various loads critical mode with highest damping ratio.

Figure 4.17 shows that the eigenvalues plotted on the left side of the complex plane, therefore indicating that the system is stable.

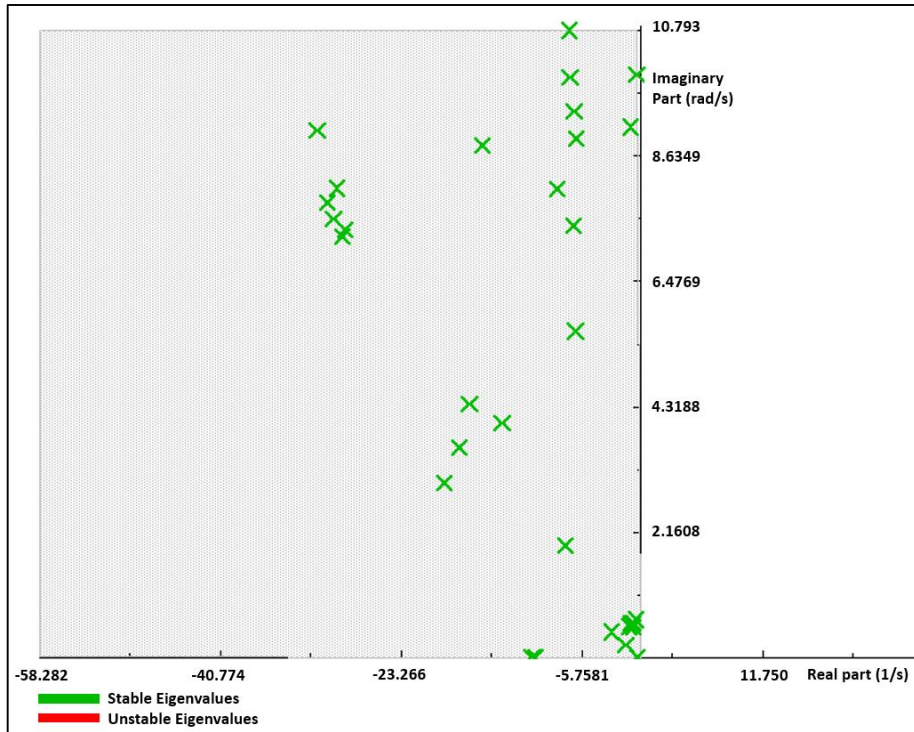


Figure 4.17. Eigenvalue plot, AC solar PV penetration of 250 MW at 15% loading.

The bar plot for participation factor in Figure 4.18 shows the lowest critical mode with lowest damping ratio at a PV penetration of 250 MW and 15% loading. The bar plot shows that the speed state variable of synchronous generator 9 still contributes to the damping ratio of this critical mode.

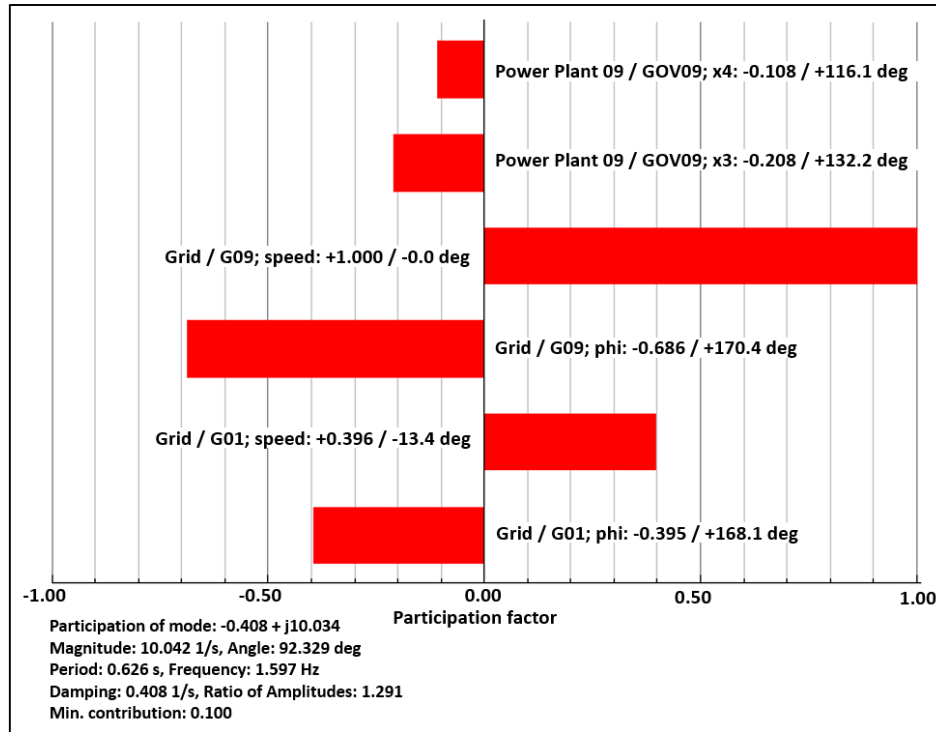


Figure 4.18. Participation factor bar plot with PV penetration of 250 MW at 15% loading (Positive imaginary part).

The 39-bus system overall load data can be referred to in Table B.2 in Appendix B. The power generation data for 5%, 10% and 15% overall load increment can be found in Table B.3, Table B.4 and Table B.5 respectively.

#### 4.5 Case 4: Incremental penetration of AC solar PV generation with various reactive load percentages

In this study, the overall reactive load of the power system is varied from 5% up to 15% increments and the small signal stability performance of the system is studied. This is similar to Case 3, but instead the overall reactive load of the power system is varied.

#### 4.5.1 Reactive load variation for various AC solar PV penetration values for the 9-bus power system

Based on the results obtained in Table 4.13, the power system is in a stable state as the reactive load is increased from its base load up to 15%. This is because the eigenvalue real part remains negative in nature. The damped frequency of the critical mode is between 0.7 Hz to 3 Hz, which indicates that it is of local mode.

Table 4.13. Lowest damping ratio eigenvalues for various AC solar PV penetration and reactive load variation.

Overall Reactive Load Variation (%)	Sync. Gen. Power (MW)	PV Penetration (MW)	Eigenvalues ( $\lambda$ )	Damped Frequency (Hz)	Damping Ratio (%)
5	163	0	$-0.9074 \pm j7.6811$	1.2225	11.73%
5	113	50	$-1.0454 \pm j7.6522$	1.2179	13.54%
5	63	100	$-1.2154 \pm j7.6431$	1.2164	15.71%
5	0	163	$-1.2190 \pm j8.7588$	1.3940	13.79%
10	163	0	$-0.9062 \pm j7.6766$	1.2218	11.72%
10	113	50	$-1.0432 \pm j7.6483$	1.2173	13.51%
10	63	100	$-1.2103 \pm j7.6393$	1.2158	15.65%
10	0	163	$-1.2229 \pm j8.7521$	1.3929	13.84%
15	163	0	$-0.9050 \pm j7.6721$	1.2211	11.72%
15	113	50	$-1.0409 \pm j7.6444$	1.2166	13.49%
15	63	100	$-1.2052 \pm j7.6355$	1.2152	15.59%
15	0	163	$-1.2260 \pm j8.7455$	1.3919	13.88%

Similar to Cases 2 and 3, as solar PV penetration increases, it is seen in Figure 4.19 that the damping ratio increases to a critical penetration at 100 MW. As the reactive load increases, the damping ratio experiences a decrease for solar PV penetrations of 0 MW, 50 MW and 100 MW. However, it is noted that at full displacement of the synchronous generator, the damping ratio is observed to increase from 13.79% to 13.88% when reactive load increases. This corresponds similarly to Case 3 for the 9-bus power system. Nevertheless, the eigenvalues are on the negative portion of the complex plane, thus the system still remains stable.

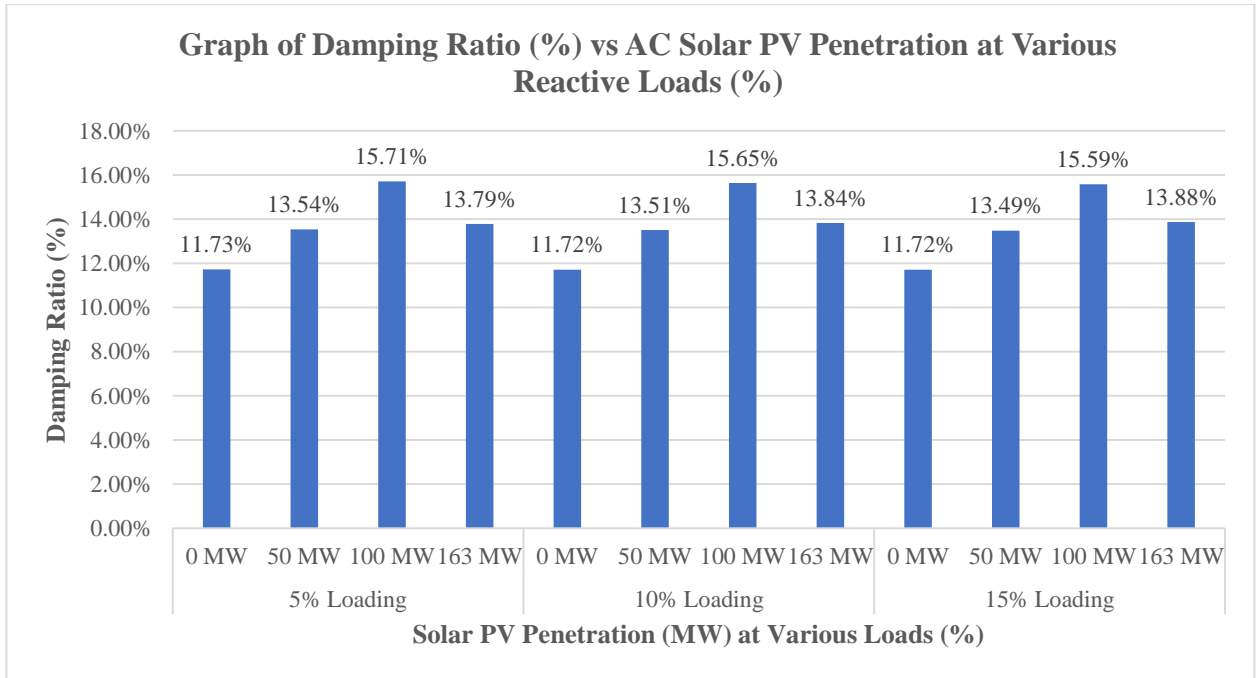


Figure 4.19. Graph of damping ratio against AC solar PV penetration at various reactive loads for lowest damping ratio mode.

The overall damping ratio for highest oscillatory modes does not have any significant changes as the loading increases. Table 4.14 shows the data obtained and trend of the damping ratio against load.

Table 4.14. Highest damping ratio eigenvalues for various AC solar PV penetration and reactive load variation.

Overall Reactive Load Variation (%)	Sync. Gen. Power (MW)	PV Penetration (MW)	Eigenvalues ( $\lambda$ )	Damped Frequency (Hz)	Damping Ratio (%)
5	163	0	$-4.9428 \pm j0.4206$	0.0669	99.64%
5	113	50	$-4.8629 \pm j0.4846$	0.0771	99.51%
5	63	100	$-4.7265 \pm j0.4726$	0.0752	99.50%
5	0	163	$-5.0602 \pm j0.3615$	0.0575	99.75%
10	163	0	$-4.9449 \pm j0.4211$	0.0670	99.64%
10	113	50	$-4.8643 \pm j0.4857$	0.0773	99.51%
10	63	100	$-4.7285 \pm j0.4739$	0.0754	99.50%
10	0	163	$-5.0612 \pm j0.3602$	0.0573	99.75%

Overall Reactive Load Variation (%)	Sync. Gen. Power (MW)	PV Penetration (MW)	Eigenvalues ( $\lambda$ )	Damped Frequency (Hz)	Damping Ratio (%)
15	163	0	$-4.9470 \pm j0.4215$	0.0671	99.64%
15	113	50	$-4.8658 \pm j0.4868$	0.0775	99.50%
15	63	100	$-4.7305 \pm j0.4752$	0.0756	99.50%
15	0	163	$-5.0621 \pm j0.3590$	0.0571	99.75%

Figure 4.20. Graph of damping ratio against AC solar PV penetration at various reactive loads for highest damping ratio mode. Figure 4.17 show the data obtained and trend of the damping ratio against load. The damping ratio values remain greater than 99%.

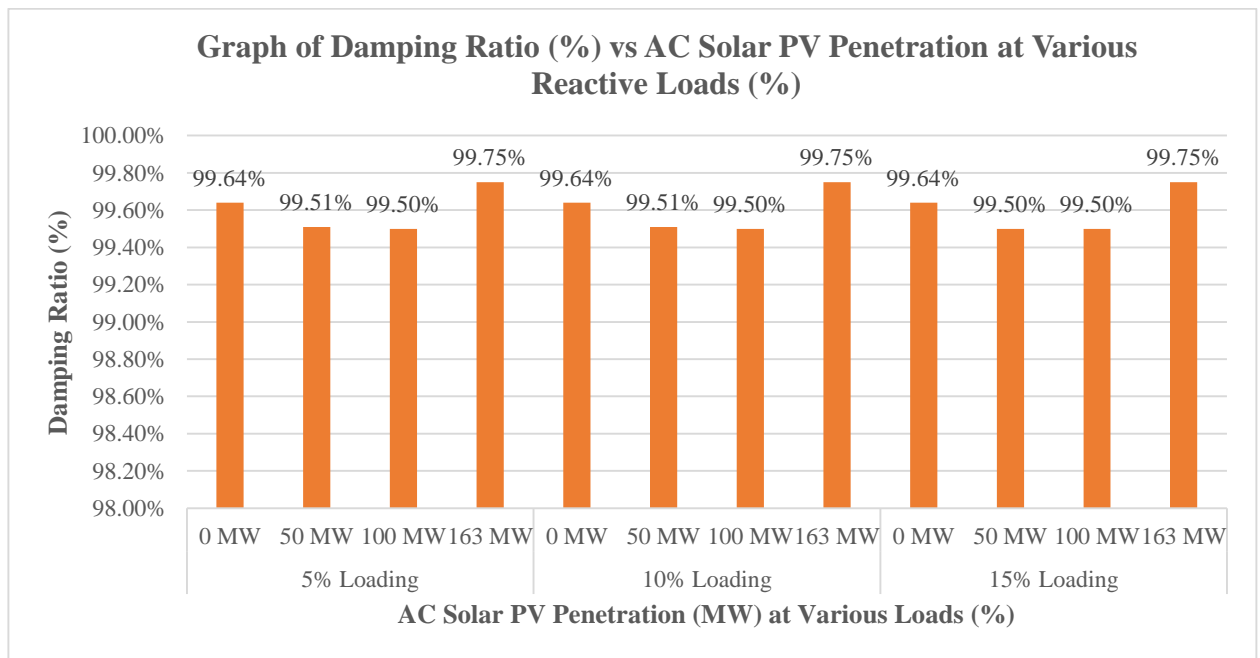


Figure 4.20. Graph of damping ratio against AC solar PV penetration at various reactive loads for highest damping ratio mode.

Based on Figure 4.21, the data shows that eigenvalues are on the negative side of the plot. This means that there are no unstable oscillatory modes in this power system.

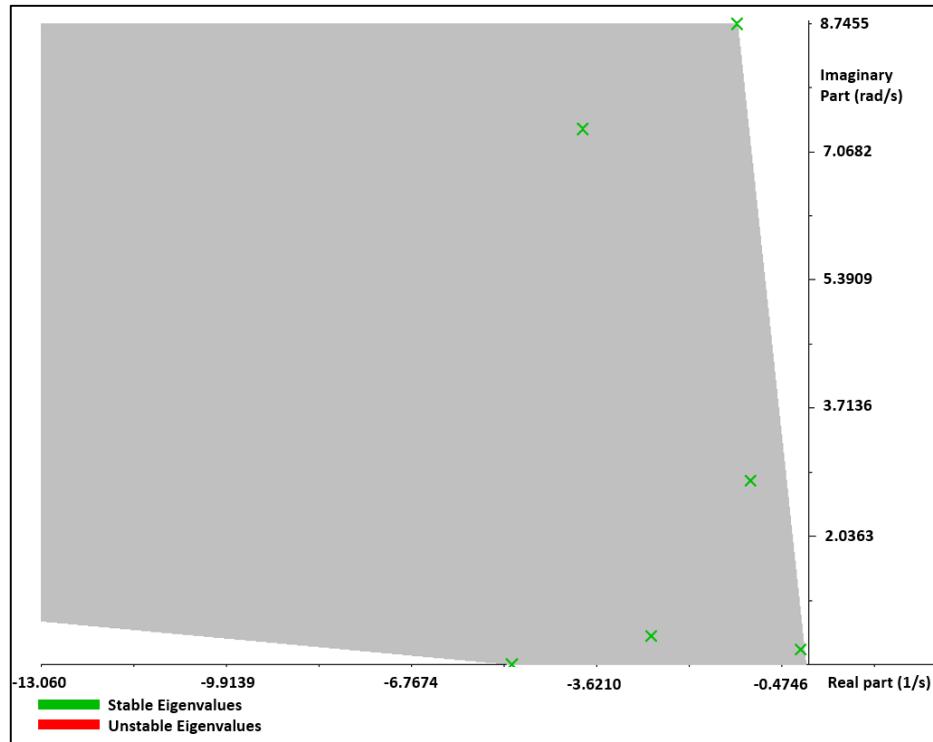


Figure 4.21. Eigenvalue plot, AC solar PV penetration of 163 MW at 15% reactive loading.

Additionally, the bar plot in Figure 4.22 shows that the speed state variable of synchronous generator 3 still contributes the highest to overall participation factor of the system.

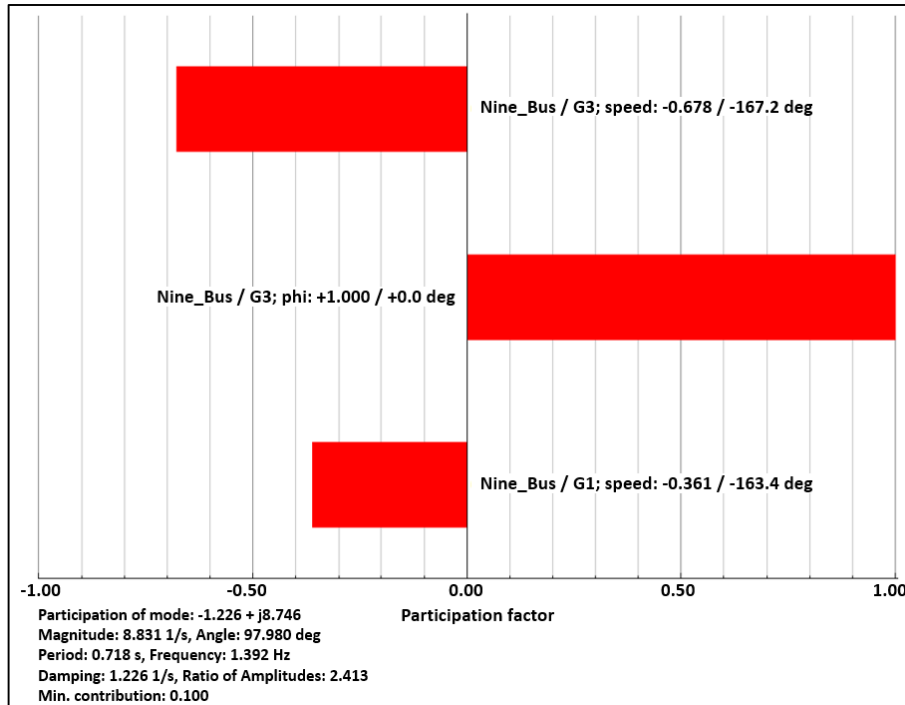


Figure 4.22. Participation factor bar plot with PV penetration of 163 MW at 15% reactive loading (Positive imaginary part).

The 9-bus system reactive load data can be referred to in Table A.6 in Appendix A. The power generation data for 5%, 10% and 15% reactive load increment can be found in Table A.7, Table A.8 and Table A.9 respectively.

#### 4.5.2 Reactive load variation for various AC solar PV penetration values for the 39-bus power system

The 39-bus power system is then used to be simulated at various reactive loads of 5% up to 15%. Table 4.15 shows the results obtained from the modal analysis. All real parts are negative in nature, thus indicating that the power system is in a stable state. Damped frequency is in the range of local mode because it is between 0.7 Hz to 3 Hz.

Table 4.15. Lowest damping ratio eigenvalues for various AC solar PV penetration and reactive load variation.

<b>Overall Reactive Load Variation (%)</b>	<b>Sync. Gen. Power (MW)</b>	<b>PV Penetration (MW)</b>	<b>Eigenvalues (<math>\lambda</math>)</b>	<b>Damped Frequency (Hz)</b>	<b>Damping Ratio (%)</b>
5	250	0	$-0.3779 \pm j10.0360$	1.5973	3.76%
5	200	50	$-0.3767 \pm j10.0359$	1.5973	3.75%
5	150	100	$-0.3756 \pm j10.0360$	1.5973	3.74%
5	100	150	$-0.3745 \pm j10.0361$	1.5973	3.73%
5	50	200	$-0.3734 \pm j10.0365$	1.5974	3.72%
5	0	250	$-0.3909 \pm j9.9975$	1.5911	3.91%
10	250	0	$-0.3802 \pm j10.0319$	1.5966	3.79%
10	200	50	$-0.3790 \pm j10.0318$	1.5966	3.78%
10	150	100	$-0.3779 \pm j10.0319$	1.5966	3.76%
10	100	150	$-0.3768 \pm j10.0321$	1.5967	3.75%
10	50	200	$-0.3757 \pm j10.0324$	1.5967	3.74%
10	0	250	$-0.3933 \pm j9.9921$	1.5903	3.93%
15	250	0	$-0.3824 \pm j10.0278$	1.5960	3.81%
15	200	50	$-0.3812 \pm j10.0277$	1.5960	3.80%
15	150	100	$-0.3801 \pm j10.0278$	1.5960	3.79%
15	100	150	$-0.3790 \pm j10.0280$	1.5960	3.78%
15	50	200	$-0.3780 \pm j10.0283$	1.5961	3.77%
15	0	250	$-0.3957 \pm j9.9867$	1.5894	3.96%

Based on the graph in Figure 4.23, the trend of the damping ratio is similar to the results obtained in Case 3 for the 39-bus system as well. The damping ratio displays an uptrend whereby it increases to 3.91%, 3.93% and 3.96% at 5%, 10% and 15% reactive loading respectively. Besides that, the data shows that as the reactive load increases, the damping ratio also increases. Take for example, at 200 MW solar PV penetration, the damping ratio changes from 3.72% to 3.77% when reactive load is increased from 5% to 15%. This trend is detected throughout all the various PV generation values.

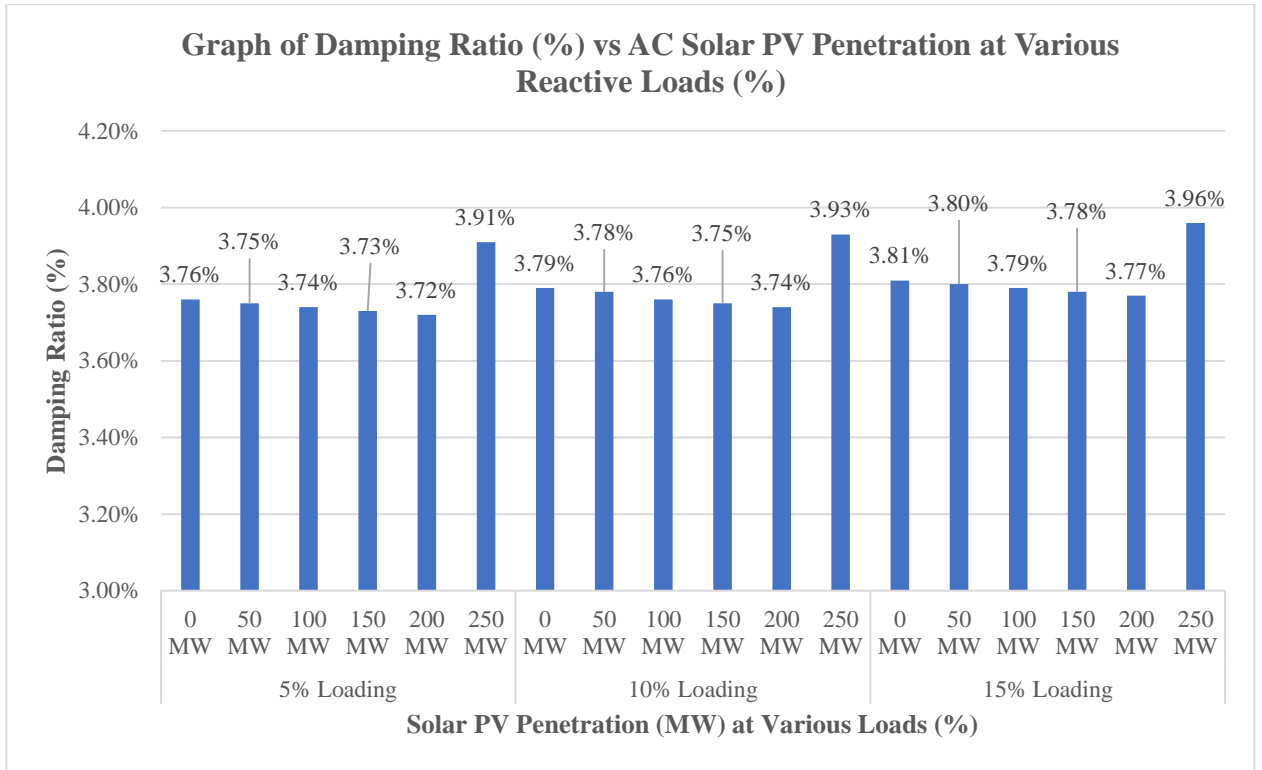


Figure 4.23. Graph of damping ratio against AC solar PV penetration at various reactive loads for critical mode with lowest damping ratio.

The highest damping ratio eigenvalue trends are displayed in Table 4.16. Based on the data shown, there is no significant change in the values obtained when the reactive load is increased from 5% up to 15% loading as the damping ratios are all above 99%.

Table 4.16. Highest damping ratio eigenvalues for various AC solar PV penetration and reactive load variation.

Overall Reactive Load Variation (%)	Sync. Gen. Power (MW)	PV Penetration (MW)	Eigenvalues ( $\lambda$ )	Damped Frequency (Hz)	Damping Ratio (%)
5	250	0	$-13.6553 \pm j0.4344$	0.0691	99.95%
5	200	50	$-13.6549 \pm j0.4361$	0.0694	99.95%
5	150	100	$-13.6556 \pm j0.4370$	0.0696	99.95%
5	100	150	$-13.6574 \pm j0.4371$	0.0696	99.95%
5	50	200	$-0.8165 \pm j0.0200$	0.0032	99.97%
5	0	250	$-13.7143 \pm j0.5009$	0.0797	99.93%
10	250	0	$-13.6931 \pm j0.4015$	0.0639	99.96%
10	200	50	$-13.6927 \pm j0.4033$	0.0642	99.96%
10	150	100	$-13.6935 \pm j0.4042$	0.0643	99.96%
10	100	150	$-13.6952 \pm j0.4042$	0.0643	99.96%
10	50	200	$-0.8152 \pm j0.0174$	0.0028	99.98%
10	0	250	$-13.7474 \pm j0.4723$	0.0752	99.94%
15	250	0	$-13.7297 \pm j0.3622$	0.0577	99.97%
15	200	50	$-13.7294 \pm j0.3642$	0.0580	99.96%
15	150	100	$-13.7301 \pm j0.3651$	0.0581	99.96%
15	100	150	$-13.7318 \pm j0.3649$	0.0581	99.96%
15	50	200	$-0.8140 \pm j0.0143$	0.0023	99.98%
15	0	250	$-13.7796 \pm j0.4395$	0.0700	99.95%

Figure 4.24 shows the graph of damping ratio against AC solar PV penetration at various reactive loads for critical mode with highest damping ratio. It is observed that damping ratio remains above 99% for all levels of loading and AC solar PV penetration.

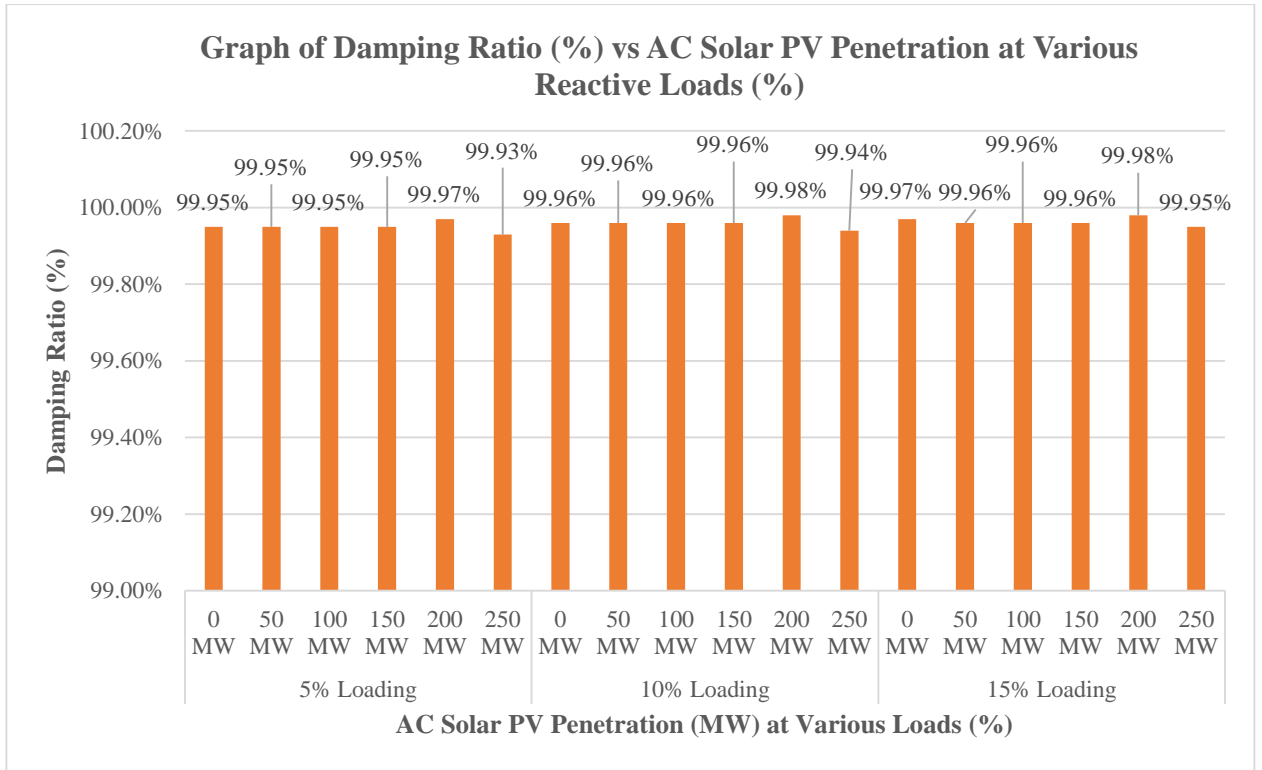


Figure 4.24. Graph of damping ratio against AC solar PV penetration at various reactive loads for critical mode with highest damping ratio.

Figure 4.25 shows the eigenvalues are on the left side of the complete plane. All real parts of the eigenvalue are on the negative left side of the complex plane, thus indicating it is in a stable state.

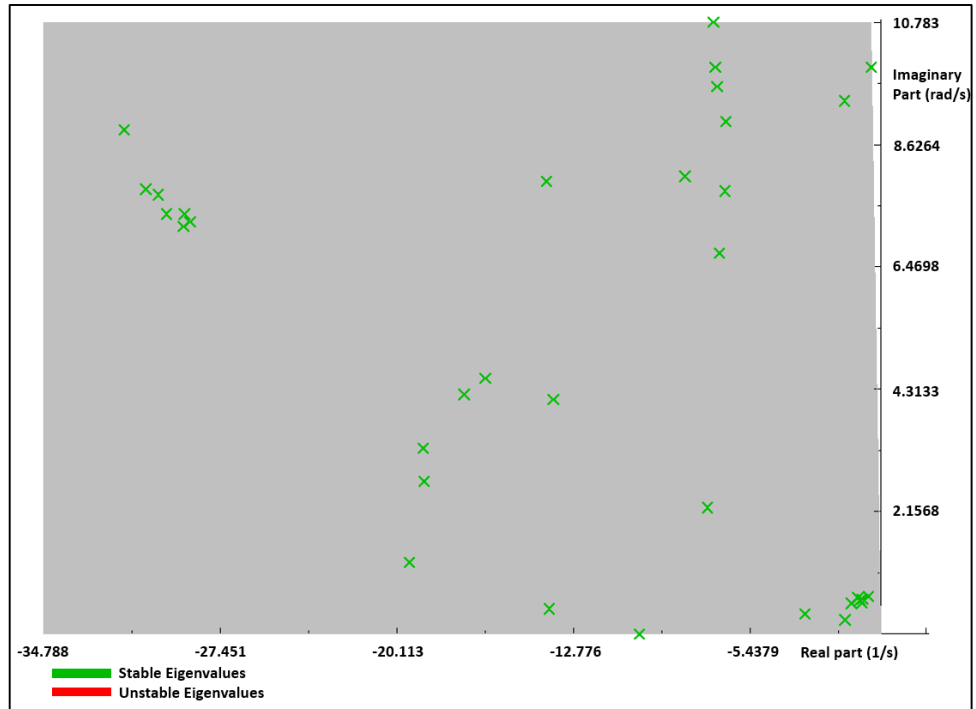


Figure 4.25. Eigenvalue plot, AC solar PV penetration of 250 MW at 15% reactive loading.

Figure 4.26 shows the participation factor bar plot for penetration of 250 MW at 15% reactive loading for the critical mode with lowest damping ratio. The bar plot shows that generator 9 still contributes the most in its speed variable state.

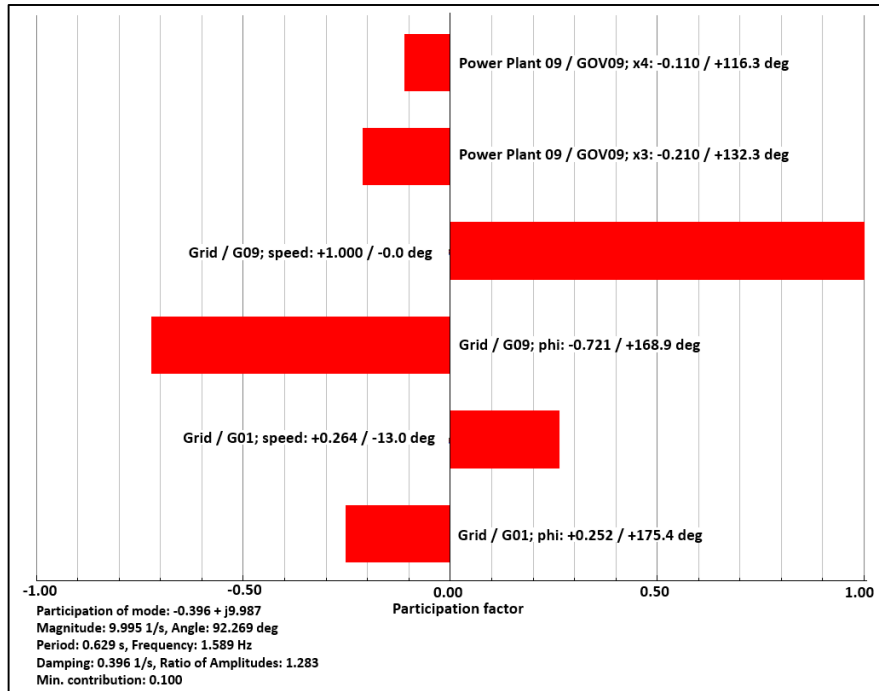


Figure 4.26. Participation factor bar plot with PV penetration of 250 MW at 15% reactive loading (Positive imaginary part).

The 39-bus system reactive load data can be referred to in Table B.6 in Appendix B. The power generation data for 5%, 10% and 15% reactive load increment can be found in Table B.7, Table B.8 and Table B.9 respectively.

## 4.6 Summary of Chapter

The results obtained from the four case studies are summarized in Table 4.17. Results summary of .

Table 4.17. Results summary of Case 1, Case 2, Case 3 and Case 4

Case No.	IEEE 9-bus Power System	IEEE 39-bus Power System
Case 1	Both power systems were in a stable condition	Both power systems were in a stable condition
Case 2	It is observed that there is an optimum solar PV penetration of 100 MW that provides the highest damping ratio of 15.78%. When generator is taken out of the equation, the damping ratio reduces slightly to 13.72% which is still higher than the base case valued at 11.74%.	The damping ratio is highest when there is complete displacement of the synchronous generator from that particular bus. This trait is also observed in similar studies.
Case 3	No significant impact is seen as the load increases. Nonetheless, the system is still stable. Similar to Case 2, the optimum solar PV penetration stands at 100 MW	The damping ratio is observed to be have peaked at 10% increase in load. This shows that it there is an optimum loading that would cause the system to be in a more stable state
Case 4	Damping ratio decreases slightly as the reactive load increases. Similar to Case 2 and Case 3, there is an optimum solar PV penetration at 100 MW. Overall system is still in a stable condition.	Damping ratio increases as reactive load increases. This may be due to the nature of a larger power system which consists of more reactive power generations and loads. Highest damping ratio seen when

## CHAPTER 5

### CONCLUSION AND RECOMMENDATIONS FOR FUTURE WORK

#### 5.1 Conclusion

The first objective of this research is to investigate the impact of increased solar PV penetration on the grid towards small signal stability. The base models of 9-bus and 39-bus power systems are investigated in terms of load flow analysis to ensure that the system is in a stable condition and the network models are suitable to be undergo small signal stability analysis. Voltage at each busbar is inspected to ensure that it is within the acceptable range. The results show that both 9-bus and 39-bus system voltage magnitude are within the 5% limit band. Various solar generation levels are induced into the power system while power generation by synchronous generator is decreased proportionally. This is to determine the small signal stability performance of the power system. For the smaller 9-bus power system, it is observed that there is an optimum solar PV penetration of 100 MW that provides the highest damping ratio of 15.78%. When the synchronous generator is taken out of the equation, the damping ratio reduces slightly to 13.72% which is still higher than the base case valued at 11.74%. In the small signal stability simulation of larger network, 39-bus power system, the data indicates the damping ratio is highest when there is complete displacement of the synchronous generator from that particular bus. This indicates that larger power systems tend to be more stable when synchronous generators are taken out of service and replaced with solar PV generation. This trait is also observed in the study done by [18][21][34], where the power system becomes more stable due to the reduction of inertia as the synchronous generator is displaced by solar PV. In both power systems, the highest damping does not vary significantly as all of them are above the 9% limit. Thus, the only significance is seen at the lowest damping ratio which was discussed.

The next objective of the research is to investigate the effect of increasing the base load by 5%, 10% and 15% at different levels of solar PV penetration in the grid towards small signal stability. In practical, the load in power systems tends to fluctuate throughout the

day when there are various power demands. In this simulation, the load is increased from its base load to 5%, 10% and up to 15%. In the 9-bus power system, the data shows as load increases, the damping ratio has a downward trend. Nonetheless, the system is still stable. The damping ratio of 39-bus system, is observed to be peaked at 10% increase in load. This shows that there is an optimum loading that would cause the system to be in a more stable state. The 9-bus and 39-bus systems do not have a similar trends observed when the load was varied, this could be due to the nature of a small power system versus a large power system. A larger power system has more inertia contributing by the all the synchronous generators as compared to the smaller scaled power system. Nevertheless, the power system is still able to maintain its state of stability throughout the variation of load.

Lastly, the final objective is to study the effect of increasing the reactive base load by 5%, 10% and 15% at different levels of solar PV penetration in the grid towards small signal stability. Similarly to Case 3, reactive power percentages of 5%, 10% and 15% are used in this simulation. Based on the results obtained for 9-bus system, it is seen that damping ratio decreases as the reactive load increases. When the synchronous generator is totally displaced, the damping ratio then shows an uptrend. These results are similar to that of Case 3. For 39-bus system, the damping ratio increases as reactive load increases. The results are not in line with the results obtained for 9-bus power system. This may be due to the nature of a larger power system which consists of more reactive power generations and loads. In addition, both systems are still in their stable states as there is no negative real components found in the eigenvalues generated from the simulation.

## **5.2 Recommendations For Future Work**

Voltage stability of grid connected solar PV generations could also be investigated. Given that the power generated by solar PV is solely based upon the level of solar irradiation, which is random in nature. It would be beneficial to investigate the ability and reliability of the power system to maintain its steady voltage on all buses after subjecting to a disturbance. Furthermore, another aspect that could be further researched is an in-depth study on the direct relationship of decreasing system inertia and system stability in the power system caused by the reduction or displacement of synchronous generators.

## REFERENCES

- [1] F. H. Anuwar and A. M. Omar. (2016, Aug.). Future Solar Irradiance Prediction using Least Square Support Vector Machine. *Int. J. Adv. Sci. Eng. Inf. Technol.* [Online]. 6 (4), pp. 520–523. Available: <http://dx.doi.org/10.18517/ijaseit.6.4.899>
- [2] C. Lins, L.E. Williamson, S. Leitner, and S. Teske. (2014). The First Decade: 2004-2014, 10 Years of Renewable Energy Progress. *OPUS.* [Online]. 20 (1), pp. 15–21. Available: <http://hdl.handle.net/10453/117208>
- [3] A. Gabbard, "Coal Combustion : Nuclear Resource or Danger ?", unpublished
- [4] T. Kaberger. (2018, January). Progress of renewable electricity replacing fossil fuels. *Glob. energy Int. Dev. Coop. Organ.* [Online]. 1 (1). pp. 48–52. Available: <https://doi.org/10.14171/j.2096-5117.gei.2018.01.006>
- [5] Suruhanjaya Tenaga Malaysia. (2014, September). Peninsular Malaysia Electricity Supply. Malaysia. [Online]. Available: <https://www.st.gov.my/contents/Peninsular%20Malaysia%20Electricity%20Supply%20Industry%20Outlook%202013.pdf>
- [6] N. A. Rahim, H. S. Che, M. Hasanuzzaman, and A. Habib. (2018, July). Toward cleaner cities: Renewable energy initiatives in Malaysia. *Devising a Clean Energy Strategy for Asian Cities.* [Online]. pp. 165–185. Available: [https://doi.org/10.1007/978-981-13-0782-9\\_8](https://doi.org/10.1007/978-981-13-0782-9_8)
- [7] M. Liserre, T. Sauter, and J. Y. Hung. (2010, March). Future Energy Systems: Integrating Renewable Energy Sources into the Smart Power Grid Through Industrial Electronics. *IEEE Ind. Electron. Mag.* [Online]. 38 (1). pp. 18–37. Available: <https://doi.org/10.1109/MIE.2010.935861>
- [8] C. Lins, L.E. Williamson, S. Leitner, and S. Teske. (2014). The First Decade: 2004-2014, 10 Years of Renewable Energy Progress. *OPUS.* [Online]. 20. pp. 15–21. Available: <http://hdl.handle.net/10453/117208>
- [9] P. Kanjiya and V. Khadkikar, "Enhancing power quality and stability of future smart grid with intermittent renewable energy sources using electric springs," in *ICRERA, Madrid, 2013*, pp. 918–922.

- [10] S. A. Papathanassiou. (2007, Jan.). A technical evaluation framework for the connection of DG to the distribution network. *Electr. Power Syst. Res.* [Online]. 77 (1), pp. 24–34. Available: <https://doi.org/10.1016/j.epsr.2006.01.009>
- [11] S. Yasmeena and G. T. Das (2015, Sept.). A Review of Technical Issues for Grid Connected Renewable Energy Sources. *International Journal of Energy and Power Engineering.* [Online]. 4 (5-1), pp. 22–32. Available: <http://article.sciencepublishinggroup.com/html/10.11648.j.ijepe.s.2015040501.14.html>
- [12] Y. Saleh, S. Ghazi, and F. Shadman, “Technical issues of grid connected renewable energy sources - A New Areas of Research,” presented at the World Renew. Energy Congr., London, Aug 3-8, 2014.
- [13] D. Gautam, V. Vittal, and T. Harbour. (2009, Aug.). Impact of increased penetration of DFIG-based wind turbine generators on transient and small signal stability of power systems. *Power Syst. IEEE Trans.* [Online]. 24 (3), pp. 1426–1434. Available: <https://doi.org/10.1109/TPWRS.2009.2021234>
- [14] V. P. B. Metha, P. Bhatt. (2013, July). Small signal stability analysis of power systems with DFIG based wind power penetration. *J. Mod. Power Syst. Clean Energy.* [Online]. 1 (3), pp. 64–74. Available: <https://doi.org/10.1007/s40565-013-0028-9>
- [15] K. G. Sharma, A. Bhargava, K. Gajrani, and R. Bansal, “Impact of integration of solar and wind power on small signal stability using wavelet transform,” in *2013 IEEE Conf. Clean Energy Technol.*, Langkawi, 2013, pp. 293–298.
- [16] Y.U. Lopez and J.A.Dominguez, “Small Signal Stability Analysis of Wind Turbines,” unpublished.
- [17] A. Talha and I. S. Qureshi, “Small Signal Stability Analysis of Power System with Wind Generation Using Optimized Wind PSS,” in *SASG*, Jeddah, 2015, pp. 2–6.
- [18] S. Dahal and N. Mithulanathan, “Investigation of Small Signal Stability of a Renewable Energy based Electricity Distribution System,” in *Power Energy Soc. Gen. Meet. 2010 IEEE*, Providence, RI, 2010, pp. 1–8.

- [19] R. H. Byrne et al., “Small Signal Stability of the Western North American Power Grid with High Penetrations of Renewable Generation,” in PVSC, Portland, 2016, pp. 1784–1789.
- [20] C. Konstantinou, “A Study on the Impact of Wind Generation on the Stability of Electromechanical Oscillations,” unpublished.
- [21] A. U. Krismanto, M. Nadarajah, and O. Krause, “Influence of renewable energy based microgrid on low frequency oscillation of power systems,” in APPEEC, Brisbane, QLD, 2015, pp. 1–5.
- [22] A.W. Azhari, K. Sopian, A. Zaharim, M.A. Ghoul. (2008, April). A new approach for predicting solar radiation in tropical environment using satellite images - Case study of Malaysia. *WSEAS Transactions on Environment and Development*. [Online] 4 (4), pp. 373- 378. Available: <http://www.scopus.com/inward/record.url?scp=46449137245&partnerID=8YFLogxK>
- [23] P. Vijayan, S. Sarkar, and V. Ajjarapu, “A novel voltage stability assessment tool to incorporate wind variability,” in *2009 PE*, Calgary, AB, 2009, pp. 1-8.
- [24] F. Wu, X. P. Zhang, and P. Ju. (2009, Dec.). Small signal stability analysis and control of the wind turbine with the direct-drive permanent magnet generator integrated to the grid. *Electr. Power Syst. Res.* [Online]. 79 (12), pp. 1661–1667. Available: <https://doi.org/10.1016/j.epsr.2009.07.003>
- [25] S. Eftekharnjad, V. Vittal, G. T. Heydt, B. Keel, and J. Loehr. (2013, Oct.). Small Signal Stability Assessment of Power Systems With Increased Penetration of Photovoltaic Generation: A Case Study. *IEEE Trans. Sustain. Energy*. [Online]. 4 (4), pp. 960–967. Available: <http://dx.doi.org/10.1109/TSTE.2013.2259602>
- [26] E. Liu and J. Bebic, “Distribution System Voltage Performance Analysis for High-Penetration Photovoltaics Distribution System Voltage Performance Analysis for High-Penetration Photovoltaics,” Natl. Renew. Energy Lab., New York, ADC-7-77032-01, Feb. 2008.
- [27] P. P. Barker and R. W. De Mello, “Determining the impact of distributed generation on power systems. I. Radial distribution systems,” *Power Eng. Soc. Summer Meet. 2000. IEEE*, Seattle, WA, 2000, pp. 1645–1656.

- [28] Y. Zhang, C. Mensah-Bonsu, P. Walke, S. Arora, and J. Pierce, "Transient over-voltages in high voltage grid-connected PV solar interconnection," in *IEEE PES Gen. Meet. PES*, Providence, RI, 2010, pp. 1–6.
- [29] S. Achilles, S. Schramm, and J. Bebic, "Transmission system performance analysis for high-penetration photovoltaics," Natl. Renew. Energy Lab., New York, ADC-7-77032-01, Feb. 2008.
- [30] R. Elliott, R. Byrne, A. Ellis, and L. Grant, "Impact of Increased Photovoltaic Generation on Inter-area Oscillations in the Western North American Power System", in *IEEE PES*, National Harbor, MD, 2014.
- [31] B. Bahmanifirouzi, E. Farjah, T. Niknam, and E. Azad Farsani. (2012, Dec.). A new hybrid HBMO-SFLA algorithm for multi-objective distribution feeder reconfiguration problem considering distributed generator units. *Iran. J. Sci. Technol. - Trans. Electr. Eng.* [Online]. 36 (1), pp. 51–66. Available: [http://ijste.shirazu.ac.ir/article\\_809.html](http://ijste.shirazu.ac.ir/article_809.html)
- [32] H. Liu, L. Jin, D. Le, and A. A. Chowdhury, "Impact of high penetration of solar photovoltaic generation on power system small signal stability," in *2010 Int. Conf. Power Syst. Technol.*, Hangzhou, 2010, pp. 1–7
- [33] S. Gurung, S. Naetiladdanon, and A. Sangswang, "Impact of large photovoltaic penetration on small signal stability," in *IEEE TENCON*, Singapore, 2017, pp. 646–650.
- [34] S. L. Shaikh, "The Effect of High Pv Penetration on the Small Signal," in *IT Research International Conf.*, Kolhapur, 2015, pp. 33–37.
- [35] S. Wellhofer, S. Hohn, and M. Luther, "Impact of load modeling on small signal stability investigations", presented at 2016 IEEE Int. Conf. Power Syst. Technol. (POWERCON), NSW, Australia, Sept. 28 - Oct. 1, 2016.
- [36] Z. A. Zhang, S. Gao, H. Cai, W. Du, T. Littler, and H. F. Wang, "Analysis of Load Impact on Small-signal Stability based on Load Active Power Sensitivity," presented at 2nd IET Renewable Power Generation Conference, Beijing, China, Sept. 9-11, 2013.
- [37] J. J. Grainger and W. D. J. Stevenson, "Power System Stability," in *Power System Analysis*, 1<sup>st</sup> ed., New York: McGraw Hill, 1994, pp. 777.

- [38] P. Kundur, "Introduction to the Power System Stability Problem", in *Power System Stability and Control*, 1<sup>st</sup> ed., New York: McGraw-Hill, 1994. pp. 17-34.
- [39] P. M. Anderson, "The Synchronous Machine ", in *Power system control and stability*, 2<sup>nd</sup> ed., USA: Wiley-IEEE Press, 1926.
- [40] E. C. Bobric, G. Cartina, and G. Grigora. (2009, Feb.). Clustering techniques in load profile analysis for distribution stations. *Adv. Electr. Comput. Eng.* [Online]. 9 (1), pp. 63–66. Available: [https://www.researchgate.net/publication/41391418\\_Clustering\\_Techniques\\_in\\_Load\\_Profile\\_Analysis\\_for\\_Distribution\\_Stations](https://www.researchgate.net/publication/41391418_Clustering_Techniques_in_Load_Profile_Analysis_for_Distribution_Stations)
- [41] Distribution Code For Peninsular Malaysia, Sabah & F.T. Labuan (Amendments) 2017, Electricity Supply Act 1990, 2017.
- [42] J. Berard, "IEEE 9 Bus System Example," unpublished. Available: [https://www.kios.ucy.ac.cy/testsystems/images/Documents/Data/IEEE9\\_model\\_documentation\\_R0.pdf](https://www.kios.ucy.ac.cy/testsystems/images/Documents/Data/IEEE9_model_documentation_R0.pdf)

## APPENDICES

### Appendix A: Power generation and load data of 9-bus power system

Table A.1. Power generation data for AC solar PV penetration of 0 MW to 163 MW

Sync. Gen. Power (MW)	PV Penetration (MW)	Component	Active Power (MW)	Reactive Power (Mvar)
163	0	G1	71.64	27.05
163	0	G2	163.00	6.65
163	0	G3	85.00	-10.86
113	50	G1	71.64	27.05
113	50	G2	113.00	6.65
113	50	G3	85.00	-10.86
63	100	G1	71.64	27.05
63	100	G2	63.00	6.65
63	100	G3	85.00	-10.86
0	163	G1	71.74	31.41
0	163	G2	0.00	0.00
0	163	G3	85.00	-5.93

Table A.2. 9-bus system overall load data at 5%, 10% and 15% increments

Overall Load Increment (%)	Component	Active Power (MW)	Reactive Power (Mvar)
0	Load A	125.00	50.00
0	Load B	90.00	30.00
0	Load C	100.00	35.00
5	Load A	131.25	52.50
5	Load B	94.50	31.50
5	Load C	105.00	36.75
10	Load A	137.81	55.13
10	Load B	99.23	33.08
10	Load C	110.25	38.59
15	Load A	143.75	57.50
15	Load B	103.50	34.50
15	Load C	115.00	40.25

Table A.3. 9-bus system generation data for AC solar PV penetration of 0 MW to 163 MW at 5% overall load increment

<b>Sync. Gen. Power (MW)</b>	<b>PV Penetration (MW)</b>	<b>Component</b>	<b>Active Power (MW)</b>	<b>Reactive Power (Mvar)</b>
163	0	G1	87.39	30.44
163	0	G2	163.00	9.29
163	0	G3	85.00	-8.53
113	50	G1	87.39	30.44
113	50	G2	113.00	9.29
113	50	G3	85.00	-8.53
63	100	G1	87.39	30.44
63	100	G2	63.00	9.29
63	100	G3	85.00	-8.53
0	163	G1	87.52	36.59
0	163	G2	0.00	0.00
0	163	G3	85.00	-1.60

Table A.4. 9-bus system generation data for AC solar PV penetration of 0 MW to 163 MW at 10% overall load increment

<b>Sync. Gen. Power (MW)</b>	<b>PV Penetration (MW)</b>	<b>Component</b>	<b>Active Power (MW)</b>	<b>Reactive Power (Mvar)</b>
163	0	G1	103.18	34.27
163	0	G2	163.00	12.03
163	0	G3	85.00	-6.10
113	50	G1	103.18	34.27
113	50	G2	113.00	12.03
113	50	G3	85.00	-6.10
63	100	G1	103.18	34.27
63	100	G2	63.00	12.03
63	100	G3	85.00	-6.10
0	163	G1	103.36	42.32
0	163	G2	0.00	0.00
0	163	G3	85.00	2.95

Table A.5. 9-bus system generation data for AC solar PV penetration of 0 MW to 163 MW at 15% overall load increment

<b>Sync. Gen. Power (MW)</b>	<b>PV Penetration (MW)</b>	<b>Component</b>	<b>Active Power (MW)</b>	<b>Reactive Power (Mvar)</b>
163	0	G1	119.02	38.56
163	0	G2	163.00	14.89
163	0	G3	85.00	-3.56
113	50	G1	119.02	38.56
113	50	G2	113.00	14.89
113	50	G3	85.00	-3.56
63	100	G1	119.02	38.56
63	100	G2	63.00	14.89
63	100	G3	85.00	-3.56
0	163	G1	119.25	48.62
0	163	G2	0.00	0.00
0	163	G3	85.00	7.73

Table A.6. 9-bus system reactive load data at 5%, 10% and 15% increments

<b>Overall Load Increment (%)</b>	<b>Component</b>	<b>Active Power (MW)</b>	<b>Reactive Power (Mvar)</b>
0	Load A	125.00	50.00
0	Load B	90.00	30.00
0	Load C	100.00	35.00
5	Load A	125.00	52.50
5	Load B	90.00	31.50
5	Load C	100.00	36.75
10	Load A	125.00	55.00
10	Load B	90.00	33.00
10	Load C	100.00	38.50
15	Load A	125.00	57.50
15	Load B	90.00	34.50
15	Load C	100.00	40.25

Table A.7. 9-bus system generation data for AC solar PV penetration of 0 MW to 163 MW at 5% reactive load increment

<b>Sync. Gen. Power (MW)</b>	<b>PV Penetration (MW)</b>	<b>Component</b>	<b>Active Power (MW)</b>	<b>Reactive Power (Mvar)</b>
163	0	G1	71.68	29.78
163	0	G2	163.00	8.74
163	0	G3	85.00	-9.11
113	50	G1	71.68	29.78
113	50	G2	113.00	8.74
113	50	G3	85.00	-9.11
63	100	G1	71.68	29.78
63	100	G2	63.00	8.74
63	100	G3	85.00	-9.11
0	163	G1	71.81	35.56
0	163	G2	0.00	0.00
0	163	G3	85.00	-2.59

Table A.8. 9-bus system generation data for AC solar PV penetration of 0 MW to 163 MW at 10% reactive load increment

<b>Sync. Gen. Power (MW)</b>	<b>PV Penetration (MW)</b>	<b>Component</b>	<b>Active Power (MW)</b>	<b>Reactive Power (Mvar)</b>
163	0	G1	71.71	32.53
163	0	G2	163.00	10.83
163	0	G3	85.00	-7.34
113	50	G1	71.71	32.53
113	50	G2	113.00	10.83
113	50	G3	85.00	-7.34
63	100	G1	71.71	32.53
63	100	G2	63.00	10.83
63	100	G3	85.00	-7.34
0	163	G1	71.88	39.76
0	163	G2	0.00	0.00
0	163	G3	85.00	0.79

Table A.9. 9-bus system generation data for AC solar PV penetration of 0 MW to 163 MW at 15% reactive load increment

<b>Sync. Gen. Power (MW)</b>	<b>PV Penetration (MW)</b>	<b>Component</b>	<b>Active Power (MW)</b>	<b>Reactive Power (Mvar)</b>
163	0	G1	71.75	35.30
163	0	G2	163.00	12.94
163	0	G3	85.00	-5.57
113	50	G1	71.75	35.30
113	50	G2	113.00	12.94
113	50	G3	85.00	-5.57
63	100	G1	71.75	35.30
63	100	G2	63.00	12.94
63	100	G3	85.00	-5.57
0	163	G1	71.96	44.00
0	163	G2	0.00	0.00
0	163	G3	85.00	4.21

## Appendix B: Power generation and load data of 39-bus power system

Table B.1. Power generation data for AC solar PV penetration of 0 MW to 250 MW

Sync. Gen. Power (MW)	PV Penetration (MW)	Component	Active Power (MW)	Reactive Power (Mvar)
250	0	G1	1000.00	88.28
250	0	G2	520.81	198.25
250	0	G3	650.00	205.14
250	0	G4	632.00	109.91
250	0	G5	508.00	165.76
250	0	G6	650.00	212.41
250	0	G7	560.00	101.18
250	0	G8	540.00	0.44
250	0	G9	830.00	22.84
250	0	G10	250.00	146.16
200	50	G1	1000.00	88.28
200	50	G2	520.81	198.25
200	50	G3	650.00	205.14
200	50	G4	632.00	109.91
200	50	G5	508.00	165.76
200	50	G6	650.00	212.41
200	50	G7	560.00	101.18
200	50	G8	540.00	0.44
200	50	G9	830.00	22.84
200	50	G10	200.00	146.16
150	100	G1	1000.00	88.28
150	100	G2	520.81	198.25
150	100	G3	650.00	205.14
150	100	G4	632.00	109.91
150	100	G5	508.00	165.76
150	100	G6	650.00	212.41
150	100	G7	560.00	101.18
150	100	G8	540.00	0.44
150	100	G9	830.00	22.84
150	100	G10	150.00	146.16
100	150	G1	1000.00	88.28
100	150	G2	520.81	198.25

<b>Sync. Gen. Power (MW)</b>	<b>PV Penetration (MW)</b>	<b>Component</b>	<b>Active Power (MW)</b>	<b>Reactive Power (Mvar)</b>
100	150	G3	650.00	205.14
100	150	G4	632.00	109.91
100	150	G5	508.00	165.76
100	150	G6	650.00	212.41
100	150	G7	560.00	101.18
100	150	G8	540.00	0.44
100	150	G9	830.00	22.84
100	150	G10	100.00	146.16
50	200	G1	1000.00	88.28
50	200	G2	520.81	198.25
50	200	G3	650.00	205.14
50	200	G4	632.00	109.91
50	200	G5	508.00	165.76
50	200	G6	650.00	212.41
50	200	G7	560.00	101.18
50	200	G8	540.00	0.44
50	200	G9	830.00	22.84
50	200	G10	50.00	146.16
0	250	G1	1000.00	122.53
0	250	G2	520.72	210.07
0	250	G3	650.00	218.60
0	250	G4	632.00	119.63
0	250	G5	508.00	170.26
0	250	G6	650.00	223.32
0	250	G7	560.00	107.36
0	250	G8	540.00	53.36
0	250	G9	830.00	39.16
0	250	G10	0.00	0.00

Table B.2. 39-bus system overall load data at 5%, 10% and 15% increments

<b>Overall Load Increment (%)</b>	<b>Component</b>	<b>Active Power (MW)</b>	<b>Reactive Power (Mvar)</b>
0	Load 03	322.00	2.40
0	Load 04	500.00	184.00
0	Load 07	233.80	84.00
0	Load 08	522.00	176.00
0	Load 12	7.50	88.00
0	Load 15	320.00	153.00
0	Load 16	329.00	32.30
0	Load 18	158.00	30.00
0	Load 20	628.00	103.00
0	Load 21	274.00	115.00
0	Load 23	247.50	84.60
0	Load 24	308.60	-92.20
0	Load 25	224.00	47.20
0	Load 26	139.00	17.00
0	Load 27	281.00	75.50
0	Load 28	206.00	27.60
0	Load 29	283.50	26.90
0	Load 31	9.20	4.60
0	Load 39	1104.00	250.00
5	Load 03	338.10	2.52
5	Load 04	525.00	193.20
5	Load 07	245.49	88.20
5	Load 08	548.10	184.80
5	Load 12	7.88	92.40
5	Load 15	336.00	160.65
5	Load 16	345.45	33.92
5	Load 18	165.90	31.50
5	Load 20	659.40	108.15
5	Load 21	287.70	120.75
5	Load 23	259.88	88.83
5	Load 24	324.03	-96.81
5	Load 25	235.20	49.56
5	Load 26	145.95	17.85
5	Load 27	295.05	79.28

<b>Overall Load Increment (%)</b>	<b>Component</b>	<b>Active Power (MW)</b>	<b>Reactive Power (Mvar)</b>
5	Load 28	216.30	28.98
5	Load 29	297.68	28.25
5	Load 31	9.66	4.83
5	Load 39	1159.20	262.50
10	Load 03	354.20	2.64
10	Load 04	550.00	202.40
10	Load 07	257.18	92.40
10	Load 08	574.20	193.60
10	Load 12	8.25	96.80
10	Load 15	352.00	168.30
10	Load 16	361.90	35.53
10	Load 18	173.80	33.00
10	Load 20	690.80	113.30
10	Load 21	301.40	126.50
10	Load 23	272.25	93.06
10	Load 24	339.46	-101.42
10	Load 25	246.40	51.92
10	Load 26	152.90	18.70
10	Load 27	309.10	83.05
10	Load 28	226.60	30.36
10	Load 29	311.85	29.59
10	Load 31	10.12	5.06
10	Load 39	1214.40	275.00
15	Load 03	370.30	2.76
15	Load 04	575.00	211.60
15	Load 07	268.87	96.60
15	Load 08	600.30	202.40
15	Load 12	8.63	101.20
15	Load 15	368.00	175.95
15	Load 16	378.35	37.15
15	Load 18	181.70	34.50
15	Load 20	722.20	118.45
15	Load 21	315.10	132.25
15	Load 23	284.63	97.29
15	Load 24	354.89	-106.03

<b>Overall Load Increment (%)</b>	<b>Component</b>	<b>Active Power (MW)</b>	<b>Reactive Power (Mvar)</b>
15	Load 25	257.60	54.28
15	Load 26	159.85	19.55
15	Load 27	323.15	86.83
15	Load 28	236.90	31.74
15	Load 29	326.03	30.94
15	Load 31	10.58	5.29
15	Load 39	1269.60	287.50

Table B.3. 39-bus system generation data for AC solar PV penetration of 0 MW to 250 MW at 5% overall load increment

<b>Sync. Gen. Power (MW)</b>	<b>PV Penetration (MW)</b>	<b>Component</b>	<b>Active Power (MW)</b>	<b>Reactive Power (Mvar)</b>
250	0	G 01	1000.00	120.56
250	0	G 02	824.99	284.74
250	0	G 03	650.00	232.61
250	0	G 04	632.00	118.46
250	0	G 05	508.00	173.02
250	0	G 06	650.00	222.70
250	0	G 07	560.00	107.34
250	0	G 08	540.00	10.69
250	0	G 09	830.00	30.27
250	0	G 10	250.00	151.93
200	50	G 01	1000.00	120.56
200	50	G 02	824.99	284.74
200	50	G 03	650.00	232.61
200	50	G 04	632.00	118.46
200	50	G 05	508.00	173.02
200	50	G 06	650.00	222.70
200	50	G 07	560.00	107.34
200	50	G 08	540.00	10.69
200	50	G 09	830.00	30.27
200	50	G 10	200.00	151.93
150	100	G 01	1000.00	120.56
150	100	G 02	824.99	284.74
150	100	G 03	650.00	232.61
150	100	G 04	632.00	118.46
150	100	G 05	508.00	173.02
150	100	G 06	650.00	222.70
150	100	G 07	560.00	107.34
150	100	G 08	540.00	10.69
150	100	G 09	830.00	30.27
150	100	G 10	150.00	151.93
100	150	G 01	1000.00	120.56
100	150	G 02	824.99	284.74
100	150	G 03	650.00	232.61

<b>Sync. Gen. Power (MW)</b>	<b>PV Penetration (MW)</b>	<b>Component</b>	<b>Active Power (MW)</b>	<b>Reactive Power (Mvar)</b>
100	150	G 04	632.00	118.46
100	150	G 05	508.00	173.02
100	150	G 06	650.00	222.70
100	150	G 07	560.00	107.34
100	150	G 08	540.00	10.69
100	150	G 09	830.00	30.27
100	150	G 10	100.00	151.93
50	200	G 01	1000.00	120.56
50	200	G 02	824.99	284.74
50	200	G 03	650.00	232.61
50	200	G 04	632.00	118.46
50	200	G 05	508.00	173.02
50	200	G 06	650.00	222.70
50	200	G 07	560.00	107.34
50	200	G 08	540.00	10.69
50	200	G 09	830.00	30.27
50	200	G 10	50.00	151.93
0	250	G 01	1000.00	156.24
0	250	G 02	824.95	297.47
0	250	G 03	650.00	246.80
0	250	G 04	632.00	128.61
0	250	G 05	508.00	177.73
0	250	G 06	650.00	234.10
0	250	G 07	560.00	113.80
0	250	G 08	540.00	65.80
0	250	G 09	830.00	47.28
0	250	G 10	0.00	0.00

Table B.4. 39-bus system generation data for AC solar PV penetration of 0 MW to 250 MW at 10% overall load increment

<b>Sync. Gen. Power (MW)</b>	<b>PV Penetration (MW)</b>	<b>Component</b>	<b>Active Power (MW)</b>	<b>Reactive Power (Mvar)</b>
250	0	G 01	1000.00	164.63
250	0	G 02	1131.58	419.82
250	0	G 03	650.00	276.56
250	0	G 04	632.00	131.10
250	0	G 05	508.00	182.26
250	0	G 06	650.00	237.42
250	0	G 07	560.00	116.01
250	0	G 08	540.00	24.36
250	0	G 09	830.00	40.14
250	0	G 10	250.00	163.23
200	50	G 01	1000.00	164.63
200	50	G 02	1131.58	419.82
200	50	G 03	650.00	276.56
200	50	G 04	632.00	131.10
200	50	G 05	508.00	182.26
200	50	G 06	650.00	237.42
200	50	G 07	560.00	116.01
200	50	G 08	540.00	24.36
200	50	G 09	830.00	40.14
200	50	G 10	200.00	163.23
150	100	G 01	1000.00	164.63
150	100	G 02	1131.58	419.82
150	100	G 03	650.00	276.56
150	100	G 04	632.00	131.10
150	100	G 05	508.00	182.26
150	100	G 06	650.00	237.42
150	100	G 07	560.00	116.01
150	100	G 08	540.00	24.36
150	100	G 09	830.00	40.14
150	100	G 10	150.00	163.23
100	150	G 01	1000.00	164.63
100	150	G 02	1131.58	419.82
100	150	G 03	650.00	276.56

<b>Sync. Gen. Power (MW)</b>	<b>PV Penetration (MW)</b>	<b>Component</b>	<b>Active Power (MW)</b>	<b>Reactive Power (Mvar)</b>
100	150	G 04	632.00	131.10
100	150	G 05	508.00	182.26
100	150	G 06	650.00	237.42
100	150	G 07	560.00	116.01
100	150	G 08	540.00	24.36
100	150	G 09	830.00	40.14
100	150	G 10	100.00	163.23
50	200	G 01	1000.00	164.63
50	200	G 02	1131.58	419.82
50	200	G 03	650.00	276.56
50	200	G 04	632.00	131.10
50	200	G 05	508.00	182.26
50	200	G 06	650.00	237.42
50	200	G 07	560.00	116.01
50	200	G 08	540.00	24.36
50	200	G 09	830.00	40.14
50	200	G 10	50.00	163.23
0	250	G 01	1000.00	203.26
0	250	G 02	1131.68	434.42
0	250	G 03	650.00	292.28
0	250	G 04	632.00	142.13
0	250	G 05	508.00	187.37
0	250	G 06	650.00	249.80
0	250	G 07	560.00	123.04
0	250	G 08	540.00	83.77
0	250	G 09	830.00	58.50
0	250	G 10	0.00	0.00

Table B.5. 39-bus system generation data for AC solar PV penetration of 0 MW to 250 MW at 15% overall load increment

Sync. Gen. Power (MW)	PV Penetration (MW)	Component	Active Power (MW)	Reactive Power (Mvar)
250	0	G 01	1000.00	223.56
250	0	G 02	1441.12	615.56
250	0	G 03	650.00	341.75
250	0	G 04	632.00	148.80
250	0	G 05	508.00	193.92
250	0	G 06	650.00	257.64
250	0	G 07	560.00	127.81
250	0	G 08	540.00	42.31
250	0	G 09	830.00	53.00
250	0	G 10	250.00	181.42
200	50	G 01	1000.00	223.56
200	50	G 02	1441.12	615.56
200	50	G 03	650.00	341.75
200	50	G 04	632.00	148.80
200	50	G 05	508.00	193.92
200	50	G 06	650.00	257.64
200	50	G 07	560.00	127.81
200	50	G 08	540.00	42.31
200	50	G 09	830.00	53.00
200	50	G 10	200.00	181.42
150	100	G 01	1000.00	223.56
150	100	G 02	1441.12	615.56
150	100	G 03	650.00	341.75
150	100	G 04	632.00	148.80
150	100	G 05	508.00	193.92
150	100	G 06	650.00	257.64
150	100	G 07	560.00	127.81
150	100	G 08	540.00	42.31
150	100	G 09	830.00	53.00
150	100	G 10	150.00	181.42
100	150	G 01	1000.00	223.56
100	150	G 02	1441.12	615.56
100	150	G 03	650.00	341.75

<b>Sync. Gen. Power (MW)</b>	<b>PV Penetration (MW)</b>	<b>Component</b>	<b>Active Power (MW)</b>	<b>Reactive Power (Mvar)</b>
100	150	G 04	632.00	148.80
100	150	G 05	508.00	193.92
100	150	G 06	650.00	257.64
100	150	G 07	560.00	127.81
100	150	G 08	540.00	42.31
100	150	G 09	830.00	53.00
100	150	G 10	100.00	181.42
50	200	G 01	1000.00	223.56
50	200	G 02	1441.12	615.56
50	200	G 03	650.00	341.75
50	200	G 04	632.00	148.80
50	200	G 05	508.00	193.92
50	200	G 06	650.00	257.64
50	200	G 07	560.00	127.81
50	200	G 08	540.00	42.31
50	200	G 09	830.00	53.00
50	200	G 10	50.00	181.42
0	250	G 01	1000.00	267.14
0	250	G 02	1441.50	633.71
0	250	G 03	650.00	360.21
0	250	G 04	632.00	161.33
0	250	G 05	508.00	199.73
0	250	G 06	650.00	271.71
0	250	G 07	560.00	135.79
0	250	G 08	540.00	108.74
0	250	G 09	830.00	73.61
0	250	G 10	0.00	0.00

Table B.6. 39-bus system reactive load data at 5%, 10% and 15% increments

<b>Overall Load Increment (%)</b>	<b>Component</b>	<b>Active Power (MW)</b>	<b>Reactive Power (Mvar)</b>
0	Load 03	322.00	2.40
0	Load 04	500.00	184.00
0	Load 07	233.80	84.00
0	Load 08	522.00	176.00
0	Load 12	7.50	88.00
0	Load 15	320.00	153.00
0	Load 16	329.00	32.30
0	Load 18	158.00	30.00
0	Load 20	628.00	103.00
0	Load 21	274.00	115.00
0	Load 23	247.50	84.60
0	Load 24	308.60	-92.20
0	Load 25	224.00	47.20
0	Load 26	139.00	17.00
0	Load 27	281.00	75.50
0	Load 28	206.00	27.60
0	Load 29	283.50	26.90
0	Load 31	9.20	4.60
0	Load 39	1104.00	250.00
5	Load 03	322.00	2.52
5	Load 04	500.00	193.20
5	Load 07	233.80	88.20
5	Load 08	522.00	184.80
5	Load 12	7.50	92.40
5	Load 15	320.00	160.65
5	Load 16	329.00	33.92
5	Load 18	158.00	31.50
5	Load 20	628.00	108.15
5	Load 21	274.00	120.75
5	Load 23	247.50	88.83
5	Load 24	308.60	-96.81
5	Load 25	224.00	49.56
5	Load 26	139.00	17.85
5	Load 27	281.00	79.28

<b>Overall Load Increment (%)</b>	<b>Component</b>	<b>Active Power (MW)</b>	<b>Reactive Power (Mvar)</b>
5	Load 28	206.00	28.98
5	Load 29	283.50	28.25
5	Load 31	9.20	4.83
5	Load 39	1104.00	262.50
10	Load 03	322.00	2.64
10	Load 04	500.00	202.40
10	Load 07	233.80	92.40
10	Load 08	522.00	193.60
10	Load 12	7.50	96.80
10	Load 15	320.00	168.30
10	Load 16	329.00	35.53
10	Load 18	158.00	33.00
10	Load 20	628.00	113.30
10	Load 21	274.00	126.50
10	Load 23	247.50	93.06
10	Load 24	308.60	-101.42
10	Load 25	224.00	51.92
10	Load 26	139.00	18.70
10	Load 27	281.00	83.05
10	Load 28	206.00	30.36
10	Load 29	283.50	29.59
10	Load 31	9.20	5.06
10	Load 39	1104.00	275.00
15	Load 03	322.00	2.76
15	Load 04	500.00	211.60
15	Load 07	233.80	96.60
15	Load 08	522.00	202.40
15	Load 12	7.50	101.20
15	Load 15	320.00	175.95
15	Load 16	329.00	37.15
15	Load 18	158.00	34.50
15	Load 20	628.00	118.45
15	Load 21	274.00	132.25
15	Load 23	247.50	97.29
15	Load 24	308.60	-106.03

<b>Overall Load Increment (%)</b>	<b>Component</b>	<b>Active Power (MW)</b>	<b>Reactive Power (Mvar)</b>
15	Load 25	224.00	54.28
15	Load 26	139.00	19.55
15	Load 27	281.00	86.83
15	Load 28	206.00	31.74
15	Load 29	283.50	30.94
15	Load 31	9.20	5.29
15	Load 39	1104.00	287.50

Table B.7. 39-bus system generation data for AC solar PV penetration of 0 MW to 250 MW at 5% reactive load increment

Sync. Gen. Power (MW)	PV Penetration (MW)	Component	Active Power (MW)	Reactive Power (Mvar)
250	0	G 01	1000.00	107.90
250	0	G 02	521.06	208.46
250	0	G 03	650.00	215.76
250	0	G 04	632.00	116.05
250	0	G 05	508.00	170.92
250	0	G 06	650.00	220.36
250	0	G 07	560.00	105.95
250	0	G 08	540.00	4.88
250	0	G 09	830.00	28.36
250	0	G 10	250.00	151.91
200	50	G 01	1000.00	107.90
200	50	G 02	521.06	208.46
200	50	G 03	650.00	215.76
200	50	G 04	632.00	116.05
200	50	G 05	508.00	170.92
200	50	G 06	650.00	220.36
200	50	G 07	560.00	105.95
200	50	G 08	540.00	4.88
200	50	G 09	830.00	28.36
200	50	G 10	200.00	151.91
150	100	G 01	1000.00	107.90
150	100	G 02	521.06	208.46
150	100	G 03	650.00	215.76
150	100	G 04	632.00	116.05
150	100	G 05	508.00	170.92
150	100	G 06	650.00	220.36
150	100	G 07	560.00	105.95
150	100	G 08	540.00	4.88
150	100	G 09	830.00	28.36
150	100	G 10	150.00	151.91
100	150	G 01	1000.00	107.90
100	150	G 02	521.06	208.46
100	150	G 03	650.00	215.76

<b>Sync. Gen. Power (MW)</b>	<b>PV Penetration (MW)</b>	<b>Component</b>	<b>Active Power (MW)</b>	<b>Reactive Power (Mvar)</b>
100	150	G 04	632.00	116.05
100	150	G 05	508.00	170.92
100	150	G 06	650.00	220.36
100	150	G 07	560.00	105.95
100	150	G 08	540.00	4.88
100	150	G 09	830.00	28.36
100	150	G 10	100.00	151.91
50	200	G 01	1000.00	107.90
50	200	G 02	521.06	208.46
50	200	G 03	650.00	215.76
50	200	G 04	632.00	116.05
50	200	G 05	508.00	170.92
50	200	G 06	650.00	220.36
50	200	G 07	560.00	105.95
50	200	G 08	540.00	4.88
50	200	G 09	830.00	28.36
50	200	G 10	50.00	151.91
0	250	G 01	1000.00	143.55
0	250	G 02	520.99	220.80
0	250	G 03	650.00	229.80
0	250	G 04	632.00	126.18
0	250	G 05	508.00	175.61
0	250	G 06	650.00	231.74
0	250	G 07	560.00	112.40
0	250	G 08	540.00	59.93
0	250	G 09	830.00	45.36
0	250	G 10	0.00	0.00

Table B.8. 39-bus system generation data for AC solar PV penetration of 0 MW to 250 MW at 10% reactive load increment

<b>Sync. Gen. Power (MW)</b>	<b>PV Penetration (MW)</b>	<b>Component</b>	<b>Active Power (MW)</b>	<b>Reactive Power (Mvar)</b>
250	0	G 01	1000.00	127.57
250	0	G 02	521.33	218.74
250	0	G 03	650.00	226.44
250	0	G 04	632.00	122.21
250	0	G 05	508.00	176.09
250	0	G 06	650.00	228.35
250	0	G 07	560.00	110.75
250	0	G 08	540.00	9.34
250	0	G 09	830.00	33.91
250	0	G 10	250.00	157.69
200	50	G 01	1000.00	127.57
200	50	G 02	521.33	218.74
200	50	G 03	650.00	226.44
200	50	G 04	632.00	122.21
200	50	G 05	508.00	176.09
200	50	G 06	650.00	228.35
200	50	G 07	560.00	110.75
200	50	G 08	540.00	9.34
200	50	G 09	830.00	33.91
200	50	G 10	200.00	157.69
150	100	G 01	1000.00	127.57
150	100	G 02	521.33	218.74
150	100	G 03	650.00	226.44
150	100	G 04	632.00	122.21
150	100	G 05	508.00	176.09
150	100	G 06	650.00	228.35
150	100	G 07	560.00	110.75
150	100	G 08	540.00	9.34
150	100	G 09	830.00	33.91
150	100	G 10	150.00	157.69
100	150	G 01	1000.00	127.57
100	150	G 02	521.33	218.74
100	150	G 03	650.00	226.44

---

100	150	G 04	632.00	122.21
100	150	G 05	508.00	176.09
100	150	G 06	650.00	228.35
100	150	G 07	560.00	110.75
100	150	G 08	540.00	9.34
100	150	G 09	830.00	33.91
100	150	G 10	100.00	157.69
50	200	G 01	1000.00	127.57
50	200	G 02	521.33	218.74
50	200	G 03	650.00	226.44
50	200	G 04	632.00	122.21
50	200	G 05	508.00	176.09
50	200	G 06	650.00	228.35
50	200	G 07	560.00	110.75
50	200	G 08	540.00	9.34
50	200	G 09	830.00	33.91
50	200	G 10	50.00	157.69
0	250	G 01	1000.00	164.63
0	250	G 02	521.28	231.62
0	250	G 03	650.00	241.09
0	250	G 04	632.00	132.77
0	250	G 05	508.00	180.98
0	250	G 06	650.00	240.21
0	250	G 07	560.00	117.47
0	250	G 08	540.00	66.54
0	250	G 09	830.00	51.59
0	250	G 10	0.00	0.00

---

Table B.9. 39-bus system generation data for AC solar PV penetration of 0 MW to 250 MW at 15% reactive load increment

<b>Sync. Gen. Power (MW)</b>	<b>PV Penetration (MW)</b>	<b>Component</b>	<b>Active Power (MW)</b>	<b>Reactive Power (Mvar)</b>
250	0	G 01	1000.00	147.29
250	0	G 02	521.61	229.09
250	0	G 03	650.00	237.20
250	0	G 04	632.00	128.42
250	0	G 05	508.00	181.27
250	0	G 06	650.00	236.39
250	0	G 07	560.00	115.58
250	0	G 08	540.00	13.82
250	0	G 09	830.00	39.47
250	0	G 10	250.00	163.50
200	50	G 01	1000.00	147.29
200	50	G 02	521.61	229.09
200	50	G 03	650.00	237.20
200	50	G 04	632.00	128.42
200	50	G 05	508.00	181.27
200	50	G 06	650.00	236.39
200	50	G 07	560.00	115.58
200	50	G 08	540.00	13.82
200	50	G 09	830.00	39.47
200	50	G 10	200.00	163.50
150	100	G 01	1000.00	147.29
150	100	G 02	521.61	229.09
150	100	G 03	650.00	237.20
150	100	G 04	632.00	128.42
150	100	G 05	508.00	181.27
150	100	G 06	650.00	236.39
150	100	G 07	560.00	115.58
150	100	G 08	540.00	13.82
150	100	G 09	830.00	39.47
150	100	G 10	150.00	163.50
100	150	G 01	1000.00	147.29
100	150	G 02	521.61	229.09
100	150	G 03	650.00	237.20

<b>Sync. Gen. Power (MW)</b>	<b>PV Penetration (MW)</b>	<b>Component</b>	<b>Active Power (MW)</b>	<b>Reactive Power (Mvar)</b>
100	150	G 04	632.00	128.42
100	150	G 05	508.00	181.27
100	150	G 06	650.00	236.39
100	150	G 07	560.00	115.58
100	150	G 08	540.00	13.82
100	150	G 09	830.00	39.47
100	150	G 10	100.00	163.50
50	200	G 01	1000.00	147.29
50	200	G 02	521.61	229.09
50	200	G 03	650.00	237.20
50	200	G 04	632.00	128.42
50	200	G 05	508.00	181.27
50	200	G 06	650.00	236.39
50	200	G 07	560.00	115.58
50	200	G 08	540.00	13.82
50	200	G 09	830.00	39.47
50	200	G 10	50.00	163.50
0	250	G 01	1000.00	185.77
0	250	G 02	521.59	242.51
0	250	G 03	650.00	252.46
0	250	G 04	632.00	139.39
0	250	G 05	508.00	186.36
0	250	G 06	650.00	248.72
0	250	G 07	560.00	122.57
0	250	G 08	540.00	73.18
0	250	G 09	830.00	57.85
0	250	G 10	0.00	0.00